ANALYSIS OF A WIND TURBINE FOUNDATION ON STIFF CLAY WITH ANALYTICAL AND 3D FINITE ELEMENT METHODS

A THESIS SUBMITTED TO
THE GRADUATE SCHOOL OF NATURAL AND APPLIED SCIENCES
OF
MIDDLE EAST TECHNICAL UNIVERSITY

BY

BAKİ EREN YAŞAR

IN PARTIAL FULFILLMENT OF THE REQUIREMENTS
FOR
THE DEGREE OF MASTER OF SCIENCE
IN
CIVIL ENGINEERING

DECEMBER 2019

Approval of the thesis:

ANALYSIS OF A WIND TURBINE FOUNDATION ON STIFF CLAY WITH ANALYTICAL AND 3D FINITE ELEMENT METHODS

submitted by **BAKİ EREN YAŞAR** in partial fulfillment of the requirements for the degree of **Master of Science in Civil Engineering Department, Middle East Technical University** by,

Prof. Dr. Halil Kalıpçılar
Dean, Graduate School of **Natural and Applied Sciences** _____

Prof. Dr. Ahmet Türer
Head of Department, **Civil Engineering** _____

Assoc. Prof. Dr. Nejan Huvaj Sarıhan
Supervisor, **Civil Engineering, METU** _____

Examining Committee Members:

Prof. Dr. Nihat Sinan Işık
Civil Engineering, Gazi University _____

Assoc. Prof. Dr. Nejan Huvaj Sarıhan
Civil Engineering, METU _____

Assoc. Prof. Dr. Zeynep Gülerce
Civil Engineering, METU _____

Assist. Prof. Dr. Onur Pekcan
Civil Engineering, METU _____

Assist. Prof. Dr. Gence Genç
Civil Engineering, Çankaya University _____

Date: 06.12.2019

I hereby declare that all information in this document has been obtained and presented in accordance with academic rules and ethical conduct. I also declare that, as required by these rules and conduct, I have fully cited and referenced all material and results that are not original to this work.

Name, Surname: Baki Eren Yaşar

Signature:

ABSTRACT

ANALYSIS OF A WIND TURBINE FOUNDATION ON STIFF CLAY WITH ANALYTICAL AND 3D FINITE ELEMENT METHODS

Yaşar, Baki Eren
Master of Science, Civil Engineering
Supervisor: Assoc. Prof. Dr. Nejan Huvaj Sarıhan

December 2019, 121 pages

Optimum design of onshore wind turbine foundations have been a topic of interest in geotechnical engineering in recent decades. However, the literature is lacking a systematic methodology for the design of onshore wind turbine foundations with three-dimensional finite element method (3D FEM) and a practical study evaluating the factors affecting the foundation design. The goals of this study are (i) to present a comprehensive design procedure by summarizing the literature, (ii) to investigate the key issues for the design of onshore wind turbine foundations using 3D FEM and (iii) to highlight the important factors for ensuring both safe and economical design. For these purposes, a wind turbine with 1.5 MW capacity on stiff clay was taken as a case study and the analyses of the foundation (in terms of bearing capacity, overturning, sliding, rocking stiffness, elastic settlement and rotation) were conducted using analytical method, probabilistic method using Monte Carlo simulation, and 3D FEM. In conclusion, to calculate the settlement and rotation of wind turbine foundations accurately, using 3D finite element analysis was recommended instead of analytical method. Furthermore, the variation in foundation diameter and soil properties, i.e., different coefficient of variation (COV) levels, on satisfactory performance was evaluated. It was noted that the increase of COV level causes an increase in the probability of unsatisfactory performance of the foundation. This study demonstrates

a foundation design methodology for practicing engineers and will be useful to reach robust, safe and economical foundation design for wind turbines considering the variability in soil properties.

Keywords: Onshore Wind Turbine Foundation, Monte Carlo, Three Dimensional Finite Element Method, Plaxis 3D

ÖZ

KATI KİL ÜZERİNE KURULU BİR RÜZGAR TÜRBİNİ TEMELİNİN ANALİTİK VE ÜÇ BOYUTLU SONLU ELEMANLAR YÖNTEMLERİ İLE ANALİZİ

Yaşar, Baki Eren
Yüksek Lisans, İnşaat Mühendisliği
Tez Danışmanı: Doç. Dr. Nejan Huvaj Sarıhan

Aralık 2019, 121 sayfa

Karadaki rüzgâr türbini temellerinin ideal tasarımı, geoteknik mühendisliğinin son yıllarda ilgi duyulan bir konusu olmuştur. Ancak, literatür, karadaki rüzgâr türbini temellerinin üç boyutlu sonlu elemanlar yöntemi (3B SEY) ile tasarımı için oluşturulmuş sistematik bir metodoloji ve tasarımı etkileyen faktörleri değerlendiren pratik bir çalışma yönünden yoksundur. Bu çalışmanın amaçları (i) literatürü özetleyerek kapsamlı bir tasarım prosedürü sunmak, (ii) 3B SEY kullanarak karadaki rüzgâr türbini temellerinin tasarımı için gerekli kilit konuları araştırmak ve (iii) hem güvenli hem de ekonomik bir tasarım için önemli olan faktörleri vurgulamaktır. Bu amaçlar için, sert kil üzerinde kurulu 1.5 MW kapasiteli bir rüzgâr türbini, örnek bir çalışma olarak ele alınmış ve temel analizleri (taşıma kapasitesi, devrilme, kayma, dönme rijitliği, elastik oturma ve dönme açısından); analitik yöntem, Monte Carlo simülasyonu kullanılarak olasılıksal yöntem ve 3B sonlu elemanlar kullanılarak yapılmıştır. Sonuç olarak, rüzgâr türbini temellerinin oturma ve dönmesini doğru bir şekilde hesaplamak için, analitik yöntem yerine 3B sonlu eleman çözümleri önerilmiştir. Ayrıca, temel çapı ve zemin özelliklerindeki değişimler, başka bir deyişle farklı değişim katsayısı (DK) seviyeleri, yeterli performanstaki değişim açısından değerlendirilmiştir. DK seviyesi artışının, temelin yetersiz performans gösterme

ihtimalinde artışa neden olduğu belirtilmiştir. Bu çalışma; mühendislere temel tasarım yöntemi sunmakta olup, onların zemin özelliklerindeki değişkenliği de hesaba katarak sağlam, güvenli ve ekonomik temel tasarımına ulaşmalarına yardımcı olacaktır.

Anahtar Kelimeler: Karadaki Rüzgâr Türbini Temelleri, Monte Carlo, Üç Boyutlu Sonlu Eleman Yöntemi, Plaxis 3D

To My Parents

ACKNOWLEDGEMENTS

I would like to express my sincere gratitude and respectful regards to my supervisor, Professor Nejan Huvaj Sarıhan, for providing me continuous and invaluable guidance throughout this thesis study. It was a great privilege to work with her. I would also like to thank her for her friendship, empathy, kindness and patience (*I have enjoyed long hours of discussions with you on various technical and non-technical topics!*).

I would also like to express my gratitude to the members of my thesis examining committee for their time, interest and insightful comments. The comments helped me in preparing the final version of this thesis.

I thank my classmates and faculty members in Department of Civil Engineering at Middle East Technical University (METU). They have taught me immensely and inspired me in some way.

I thank Mehmet Yılmaz at University of Wisconsin-Madison in USA for answering patiently my long questions about his study and providing me the information that I needed to use in this thesis.

I thank Byron Mawer at JG Afrika in South Africa for helping me when I needed further clarification to understand some key points of wind turbine foundations.

I thank my friends (*too many to list here but you know who you are!*) for providing me invaluable friendship and motivation that I needed.

I would also like to thank my dear nephew and colleague, Mehmet Ali Yaşar, for going far beyond the call of duty (*I owe you a lot!*).

Finally, but by no means least, I would like to thank my family for all their love (*words cannot express my gratitude to you!*). Their support has been unconditional all these years. Whenever I needed, they have always supported me to overcome the difficulties and be with me. This thesis would not have been possible without them..

TABLE OF CONTENTS

ABSTRACT v

ÖZ vii

ACKNOWLEDGEMENTS x

TABLE OF CONTENTS xi

LIST OF TABLES xiv

LIST OF FIGURES xvi

1. INTRODUCTION 1

1.1. General Information 1

1.2. Research Objectives 3

1.3. Research Scope 4

2. LITERATURE REVIEW 5

2.1. Wind Turbines 5

2.1.1. Energy Conversion Systems of a Wind Turbine 6

2.1.2. Supporting Systems of a Wind Turbine 7

2.1.2.1. Tower 7

2.1.2.2. Foundation 8

2.2. Geotechnical Design Considerations 11

2.2.1. Loading 11

2.2.2. Bearing Capacity 20

2.2.3. Global Stability 29

2.2.4. Stiffness 31

2.2.5. Settlement 35

2.2.5.1. Induced Vertical Stresses 36
2.2.5.2. Elastic Settlement 38
2.2.5.3. Consolidation Settlement 40
2.2.6. Rotation (Tilt) 42
2.3. Previous Studies on the Topic 43
2.3.1. Theoretical Studies 43
2.3.2. Numerical Studies 44
2.3.3. Experimental Studies 47
3. A CASE STUDY 49
3.1. General Information 49
3.2. Project Information 50
3.3. Soil Information 54
3.3.1. Index Properties of the Soil 54
3.3.2. Strength Properties of the Soil 55
3.3.3. Compression Properties of the Soil 65
4. ANALYSIS USING ANALYTICAL METHOD 67
4.1. General Information 67
4.2. Dimensions 67
4.3. Loads 68
4.4. Effective Area & Eccentricity 68
4.5. Geotechnical Design Requirements 69
4.6. Monte Carlo Simulation 71
4.6.1. The Reason 71
4.6.2. The Methodology 72

4.6.3. The Results 75
5. ANALYSIS USING 3D FINITE ELEMENT METHOD 83
5.1. Software.....83
5.2. Geometry 83
5.3. Meshing 85
5.4. Constitutive Models 89
5.5. Analysis Stages.....93
5.6. Results 96
5.7. Discussion of Results: Field Measurements, Analytical Solution and Three-Dimensional Finite Element Method 104
6. CONCLUSION.....105
6.1. Summary 105
6.2. Conclusions 105
6.3. Recommendations for Future Studies 107
REFERENCES.....109

LIST OF TABLES

TABLES

Table 2.1. Loads at the Tower Base of a ENERCON E48 Turbine (0.8 MW) 14
Table 2.2. Different Expressions for N_γ from Various Researchers 24
Table 2.3. Hansen's (1970) Geometric Factors 25
Table 2.4. Vesić's (1973; 1975) Geometric Factors 25
Table 2.5. DNV/RISØ's (2002) Geometric Factors 26
Table 2.6. Adhesion and Friction Factor for Mass Concrete on Different Soils 31
Table 2.7. Stiffness Equations for a Circular Foundation 34
Table 2.8. Rocking Stiffness Requirement for a Foundation of ENERCON E48 Turbine (0.8 MW) 35
Table 3.1. Information about Vensys 82 Turbine (1.5 MW) 50
Table 3.2. Unfactored Loads and Moments Provided for Vensys 82 Turbine (1.5 MW capacity) 51
Table 3.3. Soil Properties Obtained by Using the Laboratory Experiments (Yılmaz, 2014) 54
Table 3.4. Soil Properties Calculated by Using the Available Properties 55
Table 3.5. Variation of α' with Plasticity Index 56
Table 3.6. Undrained Young's Modulus of Clays 60
Table 3.7. The Results Based on the Average of SPT-N Values and Nonlinear Relations 63
Table 3.8. Undrained Shear Strength and OCR Values Based on Available Unconfined Compressive Strengths and Nonlinear Relations 64
Table 3.9. Different Expressions for Compression Index of the Soil 64
Table 3.10. Different Expressions for Compression Index of the Soil 65
Table 3.11. Recompression Index of the Soil 66
Table 4.1. Results of Monte Carlo Simulation for Bearing Capacity 77

Table 4.2. Results of Monte Carlo Simulation for Sliding 78
Table 4.3. Results of Monte Carlo Simulation for Rocking Stiffness 79
Table 4.4. Results of Monte Carlo Simulation for Settlement.....79
Table 5.1. Mesh Generation Options in PLAXIS 3D AE 86
Table 5.2. Results of the Mesh Sensitivity Analysis.....88
Table 5.3. Soil Properties Obtained by Using the Estimation Curve for Mohr-Coulomb Model 91
Table 5.4. Soil Properties Obtained by Using the Weighted Averages for Mohr-Coulomb Model 92
Table 5.5. Soil Properties Obtained by Using the Estimation Curve for Hardening Model 92
Table 5.6. Soil Properties Obtained by Using the Weighted Averages for Hardening Model 93
Table 5.7. Reinforced Concrete Properties for Linear-Elastic Model 93
Table 5.8. Results of the 3D Finite Element Analyses Using Estimation Curve.....102
Table 5.9. Results of the 3D Finite Element Analyses Using Weighted Averages .103

LIST OF FIGURES

FIGURES

Figure 1.1. World Electricity Generation by Fuel, 2012-40 2
Figure 1.2. World Electricity Generation from Renewable Energy by Fuel, 2012-40 2
Figure 1.3. Concrete Volume of Foundation versus Wind Turbine Rated Power. Adapted from Morgan & Ntambakwa (2008) 3
Figure 2.1. Horizontal Axis Wind Turbines with Rated Power of 7.5 MW at Noordoostpolder Windpark in the Netherlands 5
Figure 2.2. Major Structural and Mechanical Parts of a Typical Wind Turbine 6
Figure 2.3. Main Components of a Typical Wind Turbine (Lynn, 2012) 7
Figure 2.4. Approximate Component Masses and Moment at the Tower Base versus Rotor Diameter 8
Figure 2.5. An Almost Completed Wind Turbine Gravity Base Circular Foundation. Retrieved from Partnership for Renewables (2013) 9
Figure 2.6. Different Gravity Base Foundation Types and Typical Dimensions 10
Figure 2.7. Capital Cost Breakdown for a Typical Wind Turbine 11
Figure 2.8. Loads on a Wind Turbine Gravity Base Foundation 13
Figure 2.9. Bearing Pressure Distributions of Concentric and Eccentric Load 14
Figure 2.10. Effective Areas of an Eccentrically Loaded Square Foundation and Eccentrically Loaded Circular Foundation 17
Figure 2.11. Failure Modes of a Shallow Foundation 21
Figure 2.12. Vesić's (1973, 1975) Base and Ground Inclination Factors 23
Figure 2.13. Three Different Positions of Groundwater Table for Bearing Capacity Analysis 26
Figure 2.14. G/G_{max} versus γ Curves 32
Figure 2.15. ζ versus γ Curves 32

Figure 2.16. Typical Shear Modulus Reduction Curve and Applicable Range of Dynamic Laboratory and In-situ Tests (Priest, 2012) 33
Figure 2.17. Circular Foundation on Stratum over Bedrock or on Stratum over Half-Space or Embedded in Stratum over Bedrock 35
Figure 2.18. Variation of Vertical Stresses with Depth Based on Boussinesq's (1885) Equation 37
Figure 2.19. Influence Factor I_g for a Circular Foundation 39
Figure 2.20. Typical Stress-Strain Curve Appropriate for Consolidation Approach 41
Figure 2.21. Vertical Displacement, Distribution of Void Ratio and Stress Obliquity for Load Cycles N=1 and N=100,000 46
Figure 2.22. Vertical and Horizontal Displacements at the Center of the Foundation Base and Rotation for Static Loads P_A=20 kN/m, P_A=10 kN/m and Cyclic Load 46
Figure 3.1. The Wind Turbine Foundation Constructed for the Project 49
Figure 3.2. The Wind Rose for the Site 50
Figure 3.3. The Dimensions of the Foundation 51
Figure 3.4. Top View of the Instrumentation Layout 52
Figure 3.5. Sectional View of the Instrumentation Layout 53
Figure 3.6. The Soil Deformations Recorded at Different Times in 2013 and 2014 (Yılmaz, 2014) 53
Figure 3.7. The Change in SPT-N Values with Depth 55
Figure 3.8. Undrained Shear Strength Values Obtained by Using Various Nonlinear Relations 58
Figure 3.9. Undrained Shear Strength Values Obtained by Using Unconfined Compressive Strengths and Average Values Obtained by Using Various Relations 58
Figure 3.10. The Relationship between E_u/c_u Ratio and Axial Strain (Jardine et al., 1985) 59
Figure 3.11. E_u/c_u Ratio, Plasticity Index and Overconsolidaton Ratio for Clays (Duncan & Buchignani, 1976) 60
Figure 3.12. The Relationship between E_u/SPT-N Ratio and Plasticity Index (Poulos & Small, 2000) 61

Figure 3.13. The Undrained Young's Modulus Values Obtained Using Various Relations 62
Figure 4.1. Dimensions and Gravity Weights 67
Figure 4.2. Loads at Tower Base, Loads Foundation Base and Eccentricity 68
Figure 4.3. Eccentricity and Effective Area Dimensions 68
Figure 4.4. Allowable Limits and Factors of safety 69
Figure 4.5. Results of Calculations for Checking Geotechnical Considerations 70
Figure 4.6. The Location of Boreholes for Proposed 200 MW Búrfell Wind Park in Iceland (Landsvirkjun, 2015) 71
Figure 4.7. Variability of Soil Profile for Proposed 200 MW Búrfell Wind Park in Iceland 72
Figure 4.8. Input Values of Random Variables with High and Low COVs 74
Figure 4.9. Mean Factors of Safety versus Number of Runs for Bearing Capacity and Sliding Checks 74
Figure 4.10. Bearing Capacity Values of 5000 runs for High COV Level 76
Figure 4.11. Bearing Capacity Values of 5000 runs for Low COV Level 76
Figure 4.12. Probability Density Function for Bearing Capacity 77
Figure 4.13. Probability Density Function for Sliding 78
Figure 4.14. Mean Bearing Capacity versus Diameter of the Foundation 80
Figure 4.15. Probability of $FS_{bc} < 2.26$ versus Diameter of the Foundation 81
Figure 5.1. The Boundaries of the Model below the Foundation 84
Figure 5.2. The Modeled Foundation and Excavation 85
Figure 5.3. 10-node Tetrahedron 3D Soil Element in PLAXIS 3D 86
Figure 5.4. Graphical Presentation of Mesh Sensitivity Analysis 87
Figure 5.5. Meshed Model with Fine to Very Fine Sized Soil Elements 88
Figure 5.6. Hyperbolic Stress-Strain Relation in Primary Loading for a Standard Drained Triaxial Test (PLAXIS Material Models Manual, 2015) 90
Figure 5.7. Calculation Stages for Analysis of a Wind Turbine Foundation 95
Figure 5.8. The Deformed Mesh for Mohr-Coulomb Model 96
Figure 5.9. The Arrows of Total Displacement for Mohr-Coulomb Model 97

Figure 5.10. The Total Vertical Displacement for Mohr-Coulomb Model.....98
Figure 5.11. The Total Deviatoric Strain for Mohr-Coulomb Model.....98
Figure 5.12. The Pressure Distribution beneath the Foundation at Tower Loading Stage for Mohr-Coulomb Model.....99
Figure 5.13. The Pressure Distribution beneath the Foundation at Combined Loading Stage for Mohr-Coulomb Model.....100
Figure 5.14. The Cartesian Total Stress beneath the Foundation for Mohr-Coulomb Model 101
Figure 5.15. The Pressure Distribution beneath the Foundation at Combined Loading Stage for Hardening Model.....101
Figure 5.16. The Cartesian Total Stress beneath the Foundation (Centerline) for Hardening Model 102

CHAPTER 1

INTRODUCTION

1.1. General Information

Wind energy, as an alternative to fossil fuel-generated energy, is locally available, abundant, sustainable and a clean fuel. Furthermore, wind turbines are cost-effective, installed fast and occupies little land. By these means, wind farms generate electricity more affordably and without health, environmental and financial risks intrinsic to fossil fuel and nuclear power plants.

Worldwide agreement to reduce greenhouse gas emissions makes renewable energy grow globally. Over the last decade, wind energy has been extensively growing as a major source of non-hydropower renewables (U.S. EIA, 2016). To achieve a more diversified energy mix and meet the continuing demand for alternative energy sources, a great number of wind turbines are being installed on both onshore and offshore wind farms. The shares of total electricity generation for renewable energy sources are expected to increase from 22% in 2012 to 29% in 2040 as shown in Figure 1.1. While non-hydropower renewables accounted for 5% of total electricity generation in 2012, their percentage in 2040 is expected to be 14% with 49% supplied only from wind energy as shown in Figure 1.2 (U.S. EIA, 2016).

As economic and population growths lead to increase in worldwide energy demand, wind energy will obviously be an increasingly important contributor to worldwide energy supply owing to the continuous improvements in the wind turbine technology (Smil, 2010; Brown et al., 2015). As the encouraging growth of wind energy around the world necessitates larger wind turbines with higher towers to increase the power output, larger and more robust foundations will be required to ensure the reliable operations of onshore wind turbine systems over a typical service life of 20 to 25 years

(Figure 1.3). This situation obviously necessitates the thorough understanding of geotechnical design considerations, in order to develop not only more secure but also more economical designs. Convenient and cost-effective foundations will guarantee the substantial reductions in capital costs and thus ensure the proliferation of the decentralized and decarbonized energy.

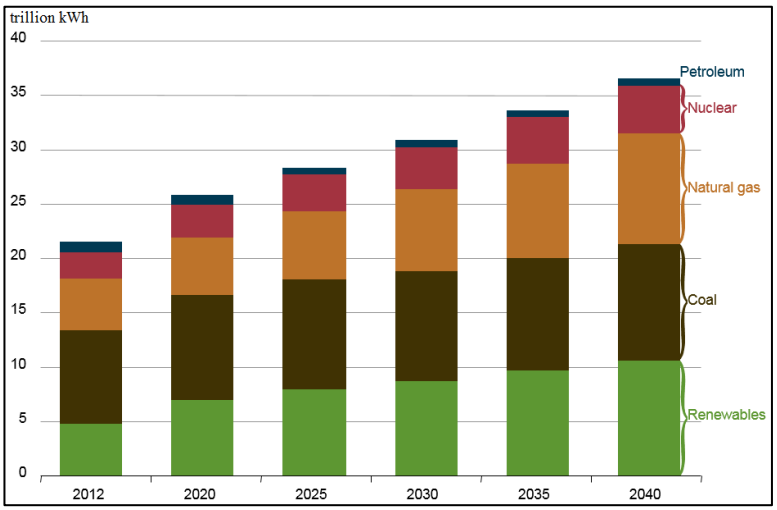

Figure 1.1. World Electricity Generation by Fuel, 2012-40

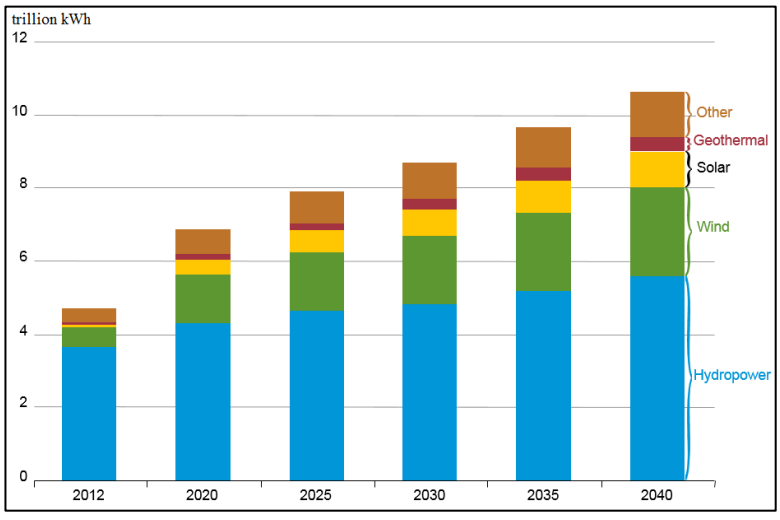

Figure 1.2. World Electricity Generation from Renewable Energy by Fuel, 2012-40

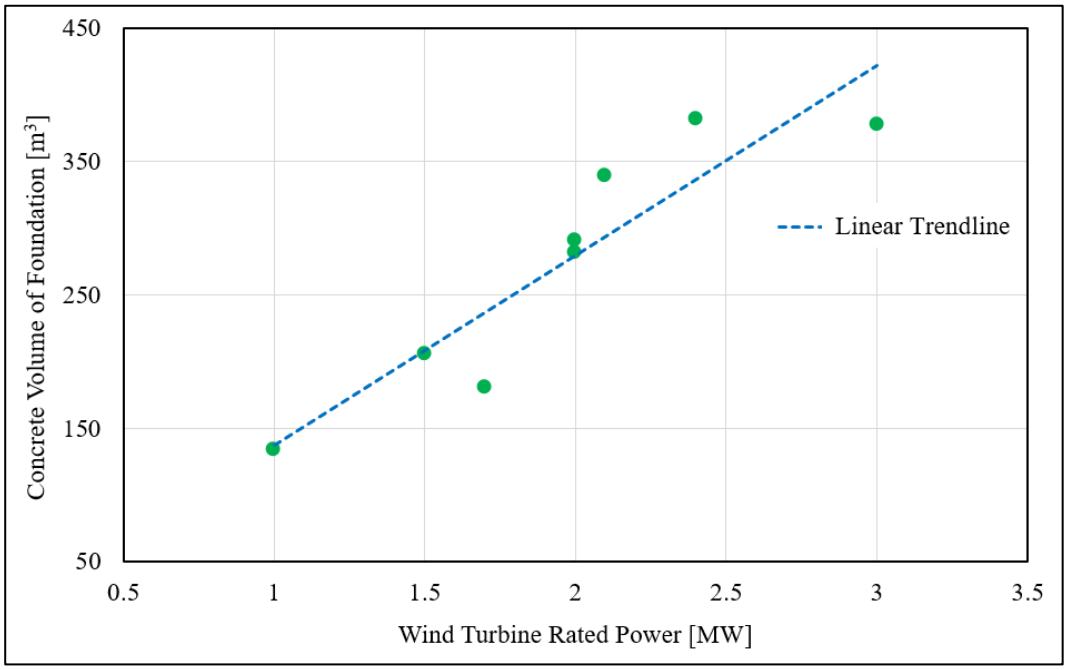

Figure 1.3. Concrete Volume of Foundation versus Wind Turbine Rated Power. Adapted from Morgan & Ntambakwa (2008)

1.2. Research Objectives

In recent years, optimum design of onshore wind turbine foundations has been in the area of interest for geotechnical engineers. Previous studies on onshore wind turbine foundations involve response of foundations to different loading and field conditions, finite element modelling and analysis to assess different behaviors of foundations (e.g. seismic, cyclic) together with analytical solutions, life cycle assessment and examining alternative foundation methods (e.g. helical piers). However, the literature is lacking a systematic methodology for the design of onshore wind turbine foundations with three-dimensional finite element method (3D FEM) and a practical study to evaluate the factors affecting the design. Therefore, the motivations of this study were (i) to demonstrate a systematic methodology to obtain both robust and safe foundation design for practicing engineers working on wind turbines and (ii) to highlight the effects and importance of the soil variability in the foundation design.

The specific objectives of this study were:

(i) to present a comprehensive geotechnical design procedure by summarizing the literature including available guidelines,

(ii) to investigate the key issues for design of onshore wind turbine foundations using analytical method with Monte Carlo simulation and 3D FEM,

(iii) to emphasize the important factors to obtain both safe and economical foundation design.

The novelty of this study is to compare the results of analyses conducted by analytical method with Monte Carlo simulation considering the variability in soil properties and 3D FEM.

1.3. Research Scope

Chapter 2 provides a literature review including fundamental information about wind turbines, geotechnical design considerations for onshore wind turbine foundations and a summary of the previous studies. Chapter 3 details a case study of a wind turbine with 1.5 MW capacity on stiff clay located in Wisconsin, USA. Chapter 4 discusses the analytical method, based on DNV/RISØ (2002), together with Monte Carlo simulation considering the variability in soil properties for the case study presented in Chapter 3. Chapter 5 presents the details of 3D finite element analyses and their results for the case study. Finally, Chapter 6 highlights the outcomes of this study and suggests topics for further studies on this subject.

CHAPTER 2

LITERATURE REVIEW

2.1. Wind Turbines

The most common design in the current megawatt-sized wind turbine market is the three-bladed horizontal axis wind turbine (hereinafter referred to as wind turbine) which has its axis of rotation horizontal to the ground as shown Figure 2.1.

A typical wind turbine has many structural, mechanical and electrical components; however, there are two major systems that are (i) energy conversion systems (i.e., rotor system and nacelle) and (ii) supporting systems (i.e., tower and foundation).

Figure 2.1. Horizontal Axis Wind Turbines with Rated Power of 7.5 MW at Noordoostpolder Windpark in the Netherlands

2.1.1. Energy Conversion Systems of a Wind Turbine

The rotor system includes blades, hub and pitch as shown in Figure 2.2. The blades capture the wind energy and the hub connects the blades and transfers the wind loads to the nacelle. The pitch system controls the power production by rotating the blades about their longitudinal axis to keep the rotational speed of the turbine within the operating limits as wind speed changes (Jain, 2011; Hemami, 2012).

The nacelle shown in Figure 2.3 contains all the components except the rotor system. These components include main shaft, gearbox, generator, yaw mechanism, brake and some other minor components. The gearbox connects the rotating blades to the generator through the main shaft and the generator converts the mechanical energy of the rotating blades into the electrical energy. The brake prevents the rotation of blades when the wind conditions are not suitable for the electricity generation. On the lower part of the nacelle, the yaw mechanism keeps the nacelle facing the wind when the wind direction changes (Lynn, 2012; El-Sharkawi, 2016).

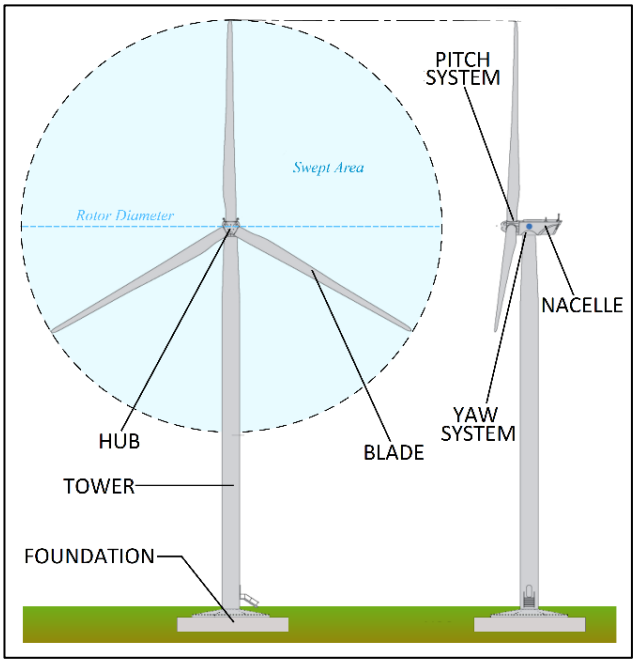

Figure 2.2. Major Structural and Mechanical Parts of a Typical Wind Turbine

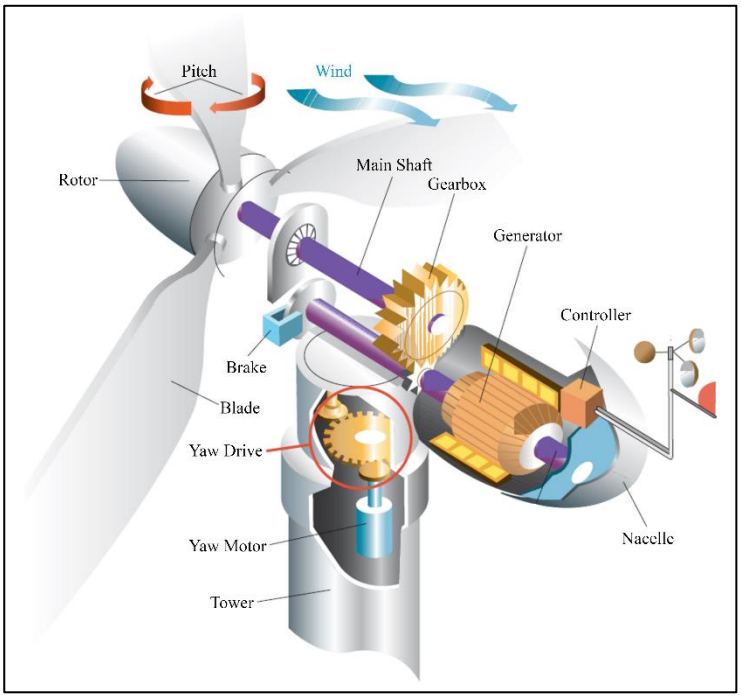

Figure 2.3. Main Components of a Typical Wind Turbine (Lynn, 2012)

2.1.2. Supporting Systems of a Wind Turbine

The major supporting systems of a wind turbine are (i) tower and (ii) foundation.

2.1.2.1. Tower

The tower is the first of the two most important supporting systems to ensure both safe and economically favorable operation. Its importance in economic efficiency results from two reasons (i) it constitutes the significant amount of the capital costs (i.e.,~20%) and (ii) the hub height directly controls the energy yield thus the profit since the wind speed increases with the height logarithmically at the most sites (Twele et al., 2012). As the size of a turbine itself increases, the rotor diameter and the wind thrust experienced by the rotor increase. Consequently, the overturning moment generated by the wind thrust at the tower base increases. This is shown in Figure 2.4.

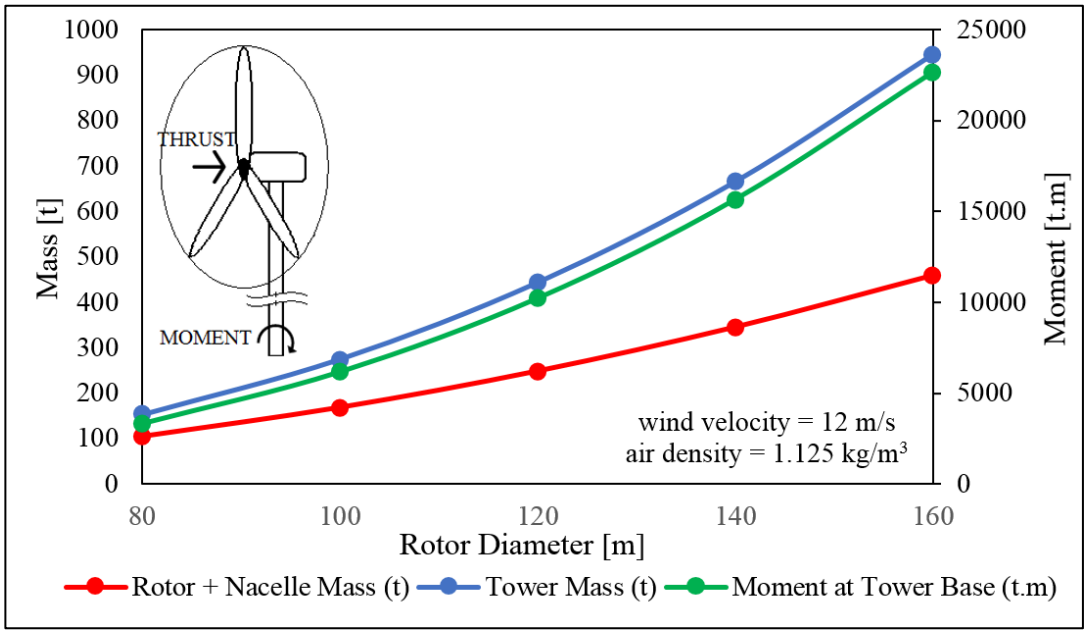

Figure 2.4. Approximate Component Masses and Moment at the Tower Base versus Rotor Diameter

Nowadays, tubular steel towers are used to support almost all megawatt-sized wind turbines. However, some limitations may be encountered as hauling the large steel sections on roads due to the width and height restrictions (e.g., low vertical clearances of overpasses). Therefore, if a tower with a diameter greater than the minimum vertical clearance of the hauling route is required, a hybrid tower can be preferred. A hybrid tower consists of a concrete base section, which is casted on site, and the upper steel sections welded on the top of the casted concrete base section (Jain, 2011; Lynn, 2012).

2.1.2.2. Foundation

The foundation, which is the second of the two most important supporting systems, transfers the total weight of the rotor system, the nacelle and the tower to the ground. It is of great importance for the stabilization of the wind turbine due to the high wind thrust caused by the large rotor area (Wagner & Mathur, 2013).

There are two basic types of wind turbine foundations (i) shallow foundations (e.g., gravity base) and (ii) deep foundations (e.g., pile). The ground conditions and the turbine size, which essentially determines the highest wind thrust acting on the turbine, specifies the foundation type (Hau, 2013).

Gravity base foundations shown in Figure 2.5 are preferred when the soils with competent strength characteristics exist within a few meters depth (Burton et al., 2011). The massive total weight of the foundation and the backfill primarily resist the overturning moment in the most extreme wind conditions. Today, these types of foundations are the most preferred options for megawatt-sized wind turbines due to their practicality and relatively low costs (Ntambakwa et al., 2016).

Figure 2.5. An Almost Completed Wind Turbine Gravity Base Circular Foundation. Retrieved from Partnership for Renewables (2013)

The ideal shape of a gravity base foundation is a circle; however, an octagon (or any centro-symmetrical plan area (Faber, 2014)) is also commonly preferred due to the construction complications of the circular formwork. Also, rock anchors may be used to reduce the foundation size (Burton et al., 2011). In general, gravity base foundations

are made of reinforced concrete with 150 to 500 m^3 of concrete and 15 to 40 tons of rebar. Their dimensions are about 15-20 m at foundation base and 4.5-5.5 m at pedestal with 0.3-1.0 m edge (or spur) height and 2.5-3.5 m center height. The foundation cost is generally about $100,000 to $300,000 (Tinjum & Christensen, 2011; Ntambakwa et al., 2016). Two most widely used gravity base foundation and their typical dimensions are shown in Figure 2.6.

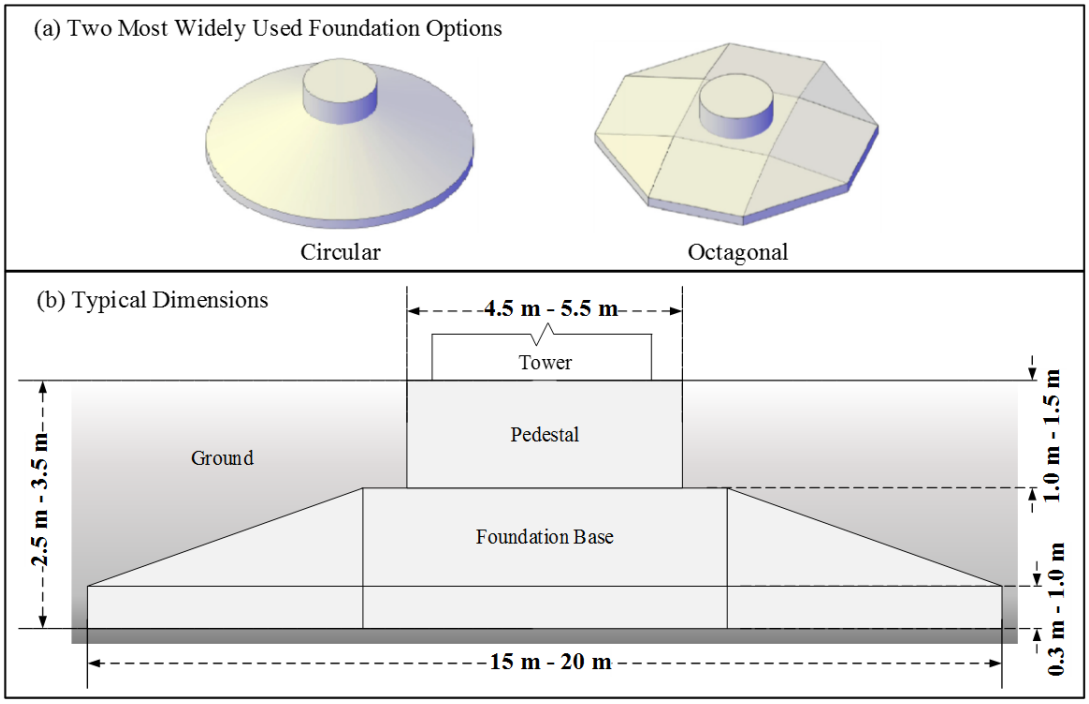

Figure 2.6. Different Gravity Base Foundation Types and Typical Dimensions

A larger rotor diameter not only increases the turbine cost but also increases the foundation cost (Jamieson, 2011). As shown in Figure 2.7, the foundation is less expensive (i.e., typically 16% of the capital cost) than the other major components. However, it is by far the heaviest component (i.e., typically 2 to 3 times the mass of the turbine itself) (Willey, 2010). The construction costs of the infrastructure and the foundation compose approximately 30% of the capital costs. Today, despite the

reductions in turbine costs, the construction costs remain relatively high (Ntambakwa et al., 2016). Therefore, the economic considerations are crucial in the design process.

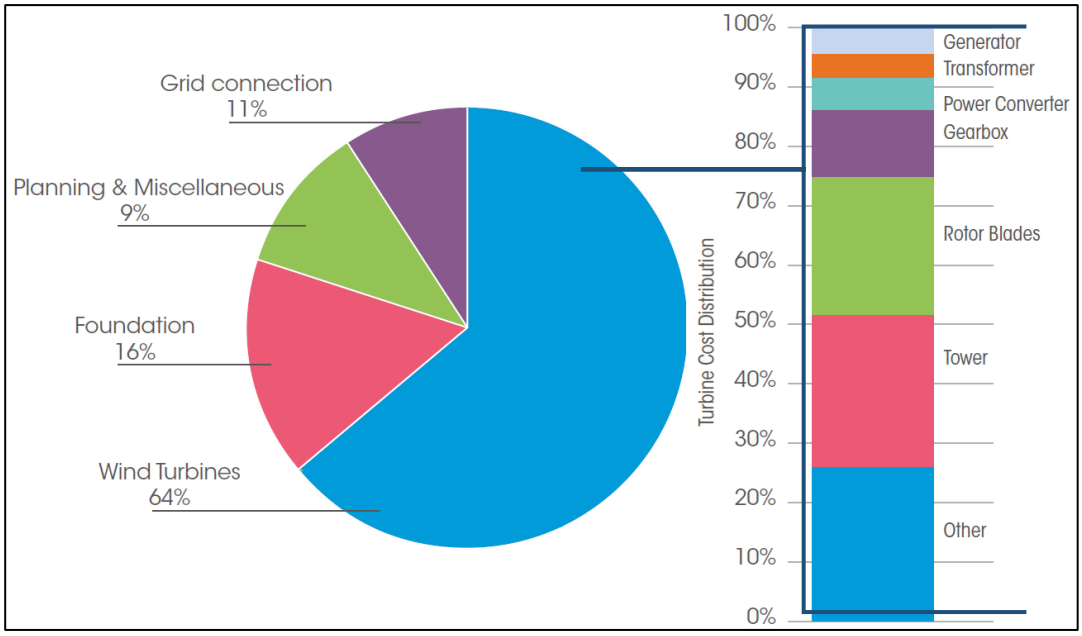

Figure 2.7. Capital Cost Breakdown for a Typical Wind Turbine

Pile foundations are more suitable than gravity base foundations for the soils with weak strength characteristics. The piles resist the high overturning moment by both vertically and laterally (Burton et al., 2011). They can be either driven (i.e., driving down a reinforced concrete or steel beam) or bored (i.e., drilling a shaft and subsequent pouring of concrete) (Jain, 2011).

2.2. Geotechnical Design Considerations

2.2.1. Loading

The sources of loading on a wind turbine are aerodynamic loads, gravitational loads, inertial loads, actuation loads arising from the operational actions of the turbine, and

other loads (e.g., ice loads) (Hau, 2013). In the worst-case scenario, these sources simultaneously produce complex and highly random dynamic loads resulting in cumulative effects on the wind turbine. In practice, the design load cases (DLCs) with sets of loads acting at the tower base covering the most extreme conditions that the foundation may experience during its service life are provided by the turbine manufacturer since the procedure to calculate the design loads requires very complex wind flow modeling and analyses.

The typical loads provided by a turbine manufacturer are shown in Figure 2.8.a:

F_x is shear force due to the aerodynamic loads,

F_z is normal force due to the weight of the structure excluding the foundation and the backfill,

M_r is overturning moment acting around y-axis due to the shear force,

M_z is torsional moment acting around z-axis mainly due to the rotations of the turbine around z-axis (Morgan & Ntambakwa, 2008).

The loads transmitted to the foundation base are shown in Figure 2.8.b:

P is characteristic or design normal force due to the weight of the structure including the weight of the foundation and the weight of the backfill,

H is characteristic or design shear force,

M is characteristic or design overturning moment,

M_{Z1} is characteristic or design torsional moment.

Hereinafter, the subscript c and d are used to refer a characteristic load (e.g., P_c, H_c, M_c) and a design load (e.g., P_d, H_d, M_d), respectively.

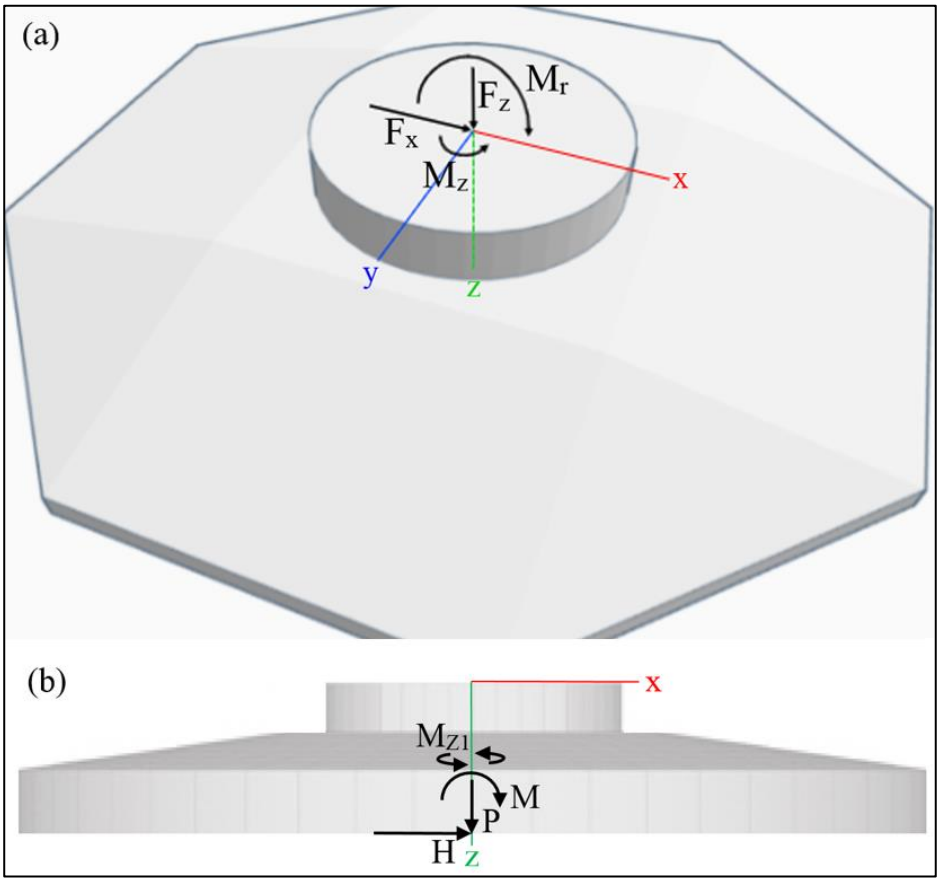

Figure 2.8. Loads on a Wind Turbine Gravity Base Foundation

For the most of the cases, the torsional moment is usually small and ignored in practice. However, when the torsional moment is non-negligible, the interaction between the torsional moment and the shear force should be accounted by replacing the shear force and the torsional moment with an equivalent shear force (DNV/RISØ, 2002) using the equation:

$$H' = \frac{2 \times M_{Z1}}{L'} + \sqrt{H^2 + \left(\frac{2 \times M_{Z1}}{L'}\right)^2} \qquad (2.1)$$

where $\mathbf{H}'$ is equivalent shear force at foundation base,

$\mathbf{M_{Z1}}$ is characteristic or design torsional moment at foundation base,

L' is effective length of foundation,

H is characteristic or design shear force at foundation base.

An example of loads at the foundation base is given in Table 2.1. The unit weight of concrete and backfill soil are 25 kN/m^3 and 18 kN/m^3, respectively.

Table 2.1. *Loads at the Tower Base of a ENERCON E48 Turbine (0.8 MW)*

Design Load Case (DLC)	M [kNm]	M_{Z1} [kNm]	P [kN]	H [kN]
Characteristic (or Unfactored) Loads				
1.0	8,100	-	4,954	180
6.1	12,366	-704	4,850	283
6.2	15,014	-704	4,857	346
Design (or Factored) Loads				
6.1	16,823	-950	4,450	382
6.1	16,729	-950	6,679	382

Note. From "Foundation Data Sheet" by ENERCON GmbH, 2010

Once the loads required to perform the geotechnical analyses are obtained, the bearing pressure needs to be calculated. In reality, the bearing pressure is not uniformly distributed; however, bearing capacity and settlement calculations based on such a distribution would be very complex (Coduto et al., 2015).

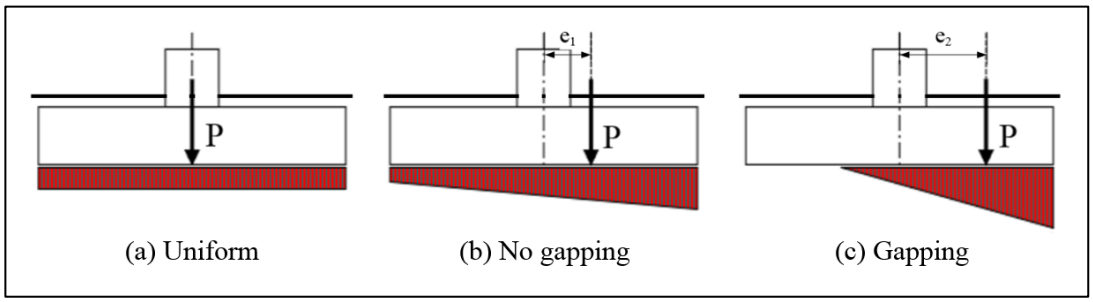

Figure 2.9. Bearing Pressure Distributions of Concentric and Eccentric Load

Therefore, if the normal force acts through the geometric center of the foundation base and no moment loads are applied, it is customary to assume that the bearing pressure is uniformly distributed as shown in Figure 2.9.a.

The gross bearing pressure is given by the equation:

$$q = \frac{P_c}{A} - u_{pd} = \frac{F_z + W_t}{A} - u_{pd} \tag{2.2}$$

where **q** is gross bearing pressure,

F_z is normal force due to weight excluding foundation and backfill,

W_t is total weight of foundation and backfill,

A is plan area of foundation base,

u_{pd} is pore water pressure at foundation base.

An alternative way to define the bearing pressure is net bearing pressure. It is a measure of the increase in vertical effective stress (i.e., induced vertical stress) at the foundation base and given by the equation:

$$q' = q - \sigma'_{z0} = \frac{P_c}{A} - u_{pd} - \sigma'_{z0} = \frac{F_z + W_t}{A} - u_{pd} - \sigma'_{z0} \tag{2.3}$$

where **q'** is net bearing pressure,

σ'_{z0} is initial vertical effective stress at foundation base before construction.

Either way of calculating the bearing pressure will produce the same design, as long as it is used consistently and correctly throughout the analyses. However, although the use of net bearing pressure simplifies the computations associated with settlements, it makes others more complex (Coduto et al., 2015).

Gravity base foundations are usually of intermediate to very high rigidity. Therefore, the actual pressure distribution beneath the foundation is not uniform. However,

bearing capacity and settlement calculations based on such a distribution would be very complex. In practice, it is reasonable to use uniformly distributed pressure beneath the centrally loaded foundations since even when the foundation is very rigid, the soil will tend to develop a uniform pressure distribution in the long term as shown in Figure 2.9.a (Briaud, 2013; Baban, 2016). However, the predominant load from a wind turbine is the high overturning moment (Morgan & Ntambakwa, 2008) and it produces a non-uniform pressure distribution in any case. Assuming a linear pressure distribution, the eccentricity of the bearing pressure is given by the equation:

$$e = \frac{M}{P} \tag{2.4}$$

where **e** is eccentricity of bearing pressure,

M is characteristic or design overturning moment at foundation base,

P is characteristic or design normal force at foundation base.

In practice, it is necessary to have pressure over the entire foundation base by either superimposing a uniform normal pressure on the soil as shown in Figure 2.9.a or limiting the eccentricity as shown in Figure 2.9.b. The gap shown in Figure 2.9.c theoretically indicates that there is tension between the soil and the one side of the foundation base. However, since the soil cannot carry any tensile load, the foundation will lose all contact pressure with the soil on the rising side of the foundation base.

When the eccentric load is applied within a limited area, which is known as the kern and shown in Figure 2.10, there will always be some contact pressure along the entire foundation base. The requirement is that there should be full contact pressure during operational conditions to minimize the vibratory compaction of the soil due to the dynamic loads by ensuring adequate foundation rotational (rocking) stiffness (Ntambakwa et al., 2016). On the other hand, the eccentricity should be limited to produce a gap no further than to the center of gravity of the plan area of the foundation base in order to prevent the failure caused by the rotation of the foundation that occurs

during extreme conditions (Germanischer Lloyd, 2010). This means that 50% of the foundation base can lose contact with the soil shortly during the extreme conditions (Branca & Ben-Hassine, 2009). However, the majority of the turbine manufacturers recommend that the gap have to be avoided even during the extreme conditions.

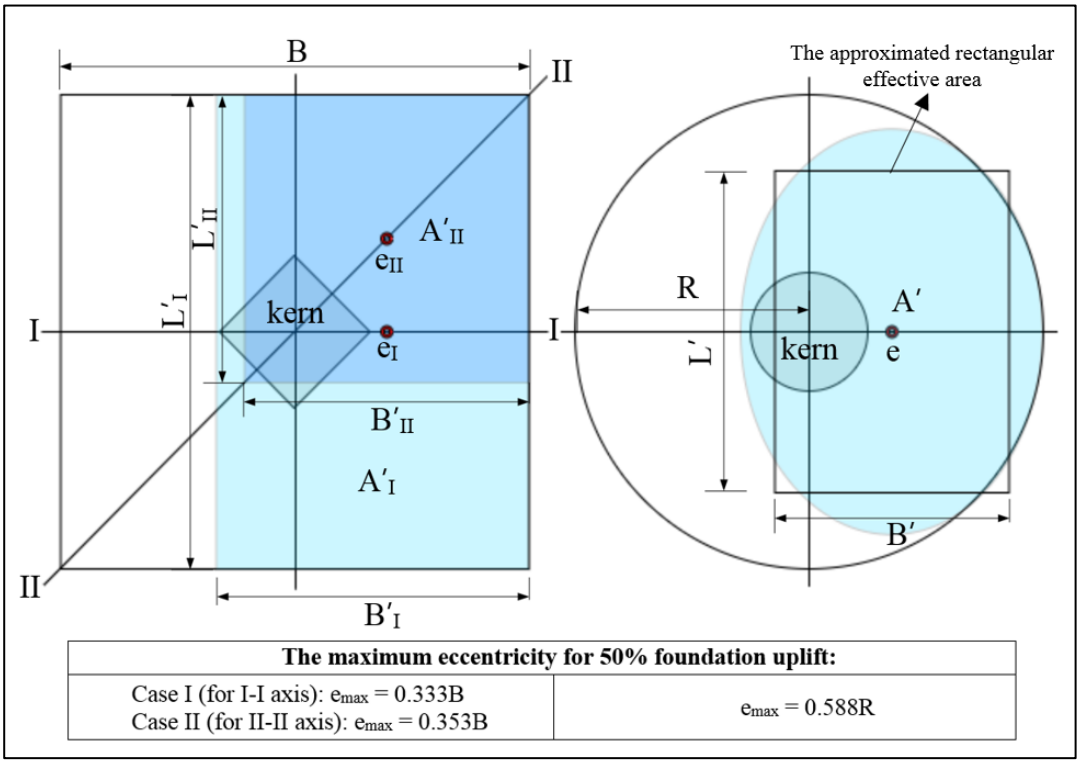

Figure 2.10. Effective Areas of an Eccentrically Loaded Square Foundation and Eccentrically Loaded Circular Foundation

The maximum and minimum values of the bearing pressure for a square foundation due to the normal force positioned within the kern is given by the equation:

$$q_{max,min} = q \times \left[1 \pm \frac{6e}{B}\right] \tag{2.5}$$

The maximum value of bearing pressure for a square foundation due to the normal force positioned outside the kern is given by the equation:

$$q_{max} = q \times \left[\frac{4B}{3B - 6e}\right] \tag{2.6}$$

The maximum and minimum values of bearing pressure for a circular foundation due to the normal force positioned within the kern is given by the equation:

$$q_{max,min} = q \times \left[1 \pm \frac{4e}{R}\right] \tag{2.7}$$

The maximum value of bearing pressure for a circular foundation due to the normal force positioned outside the kern is given by the equation:

$$q_{max} = k \times q \tag{2.8}$$

where **q** is gross (or net) bearing pressure,

e is eccentricity of normal force,

B is breadth of square foundation,

R is radius of circular foundation,

k is a function of eccentricity and radius of foundation (Rao, 2011).

For an eccentrically loaded foundation, it is necessary to obtain the equivalent uniformly loaded foundation. The effective foundation area A' is constructed such that its geometrical center coincides with the eccentric normal load and follows, as closely as possible, the nearest contour of the true area of the foundation base as shown in Figure 2.10 to ensure the uniform resulting bearing pressure (Meyerhof, 1963; DNV/RISØ, 2002).

For a square foundation, the effective area of the foundation base is given by the equation:

$$A' = B' \times L' \tag{2.9}$$

If the eccentricity of the normal force is with respect to one of the two symmetry axes (i.e., I-I axis in Figure 2.10) of the foundation, the effective dimensions are given by the equations:

$$B' = B - 2e \tag{2.10}$$
$$L' = B \tag{2.11}$$

If the eccentricity of the normal force is with respect to both symmetry axes (i.e., II-II axis in Figure 2.10) of the foundation, the effective dimensions are given by the equations:

$$B' = B - e\sqrt{2} \tag{2.12}$$
$$L' = B - e\sqrt{2} \tag{2.13}$$

where **B** is breadth of foundation,

e is eccentricity of normal force.

For a circular foundation, the elliptical effective area of the foundation base is given by the equation:

$$A' = 2\left[R^2 \cos^{-1}\left(\frac{e}{R}\right) - e\sqrt{R^2 - e^2}\right] \tag{2.14}$$

The dimensions of the approximated rectangular effective area of the foundation base, which replaces the elliptical one, are given by the equation:

$$B' = \frac{L'}{l_e} b_e \text{ and } L' = \sqrt{A' \frac{l_e}{b_e}} \tag{2.15}$$

$$\text{where } b_e = 2(R - e) \text{ and } l_e = 2R\sqrt{1 - \left(1 - \frac{b_e}{2R}\right)^2} \tag{2.16}$$

where **A'** is elliptical effective area,

e is eccentricity of normal force,

R is radius of circular foundation.

The equivalent bearing pressure for the foundation is calculated as:

$$q_{eq} = \frac{P_c}{A'} - u_{pd} = \frac{F_z + W_t}{A'} - u_{pd} \quad (2.17)$$

where $\mathbf{q_{eq}}$ is equivalent bearing pressure,

$\mathbf{F_z}$ is normal force due to weight of structure excluding foundation and backfill,

$\mathbf{W_t}$ is total weight of foundation and backfill,

A' is effective area of foundation base,

$\mathbf{u_{pd}}$ is pore water pressure at foundation base.

For an area shaped as a double symmetrical polygon (e.g., octagon), the above formulas for the circular area may be used on the condition that the radius is equal to the radius of the inscribed circle of the polygon (DNV/RISØ, 2002).

2.2.2. Bearing Capacity

Many researchers have studied the bearing capacity of shallow foundations over the years. They described three modes of bearing capacity failure (i) general shear, (ii) local shear and (iii) punching shear. Although punching shear failure mode always applies for deep foundations (i.e., $d_f/B > 4$), shallow foundations (i.e., $d_f/B < 3$) can be governed by any of the failure modes as shown in Figure 2.11. There is not any quantitative criteria to decide which mode of failure will govern in any given circumstance. However, in practice, the ground is generally improved before the construction (i.e., granular soils are densified and cohesive soils are stiffened).

Therefore, it is both reasonable and practical to consider the general shear failure mode for bearing capacity analyses (Sivakugan & Pacheco, 2011). If a shallow foundation is subjected to a dynamic load with an acceleration less than 13g, the failure is most probably by general shear (Heller, 1964). Moreover, settlement checks performed after the bearing capacity check implicitly protect the foundation against both local shear and punching shear failures (Coduto et al., 2015).

Terzaghi (1943) was the first researcher to present a comprehensive theory to calculate the bearing capacity of a shallow foundation assuming that the general shear mode of failure governs. Actually, Terzaghi's (1943) studies were a comprehensive extension of the works done by Rankine (1857), Prandtl (1921), Reissner (1924) (Reese et al., 2006), and a basis for later developments done by Skempton (1951), Meyerhof (1963), Hansen (1970), Vesić (1973; 1975) and many others (Coduto et al., 2015).

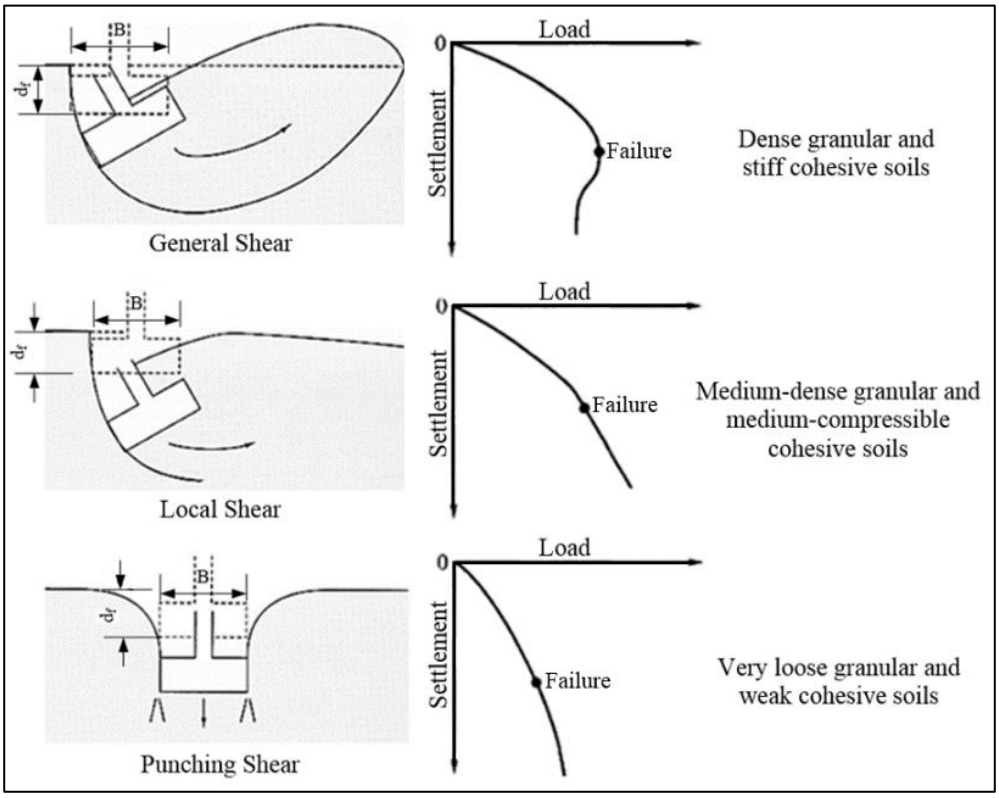

Figure 2.11. Failure Modes of a Shallow Foundation

Hansen (1970) proposed the following most commonly used bearing capacity equation. It is also well acknowledged by DNV/RISØ (2002) and given as:

$$q_n = c' N_c s_c d_c i_c b_c g_c + \sigma'_{z0} N_q s_q d_q i_q b_q g_q + 0.5 \gamma' B' N_\gamma s_\gamma d_\gamma i_\gamma b_\gamma g_\gamma \qquad (2.18)$$

where $\mathbf{q_n}$ is nominal unit bearing capacity,

$\mathbf{c'}$ effective cohesion of soil beneath foundation,

$\boldsymbol{\sigma'_{z0}}$ is initial vertical effective stress at foundation base before construction,

$\boldsymbol{\gamma'}$ is effective unit weight of soil,

B is breadth or diameter of foundation,

$\mathbf{N_c}$, $\mathbf{N_q}$, $\mathbf{N_\gamma}$ are bearing capacity factors,

$\mathbf{s_c}$, $\mathbf{s_q}$, $\mathbf{s_\gamma}$ are shape factors,

$\mathbf{d_c}$, $\mathbf{d_q}$, $\mathbf{d_\gamma}$ are depth factors,

$\mathbf{i_c}$, $\mathbf{i_q}$, $\mathbf{i_\gamma}$ are load inclination factors,

$\mathbf{b_c}$, $\mathbf{b_q}$, $\mathbf{b_\gamma}$ are base inclination factors,

$\mathbf{g_c}$, $\mathbf{g_q}$, $\mathbf{g_\gamma}$ are ground inclination factors.

Base inclination and ground inclination factors shown in Figure 2.12 are usually not necessary for design of wind turbine foundations and not addressed by DNV/RISØ (2002).

Although Hansen's (1970) formula is written in terms of effective stress parameters, it may also be used in undrained total stress analyses (Coduto et al., 2015).

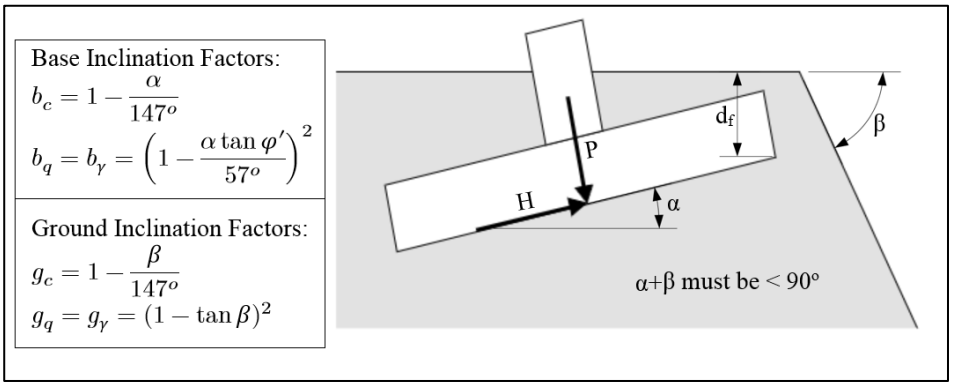

Figure 2.12. Vesić's (1973, 1975) Base and Ground Inclination Factors

In the case of extremely eccentric loading (i.e., an eccentricity in excess of 0.3 times the breadth of the foundation, e > 0.3B), DNV/RISØ (2002) proposes the following bearing capacity equation:

$$q_n = c' N_c s_c i_{ce} (1.05 + \tan^3 \varphi') + \gamma' B' N_\gamma s_\gamma i_{\gamma e} \tag{2.19}$$

The bearing capacity, which rarely governs the design, is to be taken as the smallest of the values calculated using Equation 2.18 and Equation 2.19 (DNV/RISØ, 2002).

Vesić (1973; 1975) used the following equations to calculate the bearing capacity factors N_q and N_c:

$$N_q = e^{\pi \tan \varphi'} \tan^2 \left(45 + \frac{\varphi'}{2}\right) \tag{2.20}$$

$$N_c = \left(N_q - 1\right) \cot \varphi' \ \ (\text{if } \varphi' = 0^o \text{ then } N_c = 5.14) \tag{2.21}$$

N_q factor predominates in granular soils while N_c factor predominates in cohesive soils. These two factors are well-accepted by the most authorities. However, there is considerable disagreement regarding N_γ factor (Coduto et al., 2015; Baban, 2016). N_γ may be calculated using the equations proposed by Hansen (1970), Vesić (1973; 1975), DNV/RISØ (2002) or other researchers listed in Table 2.2. The most appropriate formula is chosen considering the results of geotechnical investigations, the standard of practice and the engineering judgement (Morgan & Ntambakwa,

2008). For example, Meyerhof's (1963) N_γ term is used in North America while Hansen's (1970) N_γ term is extensively used in Europe (Sivakugan & Pacheco, 2011).

Geometric factors proposed by Hansen (1970), Vesić (1973; 1975) and DNV/RISØ (2002) are presented in Table 2.3, Table 2.4, Table 2.5, respectively.

In undrained total stress analyses, s_{co}, d_c^o, i_c^o and i_{ce}^o should be used instead of s_c, d_c, i_c and i_{ce} (DNV/RISØ, 2002).

Vesić (1973; 1975) recommended that depth factors should not be used for shallow foundations if there are uncertainties in the quality of the overburden (Bowles, 2001). Similarly, Budhu (2010) suggested that if the shear strength of the soil above the foundation base is low compared to that of the soil below the foundation, all depth factors should be set to 1.0.

Table 2.2. *Different Expressions for N_γ from Various Researchers*

Reference	Equation
Terzaghi (1943)	$\approx \frac{2(N_q + 1)\tan\varphi'}{1 + 0.4\sin 4\varphi'}$
Biarez (1961)	$1.8(N_q - 1)\tan\varphi'$
Meyerhof (1963)	$(N_q - 1)\tan(1.4\varphi')$
Booker (1969)	$0.1045e^{9.6\varphi'}$ [φ' is in radians]
Hansen (1970)	$1.5(N_q - 1)\tan\varphi'$
Davis & Booker (1971)	$0.1054e^{9.6\varphi'}$ for rough base $0.0663e^{9.3\varphi'}$ for smooth base
Vesić (1973; 1975)	$2(N_q + 1)$
Spangler & Handy (1982)	$1.1(N_q - 1)\tan(1.3\varphi')$
Michalowski (1997)	$e^{0.66+5.1\tan\varphi'}\tan\varphi'$
DNV/RISØ (2002)	$1.5(N_q - 1)\tan\varphi'$
EN 1997-1 (2004)	$2.0(N_q - 1)\tan\varphi'$
Hjiaj et al. (2005)	$e^{\frac{(\pi+3\pi^2\tan\varphi')}{6}}(\tan\varphi')^{2\pi/5}$
Martin (2005)	$(N_q - 1)\tan(1.32\varphi')$

Table 2.3. *Hansen's (1970) Geometric Factors*

Shape Factors		
$s_c = 1 + \left(\frac{B'}{L'}\right)\left(\frac{N_q}{N_c}\right)$ $s_c^o = 1 + 0.2\left(\frac{B'}{L'}\right)$	$s_q = 1 + \left(\frac{B'}{L'}\right)\sin\varphi'$	$s_\gamma = 1 - 0.4\left(\frac{B'}{L'}\right)$
Depth Factors		
$d_c = 1 + 0.4k$ $d_c^o = 0.4k$	$d_q = 1 + 2k\tan\varphi'(1-\sin\varphi')^2$ $k = d_f/B$ for $d_f/B \le 1$ $k = \tan^{-1}(d_f/B)$ for $d_f/B > 1$	$d_\gamma = 1.0$
Load Inclination Factors		
$i_c = i_q - \frac{1-i_q}{N_q - 1}$ $i_c^o = \left[1 - \frac{0.5H}{P + Ac\cot\varphi}\right]^{a_1}$	$i_q = \left[1 - \frac{0.5H}{P + Ac'\cot\varphi'}\right]^{a_1}$ $2 \le a_1 \le 5$	$i_\gamma = \left[1 - \frac{0.7H}{P + Ac'\cot\varphi'}\right]^{a_2}$ $2 \le a_2 \le 5$

Table 2.4. *Vesić's (1973; 1975) Geometric Factors*

Shape Factors		
$s_c = 1 + \left(\frac{B}{L}\right)\left(\frac{N_q}{N_c}\right)$	$s_q = 1 + \left(\frac{B}{L}\right)\tan\varphi'$	$s_\gamma = 1 - 0.4\left(\frac{B}{L}\right)$
Depth Factors		
$d_c = 1 + 0.4k$	$d_q = 1 + 2k\tan\varphi'(1-\sin\varphi')^2$ $k = d_f/B$ for $d_f/B \le 1$ $k = \tan - 1(d_f/B)$ for $d_f/B > 1$	$d_\gamma = 1.0$
Load Inclination Factors		
$i_c = 1 - \frac{mV}{Ac'N_c}$	$i_q = \left[1 - \frac{H}{P + Ac'\cot\varphi'}\right]^m$ For loads inclined in B direction: $m = \frac{2 + B/L}{1 + B/L}$ For loads inclined in L direction: $m = \frac{2 + L/B}{1 + L/B}$	$i_\gamma = \left[1 - \frac{H}{P + Ac'\cot\varphi'}\right]^{m+1}$

Table 2.5. *DNV/RISØ's (2002) Geometric Factors*

Shape Factors		
$s_c = 1 + 0.2\left(\frac{B'}{L'}\right)$ $s_c^o = 1 + 0.2\left(\frac{B'}{L'}\right)$	$s_q = 1 + 0.2\left(\frac{B'}{L'}\right)$	$s_\gamma = 1 - 0.4\left(\frac{B'}{L'}\right)$
Depth Factors		
$d_c = 1.0$ $d_c^o = 1.0$	$d_q = 1.0$	$d_\gamma = 1.0$
Load Inclination Factors		
$i_c = \left[1 - \frac{H}{P + A'c' \cot\varphi'}\right]^2$ $i_c^o = 0.5 + 0.5 + \sqrt{1 - \frac{H}{A'c}}$	$i_q = i_c$	$i_\gamma = i_q^2$
$i_{ce} = 1 + \frac{H}{P + A'c' \cot\varphi'}$ $i_{ce}^o = \sqrt{0.5 + 0.5 + \sqrt{1 + \frac{H}{A'c}}}$	$i_{qe} = i_{ce}$	$i_{\gamma e} = i_{qe}^2$

If there exist a groundwater table within the potential shear zone, the nominal unit bearing capacity will reduce since the shear strength along the failure surface will be smaller due to the presence of pore water. Three different cases may arise regarding the location of the highest possible groundwater table as shown in Figure 2.13.

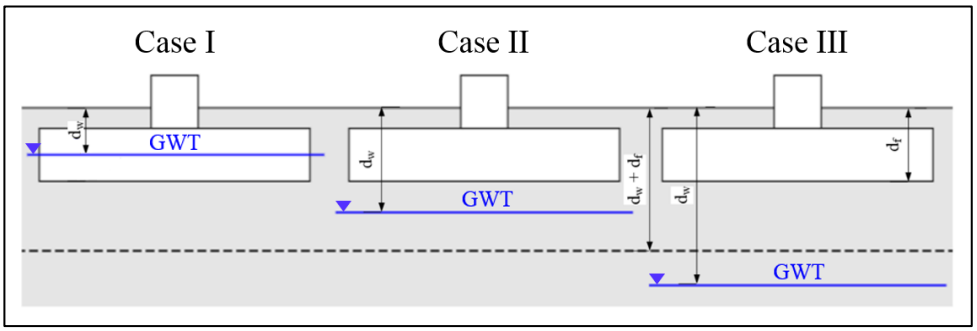

Figure 2.13. Three Different Positions of Groundwater Table for Bearing Capacity Analysis

The effective unit weight in the N_γ term of the bearing capacity equations are calculated using the following equations assuming that there is no seepage force in the soil (Das, 2015):

(i) Case I ($d_w \leq d_f$):

$$\overline{\gamma} = \gamma' = \gamma_{sat} - \gamma_w \tag{2.22}$$

(ii) Case II ($d_f < d_w < d_f + B$):

$$\overline{\gamma} = \gamma' + \left(\frac{d_w - d_f}{B}\right)[\gamma - \gamma'] \tag{2.23}$$

(iii) Case III ($d_f + B < d_w$):

$$\overline{\gamma} = \gamma \tag{2.24}$$

If undrained total stress analysis is performed, any groundwater correction is not applied since the groundwater is implicitly considered in undrained total stress analysis (Coduto et al., 2015).

To use the Allowable Stress Design (ASD) Method, the nominal bearing capacity is divided by a factor of safety to obtain the safe bearing capacity:

$$q_s = \frac{q_n}{FS_b} \tag{2.25}$$

where $\mathbf{q_s}$ is safe bearing capacity,

$\mathbf{q_n}$ is nominal bearing capacity,

FS is factor of safety.

The net safe bearing capacity can be calculated by dividing the net ultimate bearing capacity q_{nn} to a factor of safety (Baban, 2016):

$$q_{sn} = \frac{q_{nn}}{FS_b} = \frac{q_n - \sigma'_{z0}}{FS_b} \quad (2.26)$$

The foundation is then designed so that the bearing pressure does not exceed the safe bearing capacity shown as:

$$q \leq q_s \text{ or } q' \leq q_{sn} \quad (2.27)$$

Chen & McCarron (1991) suggested that the factor of safety for bearing capacity should be between 2.5 and 3.5 for light structures where maximum design load may occur occasionally. Bowles (2001) recommended 3.0 for operational and 2.26 for extreme conditions. ASCE/AWEA (2011) reported that the factor of safety should be 2.26 under extreme conditions. Coduto et al. (2015) presented that the typical range of factor of safety for bearing capacity analyses of shallow foundations is between 2.5 and 3.5.

The ASD Method is a conservative approach and the real factor of safety is probably much greater than the design factor of safety (Coduto et al., 2015).

The Load and Resistance Factor Design (LRFD) Method uses load and resistance factors instead of a single, lumped factor of safety used in the ASD Method. The foundation is designed so that the following condition is satisfied:

$$P_d \leq \psi_r q_n A' \quad (2.28)$$

where $\mathbf{P_d}$ is design normal force at bottom of foundation,

$\boldsymbol{\psi_r}$ is resistance factor,

$\mathbf{q_n}$ is nominal bearing capacity,

$\mathbf{A'}$ is effective area of foundation base.

Resistance factor is recommended as 0.7 by EN 1997-1 (2004) and as 0.45 to 0.55 by AASHTO (2012). However, the appropriate code should be used consistently

throughout the design process while using the LRFD Method. Different codes specify different design methods each with its associated design loads. The code used for design and analysis of the foundation has to match the code used to determine design loads at the tower base because mixing resistance factors from one code with load factors from another code nullifies the reliability calibration and may produce unsafe foundation designs (Coduto et al., 2015; Ntambakwa et al., 2016).

2.2.3. Global Stability

The foundation of a wind turbine is designed to provide adequate resistance to the overturning due to the loads imposed by the turbine. Overturning stability of the wind turbine foundation is evaluated in an ASD framework. The overturning moments about an axis at the downwind edge of the foundation is compared with the resisting moments to confirm adequate factors of safety for resistance to overturning (Morgan & Ntambakwa, 2008; Ntambakwa et al., 2016). The factor of safety for overturning stability is calculated using the following equation (ASCE/AWEA, 2011):

$$FS_o = \frac{P_c(B/2)}{M_c} \tag{2.29}$$

where $\mathbf{P_c}$ is characteristic normal force at foundation base,

B is breadth of square foundation or diameter of circular foundation,

$\mathbf{M_c}$ is characteristic overturning moment at foundation base.

The factor of safety for overturning stability should be at least 1.5 (ASCE/AWEA, 2011).

In the most of the cases, a gravity base foundation is first proportioned for bearing capacity and overturning stability, then sliding stability is evaluated (Morgan & Ntambakwa, 2008). The sliding resistance is obtained from the sliding friction between the foundation base and the soil beneath the foundation and the passive

resistance of the backfill. However, due to the large contact area of the foundation base, the passive resistance of the backfill is usually ignored (Tinjum & Christensen, 2011).

The equations below may be used for the sliding stability depending on the design framework employed (Tinjum & Christensen, 2011; DNV/RISØ, 2002).

(i) For granular soils:

$$FS_s = \frac{P_c \tan \delta}{H_c} \text{ or } H_d < A'c + (P_d) \tan \varphi' \tag{2.30}$$

(ii) For cohesive soils:

$$FS_s = \frac{A'c_a}{H_c} \text{ or } H_d < A'c_u \tag{2.31}$$

where **tanδ** is friction factor between foundation and soil,

$\mathbf{c_a}$ is adhesion between foundation and soil,

φ is friction angle of soil beneath foundation,

$\mathbf{c_u}$ is undrained shear strength of soil beneath foundation.

In addition to this, it must also be verified that (DNV/RISØ, 2002):

$$\frac{H_d}{P_d} < 0.4 \tag{2.32}$$

Adhesion and friction factors for mass concrete on different soils are presented in Table 2.6.

A factor of safety at least 1.5 is generally recommended for sliding resistance of shallow foundations in the literature. Similarly, ASCE/AWEA (2011) suggested that the factor of safety should not be less than 1.5 and only the dead weight of the

structure, the foundation and the backfill above the foundation should be considered in the sliding stability calculations.

Table 2.6. *Adhesion and Friction Factor for Mass Concrete on Different Soils*

Interface Material	Adhesion [kPa]	Interface Material	Friction Factor [-]
Very Soft Cohesive	0 - 12	Coarse Sand	0.55 to 0.60
Soft Cohesive	12 - 24	Fine - Medium Sand	0.45 to 0.55
Medium Stiff Cohesive	24 - 36	Fine sand	0.35 to 0.45
Stiff Cohesive	36 - 45	Fine Sandy Silt	0.30 to 0.35
Very Stiff Cohesive	45 - 62	Medium - Stiff Clay	0.30 to 0.35

Note. From "Foundations and Earth Structures" by Department of the Navy, 1982

2.2.4. Stiffness

The actual soil behavior is nonlinear under cyclic loadings. The magnitude of a cyclic load is generally much smaller than a static load and generally develops shear strains of the level of 10^{-3} to 10^{-6} in a soil. The shear modulus G of the soil varies with the shear strain γ throughout the soil as shown Figure 2.14. It is the highest (i.e., G_{max}) at zero shear strain, but it decreases as the shear strain increases. At very small shear strains (e.g., 10^{-6} to 10^{-4}), the response of the soil is elastic. At these shear strains, the effects of the number of loading cycles and the rate of loading on the soil are negligible and the real behavior of the soil can be represented quite well as that of a linear hysteretic solid. As shear strains develop further, the effects of nonlinearity and inelasticity increase. The soil is then elasto-plastic at intermediate shear strains (e.g., 10^{-4} to 10^{-2}) and it exhibits failure at higher shear strains (e.g., 10^{-2} to 10^{0}) (Priest, 2012; Gazetas, 1991; Kramer, 1996). On the contrary, the damping ratio ζ increases with the increasing shear strain as shown Figure 2.15.

Many empirical and graphical relations can be used to estimate the shear modulus and the damping ratio of a soil. Some of the published data are presented in Figure 2.14 and Figure 2.15. The actual values of the soil properties may only be determined through well-performed laboratory or in-situ tests.

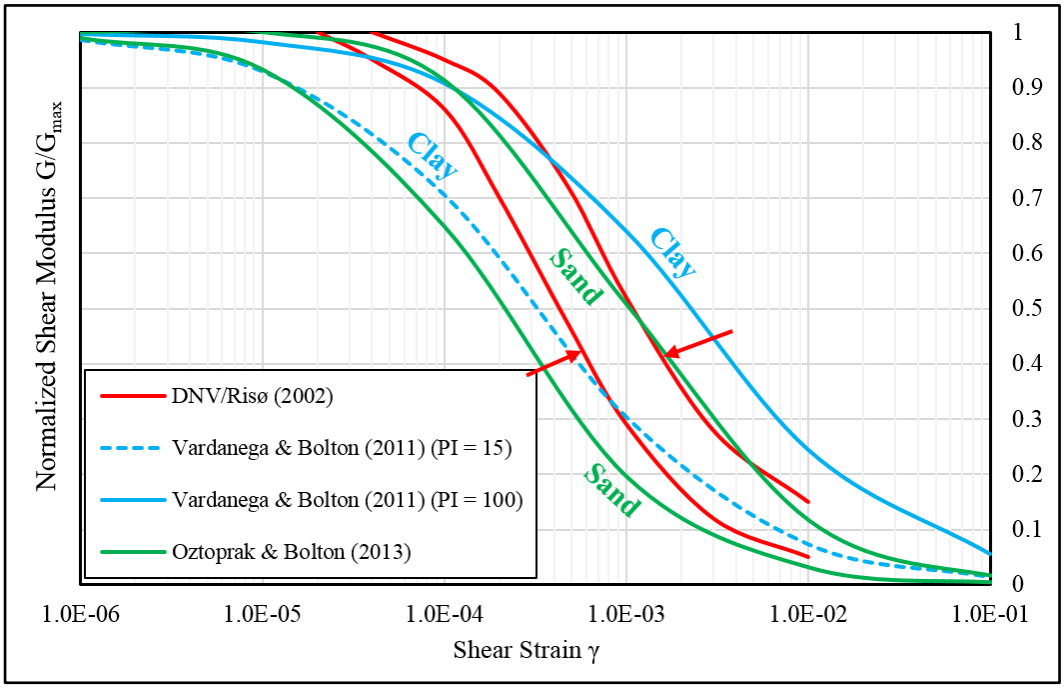

Figure 2.14. G/G_{max} versus γ Curves

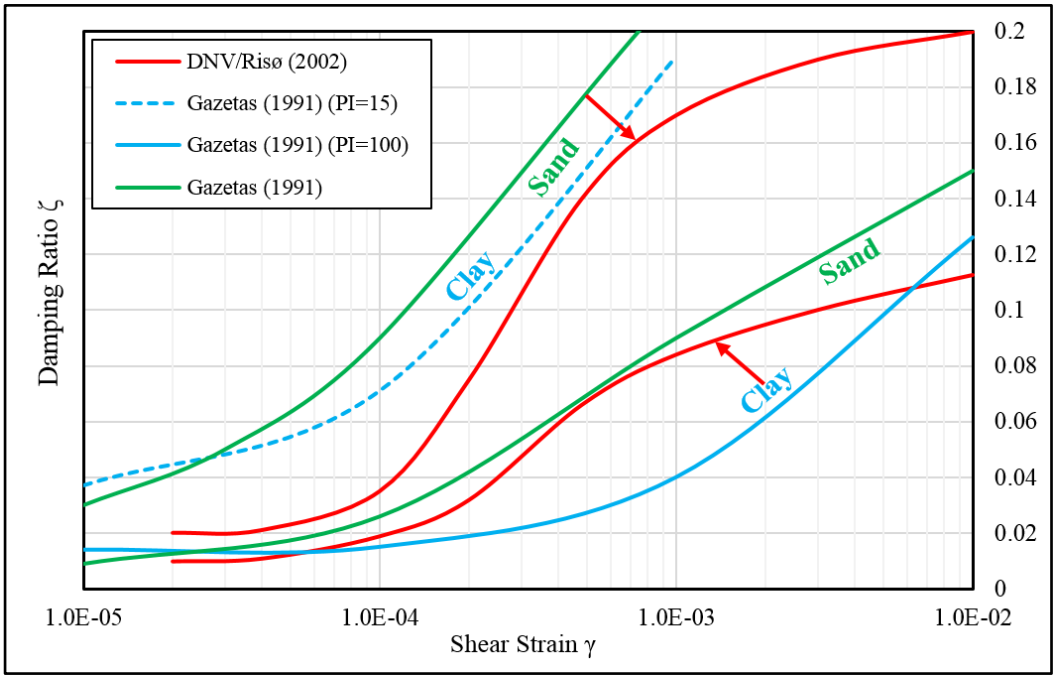

Figure 2.15. ζ versus γ Curves

Some of these tests are convenient to measure soil behavior at low shear strains and others are designed to measure soil behavior at high shear strains. Applicable ranges of dynamic laboratory and in-situ tests are shown in Figure 2.16. The soil properties obtained using very small shear strains may not be well representative for a case in which large shear strains are expected in practice. Therefore, it is important to perform the most suitable test to obtain the soil parameters at expected shear strain levels.

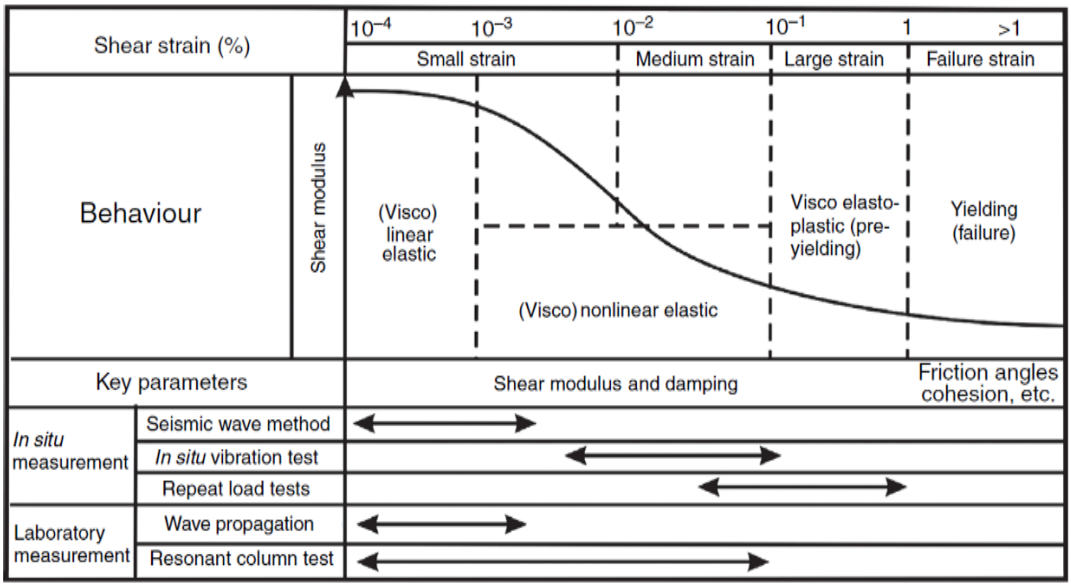

Figure 2.16. Typical Shear Modulus Reduction Curve and Applicable Range of Dynamic Laboratory and In-situ Tests (Priest, 2012)

The equations provided by DNV/RISØ (2002) to calculate the stiffness of a circular foundation are presented in Table 2.7 for three different cases shown in Figure 2.17. The stiffness, which are sets of linear spring constants, are all static stiffness (i.e., stiffness values for frequency approaching zero). The stiffness of any foundation supporting vibratory equipment are frequency-dependent and static stiffness may considerably deviate from dynamic stiffness for high frequencies. However, induced vibrations of wind turbine foundations are of such a nature that static stiffness are representative for dynamic stiffness (DNV/RISØ, 2002).

Table 2.7. *Stiffness Equations for a Circular Foundation*

Case I	Vertical Stiffness	$\frac{4GR}{1-\nu}[1+(32R/25H)]$
	Sliding Stiffness	$\frac{8GR}{2-\nu}[1+(R/2H)]$
	Rocking Stiffness	$\frac{8GR^3}{3(1-\nu)}[1+(R/6H)]$
	Torsional Stiffness	$\frac{16GR^3}{3}$
Case II	Vertical Stiffness	$\frac{4G_1R}{1-\nu_1}\left[\frac{1+(32R/25H)}{1+(32RG_1/25HG_2)}\right]$
	Sliding Stiffness	$\frac{8G_1R}{2-\nu_1}\left[\frac{1+(R/2H)}{1+(RG_1/2HG_2)}\right]$
	Rocking Stiffness	$\frac{8G_1R^3}{3(1-\nu_1)}\left[\frac{1+(R/6H)}{1+(RG_1/6HG_2)}\right]$
	Torsional Stiffness	-
Case III	Vertical Stiffness	$\frac{4GR}{1-\nu}[1+(32R/25H)]\times\left[\left(1+\frac{d_f}{2R}\right)\left(1+\left(0.85-(7\,d_f/25R)\right)\left(\frac{d_f/H}{1-d_f/H}\right)\right)\right]$
	Sliding Stiffness	$\frac{8GR}{2-\nu}[1+(R/6H)][1+(2d_f/3R)][1+(5d_f/4H)]$
	Rocking Stiffness	$\frac{8GR^3}{3(1-\nu)}[1+(R/6H)][1+(2d_f/R)][1+(7d_f/10H)]$
	Torsional Stiffness	$\frac{16GR^3}{3}[1+(8d_f/3R)]$

Although DNV/RISØ (2002) provides the equations to calculate vertical, horizontal and torsional stiffness, they are not generally considered in practice (Tinjum & Christensen, 2011).

The rocking stiffness requirement for the wind turbine foundation mentioned in Table 2.1 is given as an example in Table 2.8.

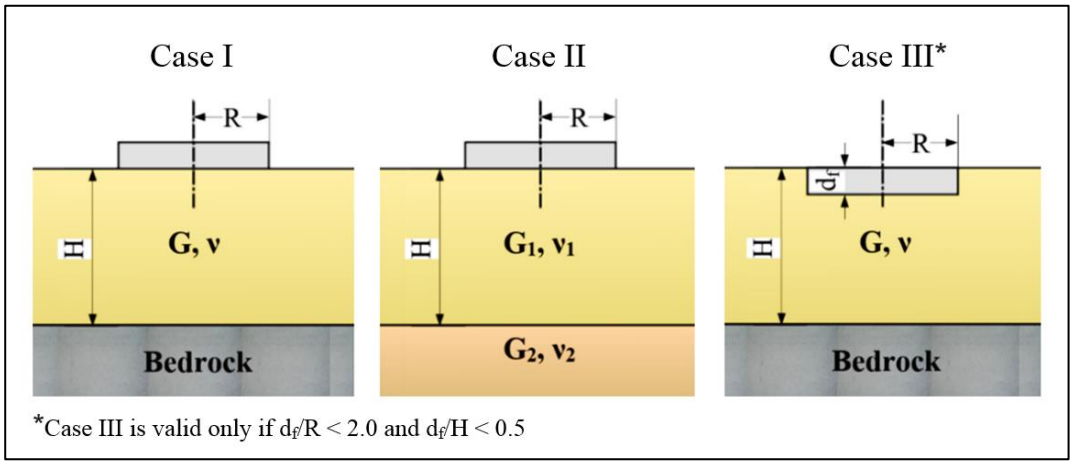

Figure 2.17. Circular Foundation on Stratum over Bedrock or on Stratum over Half-Space or Embedded in Stratum over Bedrock

Table 2.8. *Rocking Stiffness Requirement for a Foundation of ENERCON E48 Turbine (0.8 MW)*

Minimum Static Rocking Stiffness	1,500 [M.Nm/rad]

Note. From "Foundation Data Sheet" by ENERCON GmbH, 2010

2.2.5. Settlement

The settlement may be formed of three components (i) immediate settlement δ_i, (ii) consolidation settlement δ_c and (iii) secondary compression settlement δ_{sc}. One or more of the components may be zero or negligible for any foundation. Although these three components are dependent and cannot be directly added to give a sum, the settlement of a foundation is generally expressed as (Lommler, 2012):

$$\delta = \delta_i + \delta_c + \delta_{sc} \tag{2.33}$$

A foundation may have both short-term settlement and long-term settlement. The settlement in granular soils will generally be dominated by the short-term settlement while the settlement in cohesive soils will generally be dominated by the long-term settlement (Coduto et al., 2015). If a foundation will rest on inorganic soils (e.g., sand

and clay), the secondary compression settlement is very small and it is often ignored in practice (Xiao & Barreto, 2015).

2.2.5.1. Induced Vertical Stresses

The settlement is a function of induced vertical stresses. Boussinesq (1885) developed a well-accepted equation for the induced vertical stress due to a point load in a homogenous, isotropic, elastic half-space. Boussinesq's (1885) equation then was integrated to produce solutions for area loads as shown in Figure 2.18.

The induced vertical stress below the center of a uniformly loaded rectangular area is given by the equation (Das, 2017):

$$\Delta\sigma'_z = \frac{2q'}{\pi}\left[\frac{mn}{\sqrt{1+m^2+n^2}}\left(\frac{1+m^2+n^2}{(1+n^2)(m^2+n^2)}\right) + sin^{-1}\left(\frac{m}{\sqrt{m^2+n^2}\sqrt{1+n^2}}\right)\right] \quad (2.34)$$

where $m = \frac{L}{B}$ and $n = \frac{z}{(B/2)}$

where **q**' is net bearing pressure,

z is depth beneath center of foundation,

L is length of foundation,

B is breadth of foundation.

The induced vertical stress below the center of a uniformly loaded circular area is given by the equation (Das, 2017):

$$\Delta\sigma'_z = q'\left[1 - \frac{z^3}{(R^2+z^2)^{3/2}}\right] \quad (2.35)$$

where **q**' is net bearing pressure,

R is diameter of foundation,

z is depth beneath center of foundation.

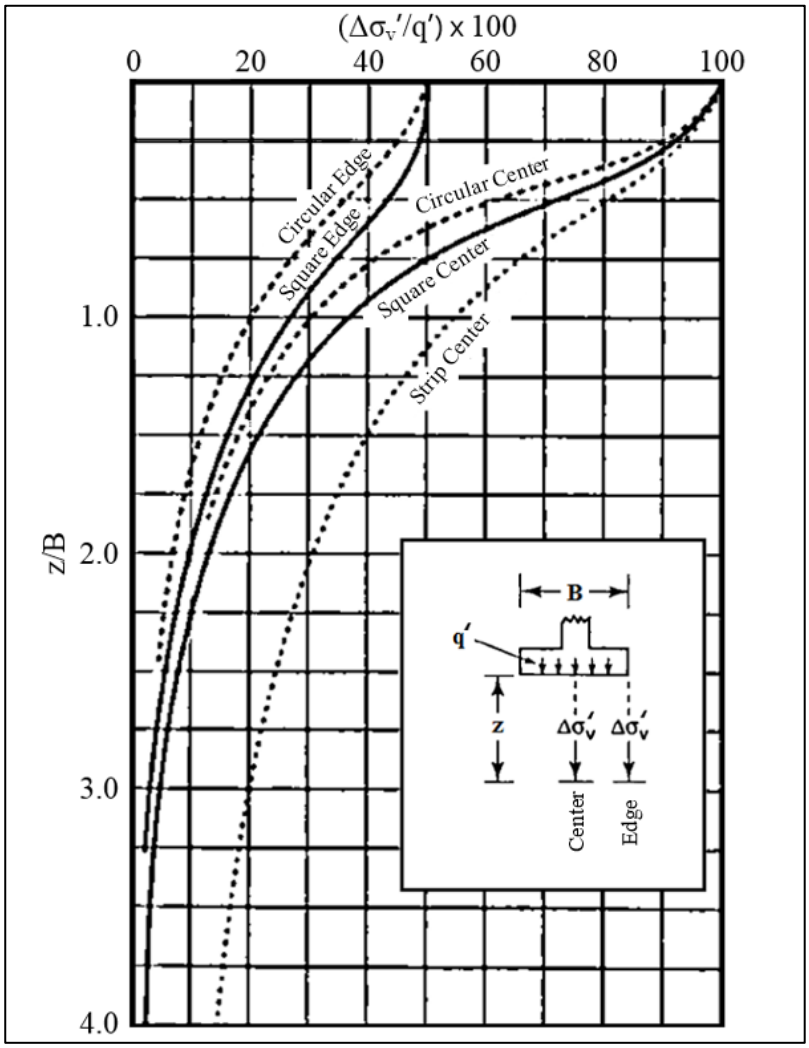

Figure 2.18. Variation of Vertical Stresses with Depth Based on Boussinesq's (1885) Equation

Approximate solutions (e.g., 2V:1H method) and chart solutions (e.g., Newmark's chart for irregular shaped foundations) are other approaches to estimate induced vertical stresses. However, the availability of computers considerably diminished the use of these approaches. In practice, they may only be needed to get a visual sense of how induced stresses are distributed in the soil. If the shape of the foundation is complex (e.g., octagonal), it is necessary to use computer-aided methods (e.g., 2D or 3D FEM) to calculate the settlements.

2.2.5.2. Elastic Settlement

Mayne & Poulos (1999) developed a versatile equation to calculate the settlement by extending Janbu, Bjerrum, & Kjaernsli's (1956) well-known equation as (Coduto et al., 2015):

$$\delta = I_g I_f I_e \frac{q' B_e}{E_0}(1-\nu^2)$$
$$\text{where } B_e = \sqrt{\frac{4BL}{\pi}} \text{ and } \beta = \frac{E_0}{kB_e} \text{ and } E_z = E_0 + kz$$
$$\text{and } I_f = \frac{\pi}{4} + \frac{1}{4.6 + 10\left(\frac{E_f}{E_0 + \frac{kB_e}{2}}\right)\left(\frac{2t}{B_e}\right)^3} \tag{2.36}$$
$$\text{and } I_e = 1 - \frac{1}{3.5\left(1.6 + \frac{B}{d_f}\right)e^{(1.22\nu - 0.4)}}$$

where $\mathbf{I_f}$, $\mathbf{I_e}$, $\mathbf{I_g}$ are influence factors,

$\mathbf{E_0}$ is modulus of soil at depth of foundation base,

$\mathbf{B_e}$ is equivalent circular diameter of foundation,

t is equivalent thickness of foundation,

$\mathbf{E_f}$ is modulus of foundation,

β is normalized modulus,

ν is Poisson's ratio,

$\mathbf{E_s}$ is modulus of soil at depth z below foundation base,

k is increase rate of modulus of soil with depth below foundation base.

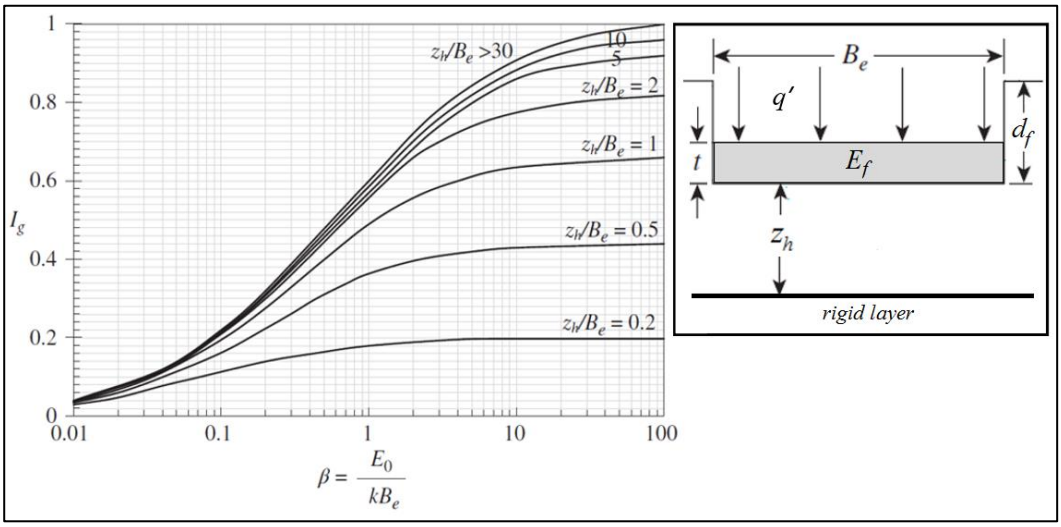

Figure 2.19. Influence Factor I_g for a Circular Foundation

Another simple solution is to decompose the depth of influence into several layers and calculate the settlement of each layer (Briaud, 2013). Then, the settlement can be calculated using the following equation:

$$\delta = \sum_{i=1}^{n} \Delta H_i = \sum_{i=1}^{n} \frac{\Delta\sigma_{vi}}{E_i} H_i \qquad (2.37)$$

where **n** is number of layers within depth of influence,

i refers to i^{th} layer,

$\mathbf{H_i}$ is thickness of i^{th} layer,

$\mathbf{\Delta H_i}$ is settlement of i^{th} layer,

$\mathbf{\Delta\sigma_{vi}}$ is induced vertical stress at midpoint of i^{th} layer.

Marchetti (1997) recommended a similar approach with constrained modulus M instead of Young's modulus E. Marchetti's (1997) equation may be used with any method which can give constrained modulus as a function of depth. Schmertmann (1978) also developed a similar approach with equivalent modulus E_{eq} (or E_s) to

calculate the settlement of the foundation resting on a granular soil considering additional factors for the embedment depth of the foundation, the shape of the foundation and the time. Equivalent modulus is greater than Young's modulus and lower than constrained modulus (Briaud, 2013; Coduto et al., 2015).

2.2.5.3. Consolidation Settlement

To calculate the consolidation settlement, the stress-strain curve should be represented by two lines (i.e., the preconsolidation stress σ'_c is readily apparent) as shown in Figure 2.20.

Consolidation settlement occurs in normally consolidated or lightly overconsolidated clays. Using consolidation approach for highly overconsolidated clays, sands and gravels may be very misleading. Therefore, selecting the most applicable stress-strain curve to link the stress increment to the strain increment requires good engineering judgment (Coduto et al., 2015).

For normally consolidated soils (i.e., $\sigma'_{z0} = \sigma'_c$), the settlement is calculated as:

$$\delta = \sum_{i=1}^{n} \left(\frac{c_c}{1+e_0}\right) H_i \log\left(\frac{\sigma'_{zfi}}{\sigma'_{z0i}}\right) \tag{2.38}$$

For overconsolidated soils (i.e., $\sigma'_{zf} < \sigma'_c$), the settlement is calculated as:

$$\delta = \sum_{i=1}^{n} \left(\frac{c_r}{1+e_0}\right) H_i \log\left(\frac{\sigma'_{zfi}}{\sigma'_{z0i}}\right) \tag{2.39}$$

For overconsolidated soils (i.e., $\sigma'_{zf} > \sigma'_c$), the settlement is calculated as:

$$\delta = \sum_{i=1}^{n} \left[\left(\frac{c_r}{1+e_0}\right) H_i \log\left(\frac{\sigma'_{ci}}{\sigma'_{z0i}}\right) + \left(\frac{c_c}{1+e_0}\right) H_i \log\left(\frac{\sigma'_{zfi}}{\sigma'_{ci}}\right)\right] \tag{2.40}$$

where $\sigma'_{ci} = \sigma'_{z0i} + \sigma'_m$

where **n** is total number of layers considered,

$\mathbf{c_r}$ is recompression index,

$\mathbf{c_c}$ is compression index,

$\mathbf{e_0}$ is initial void ratio,

$\mathbf{H_i}$ is thickness of i^{th} layer,

$\mathbf{\sigma'_{z0i}}$ is initial vertical effective stress at midpoint of i^{th} layer,

$\mathbf{\sigma'_{zfi}}$ is final vertical effective stress at midpoint of i^{th} layer,

$\mathbf{\sigma'_{ci}}$ is preconsolidation stress at midpoint of i^{th} layer,

$\mathbf{\sigma'_{m}}$ is overconsolidation margin.

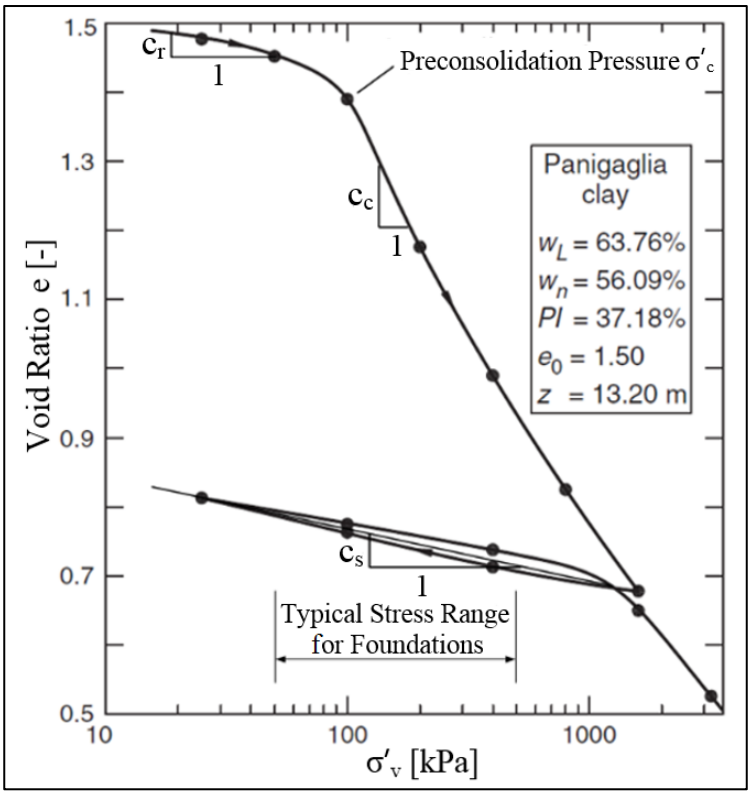

Figure 2.20. Typical Stress-Strain Curve Appropriate for Consolidation Approach

The calculations that use a large number of thin layers obviously provide more precise results than those that use a few number of thick layers. However, this is too laborious to do by hand. Therefore, FEM is generally the most efficient way to calculate the settlement.

In both elastic and consolidation approaches, the settlement is considered either for the depth at which the stress increase in the soil has decreased to ~15% of the stress increase at foundation base or where there is an underlying firm layer with negligible compressibility (Tinjum & Christensen, 2011; Xiao & Barreto, 2015).

Finally, the settlement is usually not a major concern for a wind turbine foundation since the permanent normal force is relatively light and wind turbines are not constructed on weak soils without doing ground improvement. The soils that have adequate bearing capacity and rocking stiffness usually settle less than 2.5 cm since the bearing pressure is quite low (e.g., about 50 - 75 kPa) (Tinjum & Christensen, 2011).

2.2.6. Rotation (Tilt)

The rotation of a wind turbine foundation due to the differential settlement within 20 - 25 years should be estimated. The differential settlement is more troublesome than total settlement because if the differential settlement is allowed and it progresses to an extreme value, the integrity of the wind turbine will be in great danger. Since wind turbine foundations are designed assuming rigid behavior, a uniform rotation where the entire foundation rotates can be calculated once the displacements under the edges of the foundation are obtained.

If total and differential settlement limits are absent, an allowable differential settlement approximately 3 mm/m to 4.5 mm/m is usually acceptable (ASCE/AWEA, 2011; Ntambakwa et al., 2016). The differential settlement of the foundation as much

as 40 mm is also a tolerable differential settlement when there is an absence of differential settlement limit (Grünberg & Göhlmann, 2013).

Design codes for wind turbines (e.g., DNV/RISØ (2002)) provide significant guidance for defining requirements for ultimate states (e.g., bearing capacity, stability). However, very little guidance is provided for serviceable limit states (e.g., settlement, rotation) because a serviceability limit is immensely dependent upon the type and use of a particular wind turbine in a particular location for a particular soil condition. Moreover, the purpose of a design code is to assure the public safety not to prevent the monetary losses of owners or turbine manufacturers. Therefore, the serviceability requirements for a wind turbine foundation may only be determined through good communication between the turbine manufacturer and the geotechnical engineer.

2.3. Previous Studies on the Topic

2.3.1. Theoretical Studies

Morgan & Ntambakwa (2008) briefly discussed geotechnical and structural design of wind turbine gravity base foundations including stiffness, differential settlement, stability, bearing capacity, internal forces in a foundation and bearing stresses in the flange of a tower base. The authors also evaluated the effects of growing size of wind turbines on each sub-topic mentioned.

Tinjum & Christensen (2011) reviewed geotechnical investigation methods, geotechnical design parameters and geotechnical design of wind turbine gravity base foundations including bearing capacity, settlement, sliding and stiffness. Geotechnical design considerations of access roads, crane pads and collector trenches were also briefly discussed.

Warren-Codrington (2013) discussed almost every aspect of onshore wind turbines including the mechanics and dynamics of the supporting systems of wind turbines, geotechnical design of wind turbine gravity base foundations, a discussion of the

foundations under dynamic loadings and geotechnical design of wind turbine gravity base foundations resting on pedocretes.

Mawer (2015) presented a discussion of geotechnical design of wind turbine gravity base foundations including the mechanics of a wind turbine and its supporting systems. To address the each phase of the geotechnical design discussed, the author selected three representative wind turbine sites and used them as practical design examples.

Ntambakwa et al. (2016) presented a discussion of geotechnical design and construction of wind turbine gravity base foundations including geotechnical investigation methods, geotechnical hazard evaluation, stability, stiffness, bearing capacity and differential settlement. The authors also evaluated the merits and limitations of the design methods with an example to evaluate the ASD method versus the LRFD method considering only the bearing capacity criteria.

2.3.2. Numerical Studies

Branca & Ben-Hassine (2009) focused on the dynamic modeling of a wind turbine, tower and foundation system. The authors modeled a wind turbine and tower under infinitely rigid support conditions using a finite element method software. The natural frequencies were obtained and compared with the data provided by the turbine manufacturer. The wind turbine, tower and foundation system then was broken down into pieces in order to calculate the mass moment of inertia of the system about the foundation base for rocking motion and about the vertical axis for torsional motion. The spring constants and damping ratio were calculated using the equations for a rigid circular foundation on an elastic half-space. The rigid supports were then replaced with the supports with finite stiffness and damping ratios. The natural frequencies were obtained again and compared with the data provided by the turbine manufacturer. Finally, the transient wind loads provided by the manufacturer were applied and the liquefaction potential was briefly evaluated.

Szerző (2012) compared the different foundation types for variable soil and loading conditions using hand calculations and the Group software. Two different foundation types, which are gravity base and piled raft, resting on four different soil conditions were examined. Five sets of design loads and two design criteria, which are bearing capacity and gapping, were considered for each case. The conclusion of the study was that gravity base foundations are suitable for competent soils (e.g., stiff clay) and moderate design loads. However, extreme design loads or soils with inadequate strength properties (e.g., soft clay over bedrock) generally necessitate the use of piled raft foundations.

Pasten et al. (2013) proposed a numerical scheme to analyze the long-term response to cyclic loading of foundations resting on granular soils. The study involved the modified Cam clay model to analyze the static load and the first load cycle and empirical strain accumulation functions to estimate the vibratory compaction during the cyclic loading. The algorithm consisted of four modules. Firstly, the stress field induced by the static loading were computed using Modified Cam-Clay model. The authors noted that constitutive models with irreducible plastic potentials during unloading are not suitable to simulate strain accumulation. Secondly, the first load cycle was computed using the same constitutive model. Thirdly, the accumulated volumetric and shear strains during cyclic loading were calculated using the empirical strain accumulation functions. Fourthly, the compatibility and equilibrium conditions were satisfied. The authors used the ABAQUS software and calibrated the model by using the published triaxial test results. The proposed numerical scheme was implemented considering two examples (i) a flexible foundation subjected to concentric cyclic loading and (ii) a wind turbine foundation subjected to cyclic eccentric loading considering rigid foundation behavior. The results of the implementation of the second case as shown in Figure 2.21 and Figure 2.22 showed that (i) the cyclic force causes settlement and rotation, (ii) vertical displacement, horizontal displacement and rotation increase as the factor of safety decreases and the

amplitude of cyclic force increases and (iii) settlement and rotation may advance with increasing load cycles until the soil approaches its terminal void ratio.

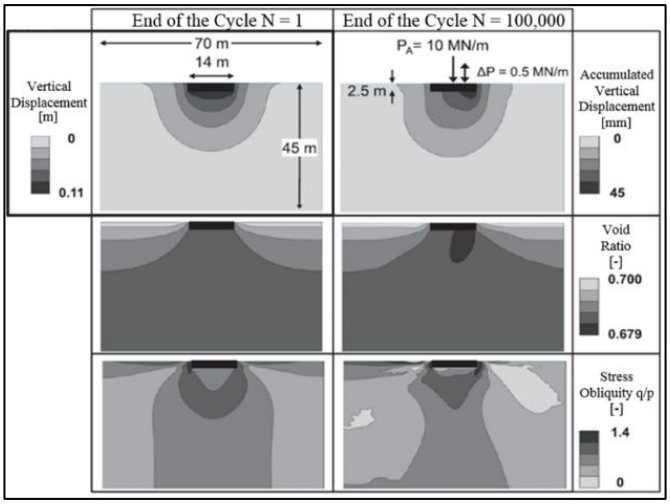

Figure 2.21. Vertical Displacement, Distribution of Void Ratio and Stress Obliquity for Load Cycles N=1 and N=100,000

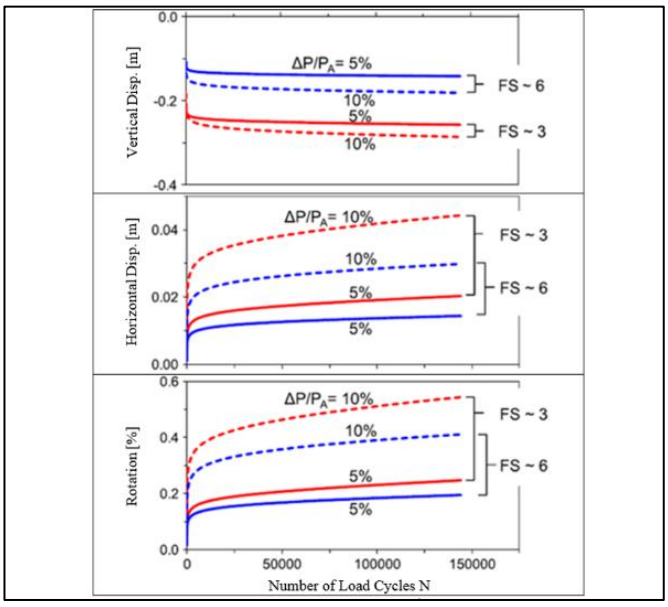

Figure 2.22. Vertical and Horizontal Displacements at the Center of the Foundation Base and Rotation for Static Loads P_A=20 kN/m, P_A=10 kN/m and Cyclic Load

Li et al. (2014) simulated the wind loading acting on a wind turbine foundation. The authors used the collected wind statistical data over the past 50 years to make the wind velocity spectrum. The time series of fluctuating wind velocity were simulated using Harmony Superposition Method. A multi-particle mass-spring-damper system with seven point masses for the upper structure was used. Three blades of the wind turbine were modeled as three and the tower as four point masses. Seven wind loading data were applied to each point mass at the same time and the dynamic responses (e.g., bending moment time series) on the foundation were computed. The soil was then modeled and simulated using the ABAQUS software to compute the settlement and rotation of the foundation for three consecutive loading cycles.

Xu et al. (2015) examined fifteen models of foundations of three different shapes, which are five circular, five hexagonal and five triangular, with assigning five different ratios of foundation width to foundation height for each shape. The authors analyzed the models using the ANSYS software and observed that if the ratios of foundation width to foundation height increase, factors of safety for bearing capacity, overturning and sliding increase irrespective of the foundation shape. Circular and hexagon foundations performed almost identically and better than triangular foundations as expected.

2.3.3. Experimental Studies

Yilmaz (2014) collected and analyzed the field data from two wind turbine sites. The foundations were instrumented with strain and pressure gauges prior to construction. The towers were also instrumented with strain gauges. The author monitored soil deformations and bearing pressure distributions beneath the foundation and moments at the tower base for the selected site.

Madaschi et al. (2016) described an experimental analysis on the dynamic behavior of a foundation consisting of a square plinth resting on a coarse granular soil. The tower, which supports a wind turbine with rated power of 11 kW, was subjected to five snap-

off tests. The displacements of the tower, the accelerations of the tower and foundation, and the velocity of the ground surface surrounding the foundation were monitored during the free vibrations of the wind turbine system. After describing the recorded measurements, a kinematic analysis of the response recorded at the top of the tower was conducted to identify the relationship describing how the frequency and damping rate depended on the vibration amplitude. A nonlinear equivalent mechanical model of the structure-soil system was then defined. The results showed that (i) the rocking stiffness of the foundation slightly decreases with the increasing rotation of the foundation as expected, (ii) the rocking stiffness of the foundation depends only on the rotation of the foundation and fairly independent of the initial pulling force applied during the snap-off tests and (iiih) the rocking stiffness of the foundation has negligible effects on the response of the tower (i.e., the vibration of the tower and the rocking vibration of the foundation are decoupled). The authors also analyzed the attenuation of the velocity at the ground surface around the foundation.

CHAPTER 3

A CASE STUDY

3.1. General Information

A wind turbine foundation shown in Figure 3.1, which was formerly studied by Yılmaz (2014), was analyzed using analytical method with Monte Carlo simulation and 3D FEM. Yılmaz's (2014) research was to measure and interpret the contact pressure distribution and the soil strain data collected beneath the wind turbine foundation constructed in Wisconsin, USA. The site was instrumented prior to the construction. The instruments were installed into the soil beneath the foundation and on the interior wall of the tower. Data relating to the contact pressure distribution and the soil strain were recorded at different times between 2013 and 2014.

Figure 3.1. The Wind Turbine Foundation Constructed for the Project

3.2. Project Information

Vensys 82 direct drive turbine was preferred for the site. The brief information about the turbine is listed in Table 3.1.

Table 3.1. *Information about Vensys 82 Turbine (1.5 MW)*

Characteristic	Value	Unit
Nominal Power	1.5	MW
Rotor Diameter	82.3	m
Hub Height	85	m
Nacelle and Rotor Weight	95,000	kg
Start-up, Nominal, Maximum Wind Speeds	2.5, 13, 22.5	m/s

Note. "Technical Data" by Vensys Energy AG, 2010
"Wind Turbine Technology Principles and Design" by Adaramola, 2014

The wind rose for the site is shown in Figure 3.2. The wind data showed that westerly winds blow frequently during a year. Therefore, westerly wind was chosen as the predominant wind direction and the instrumentation layout was aligned accordingly.

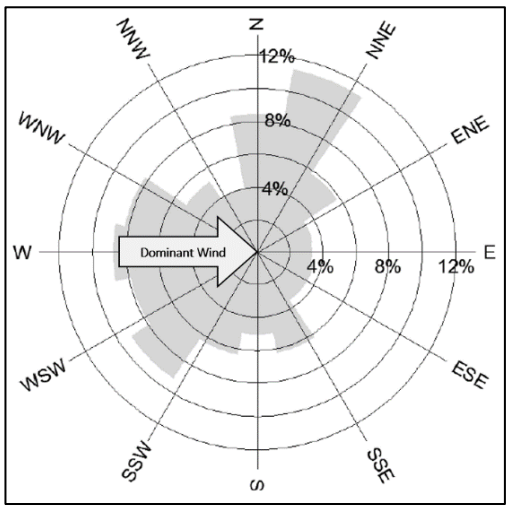

Figure 3.2. The Wind Rose for the Site

The unfactored loads and moments provided by the turbine manufacturer are given in Table 3.2.

Table 3.2. *Unfactored Loads and Moments Provided for Vensys 82 Turbine (1.5 MW capacity)*

Unfactored Load or Moment	Value	Unit
Vertical Load V	2,269.1	kN
Horizontal Load H	667.4	kN
Overturning Moment M	47,736.0	kN.m

An octagonal foundation was designed. The dimensions of the foundation is shown in Figure 3.3. The embedment of the foundation is 3.05 m below the ground surface.

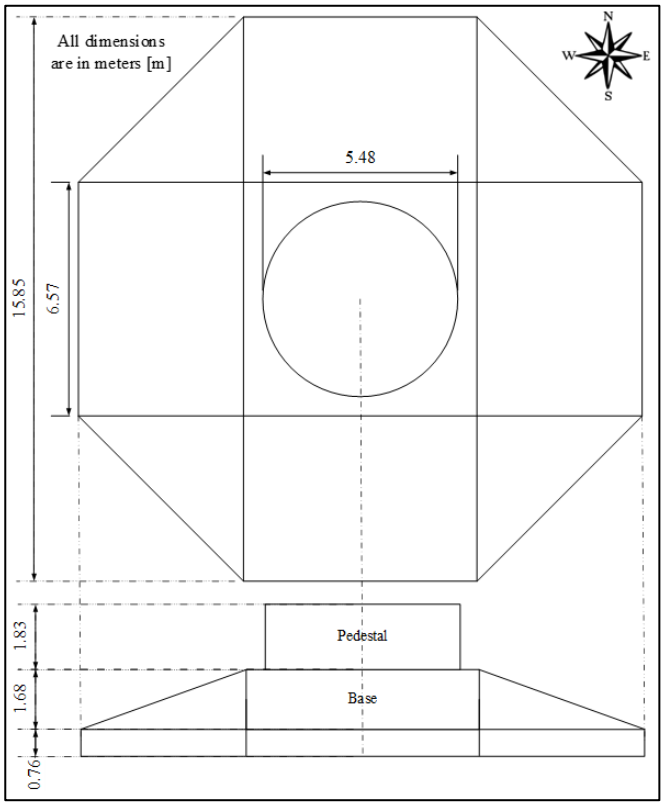

Figure 3.3. The Dimensions of the Foundation

Nine earth pressure cells and ten soil deformation meters were installed beneath the foundation. The instrument layout was employed considering the predominant wind direction obtained using the wind rose for the site. Five of the earth pressure cells were installed along the predominant wind direction and four pressure cells were located at different locations from the center of the foundation and along the lines 70^{o} from the predominant wind direction. Eight soil deformation meters were installed along the predominant wind direction at different depths and two soil deformation meters have been located along the line perpendicular to the predominant wind direction. Top and sectional views of the instrumentation layout for the site is shown in Figure 3.4 and Figure 3.5, respectively.

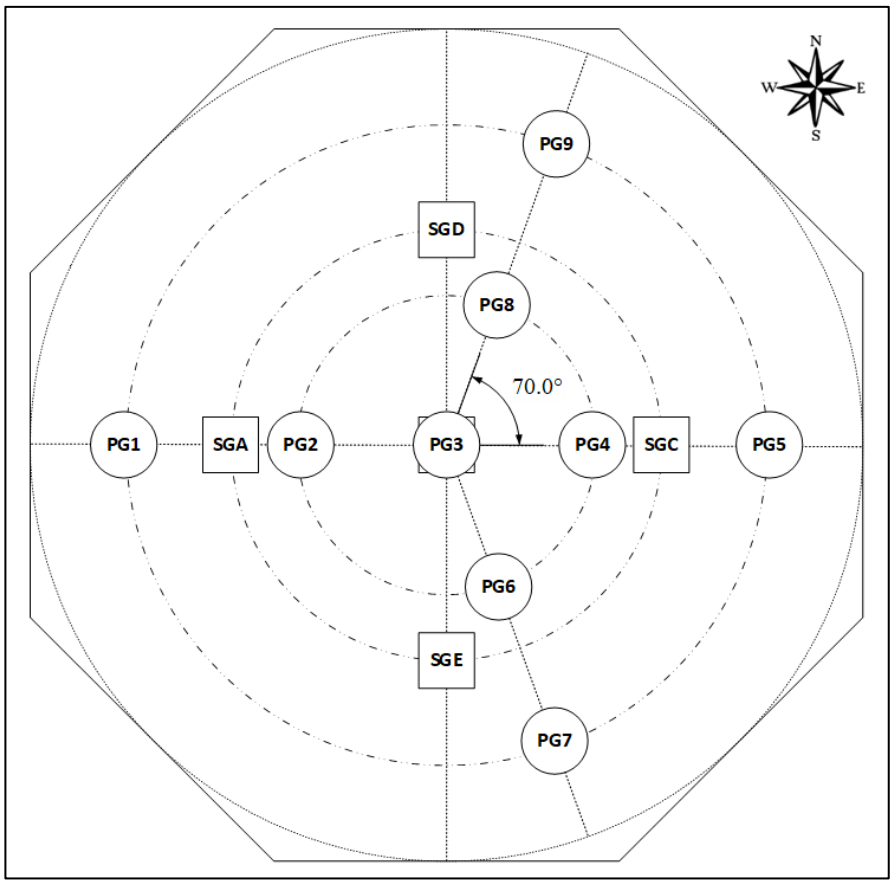

Figure 3.4. Top View of the Instrumentation Layout

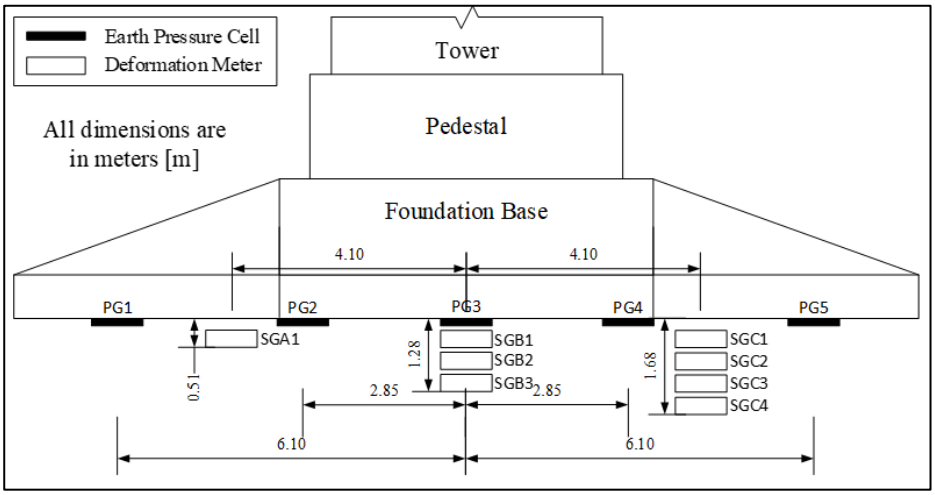

Figure 3.5. Sectional View of the Instrumentation Layout

The settlements along the predominant wind direction is shown in Figure 3.6.a. It can be observed that the settlements were highly correlated with the predominant wind direction. All settlements are presented on the same plot in Figure 3.6.b. Soil deformation meters in borehole C and E showed the highest deformation due to incipient wind direction, as expected.

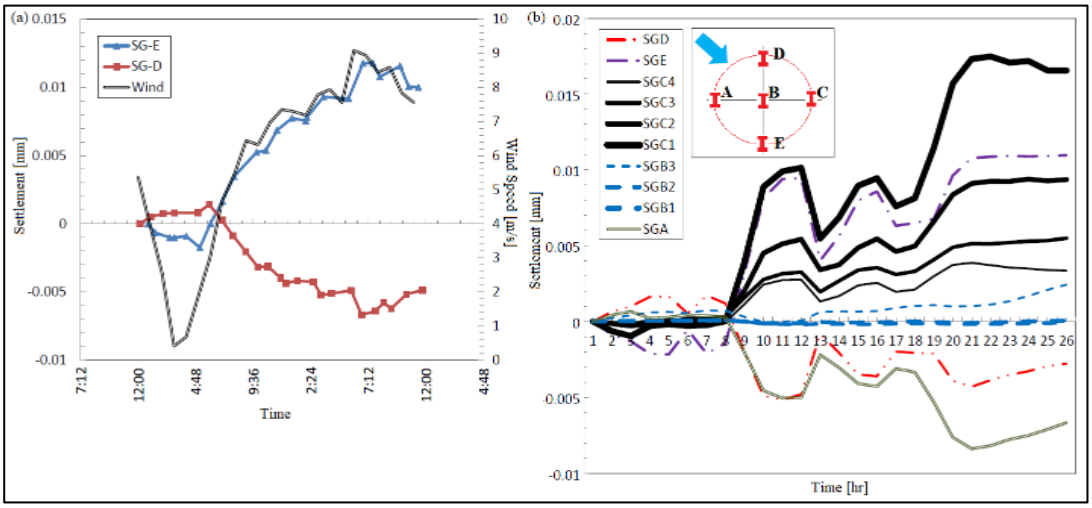

Figure 3.6. The Soil Deformations Recorded at Different Times in 2013 and 2014 (Yılmaz, 2014)

3.3. Soil Information

Prior to the construction, three soil borings were advanced. Standard Penetration Tests (SPTs) were performed from the ground surface to the depth of 15.2 m. Soil samples were collected along with the SPTs. The majority of the soil beneath the foundation was either lean clay (low plasticity clay) or silty clay (Yılmaz, 2014).

3.3.1. Index Properties of the Soil

One uniform soil layer was considered and it was classified as lean clay. The properties obtained using the laboratory experiments are presented in Table 3.3 (Yılmaz, 2014).

Some of the remaining properties can be calculated by using the simple soil phase relationships. Since the depth of the ground water table is 2.08 m below the ground surface, fully saturated condition can be considered for the phase relationships. The results of the calculations are presented in Table 3.4.

Table 3.3. *Soil Properties Obtained by Using the Laboratory Experiments (Yılmaz, 2014)*

Property	Value	Unit
Classification	CL	-
Liquid Limit LL	23	-
Plastic Limit PL	11	-
Specific Weight G_s	2.7	-
Bulk Density ρ_b	2.125	g/cm^3
Dry Density ρ_{dry}	1.897	g/cm^3
Water Content w	12%	-
Dry Unit Weight γ_{dry}	18.42	kN/m^3

Table 3.4. *Soil Properties Calculated by Using the Available Properties*

Property	Value	Unit
Plasticity Index PI	12	-
Liquidity Index LI	0.08	-
Initial Void Ratio e_0	0.324	-
Total Unit Weight γ_{tot}	22.95	kN/m^3

3.3.2. Strength Properties of the Soil

Undrained Shear Strength

The change of SPT-N values with depth is shown in Figure 3.7. It can be observed that the SPT-N values are mainly ranging from 10 to 30.

In the literature, there are various correlations to obtain undrained shear strength of clay soil. The correlations proposing a relation between SPT-N value and undrained shear strength or effective overburden pressure σ'_{v0} and undrained shear strength were used in this study to estimate the undrained shear strength of the soil.

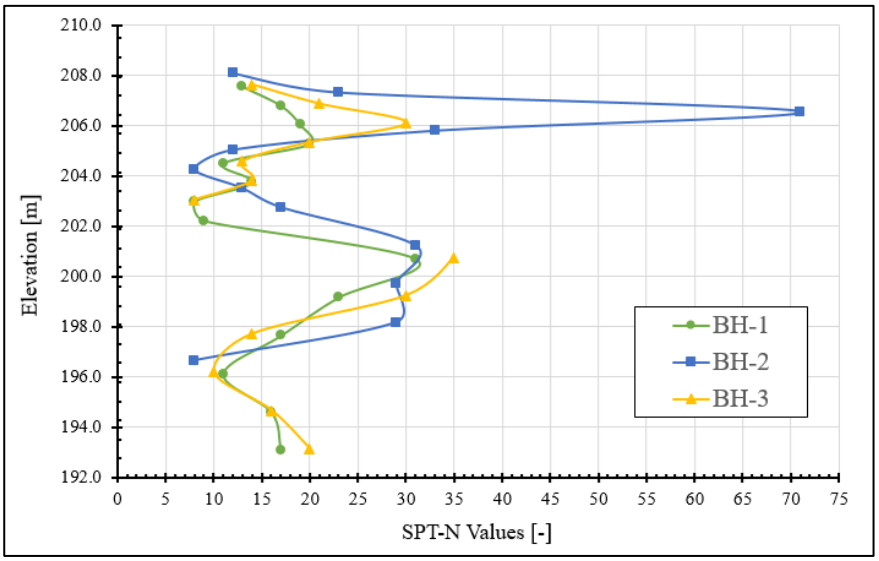

Figure 3.7. The Change in SPT-N Values with Depth

Hara et al. (1971) and Kulhawy & Mayne (1990) proposed the following relation between SPT-N_{60} value and undrained shear strength:

$$\frac{c_u}{P_a} = 0.29 \times {N_{60}}^{0.72} \tag{3.1}$$

where $\mathbf{P_a}$ is atmospheric pressure and generally taken as 100 kPa.

Stroud (1975) provided the following relation for clays:

$$\frac{c_u}{P_a} = \alpha \times N \tag{3.2}$$

Salgado (2008) modified Stroud's (1975) equation as:

$$\frac{c_u}{P_a} = \alpha' \times N_{60} \tag{3.3}$$

where $\boldsymbol{\alpha'}$ is a value interpolated with plasticity index.

Table 3.5. *Variation of α' with Plasticity Index*

Plasticity Index	**α'**
15	0.068
20	0.055
25	0.048
30	0.045
40	0.044
60	0.043

Skempton (1957) suggested the following relation for normally consolidated clays:

$$\left(\frac{c_u}{{\sigma'}_{v0}}\right)_{NC} = 0.0037\text{PI} + 0.11 \tag{3.4}$$

The c_u/σ'_{v0} ratio is larger and increases with overconsolidation ratio (Ameratunga et al., 2016).

Ladd et al. (1977) proposed the following relation by using overconsolidation ratio:

$$\left(\frac{c_u}{\sigma'_{v0}}\right)_{OC} = \left(\frac{c_u}{\sigma'_{v0}}\right)_{NC} \times \mathrm{OCR}^{0.8} \tag{3.5}$$

Correspondingly, Mayne & Kemper (1988) proposed the following relation to calculate OCR:

$$OCR = 0.193 \times \left(\frac{N}{\sigma'_{v0}\ [\mathrm{MPa}]}\right)^{0.689} \tag{3.6}$$

Jamiolkowski et al. (1985) suggested the following equation:

$$\left(\frac{c_u}{\sigma'_c}\right)_{OC} = 0.23 \pm 0.04 \tag{3.7}$$

Mesri (1989) provided the following equation:

$$\frac{c_u}{\sigma'_c} = 0.22 \tag{3.8}$$

Nonlinear relations between undrained shear strength, overburden pressure and SPT-N value can be obtained by combining the equations proposed by Hara et al. (1971), Ladd et al. (1977), Jamiolkowski et al. (1985) and Mesri (1989).

Undrained strength values (i.e., BH1, BH2 and BH3) obtained by using the available unconfined compressive strength Q_u values and the ones obtained by using the aforementioned nonlinear relations are presented in Figure 3.8. Average values presented here are the average of the values obtained by using the nonlinear relations only. The Estimation curve shown in Figure 3.8 and Figure 3.9 was plotted to get a linear relation between undrained shear strength and depth. The Average curve shown

in Figure 3.9 is the average of the Average of BHs curve and the Average of Nonlinear Relations curve.

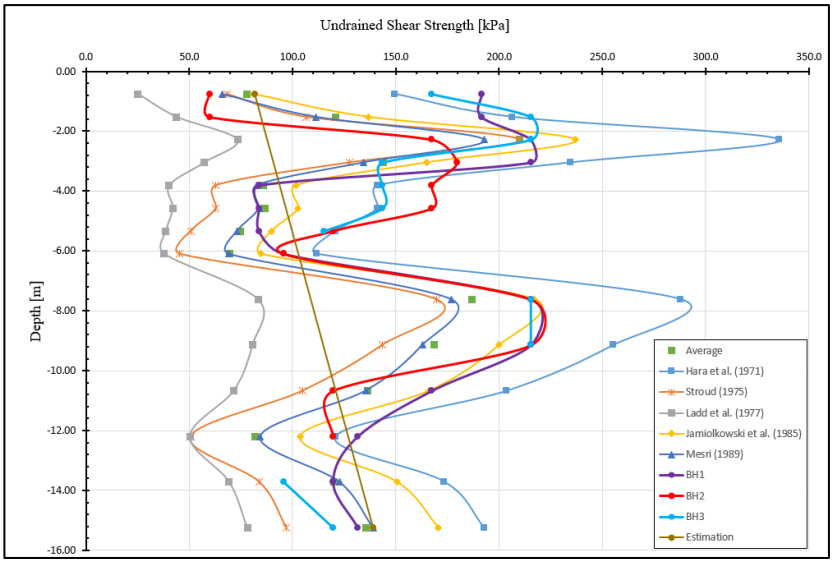

Figure 3.8. Undrained Shear Strength Values Obtained by Using Various Nonlinear Relations

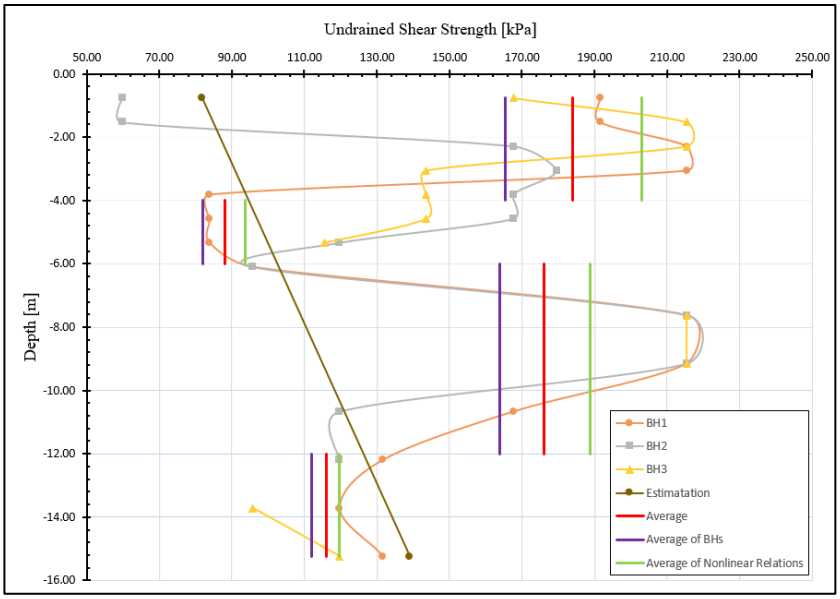

Figure 3.9. Undrained Shear Strength Values Obtained by Using Unconfined Compressive Strengths and Average Values Obtained by Using Various Relations

Undrained Young's Modulus

Undrained Young's modulus E_u of clays is generally obtained by using an appropriate value of the E_u/c_u ratio (Ameratunga et al., 2016). The E_u/c_u ratio is strain dependent and reduced by increasing strain. This is shown in Figure 3.10 plotted by Jardine et al. (1985) (Tomlinson & Woodward, 2015).

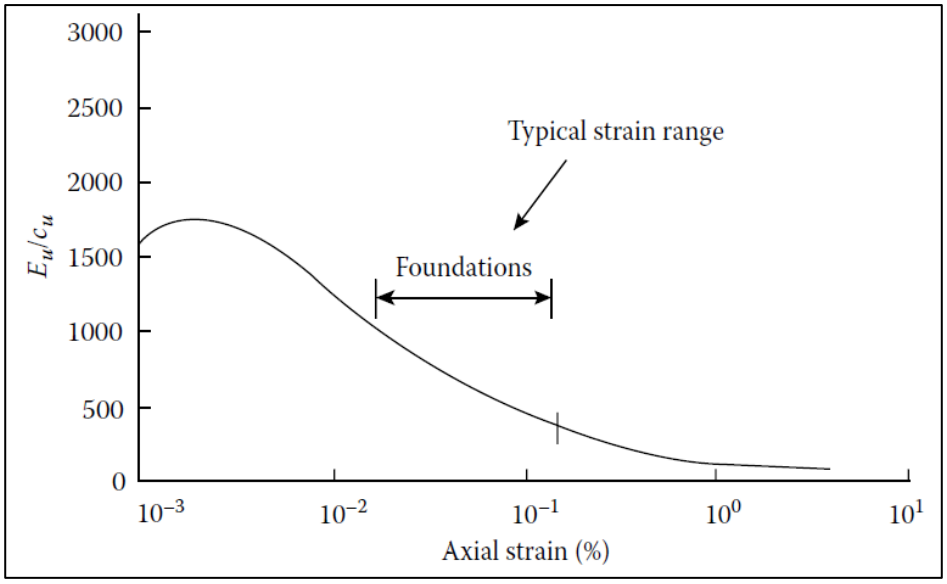

Figure 3.10. The Relationship between E_u/c_u Ratio and Axial Strain (Jardine et al., 1985)

The E_u/c_u ratio is in the order of 1000 for typical building foundations as shown in Figure 3.10. However, the permanent vertical load is relatively light for wind turbines. Therefore, the E_u/c_u ratio is expected to be greater than 1000.

CIRIA (1995) proposed data for undrained Young's modulus of very soft clays to clay shale. Table 3.6 presented these data. E_u/SPT-N ratio is expected to be between 6.3 MPa to 10.4 MPa for clays.

Table 3.6. *Undrained Young's Modulus of Clays*

Clay	Undrained Young's Modulus [MPa]
Very Soft Clay	0.5 - 5
Soft Clay	5 - 20
Medium Clay	20 - 50
Stiff Clay	50 - 100
Sandy Clay	25 - 200
Clay Shale	100 - 200

Duncan & Buchignani (1976) presented the variation of E_u/c_u ratio with plasticity index and overconsolidation ratio as shown in Figure 3.11. The E_u/c_u ratio can be estimated 1000 for plasticity index of 12.

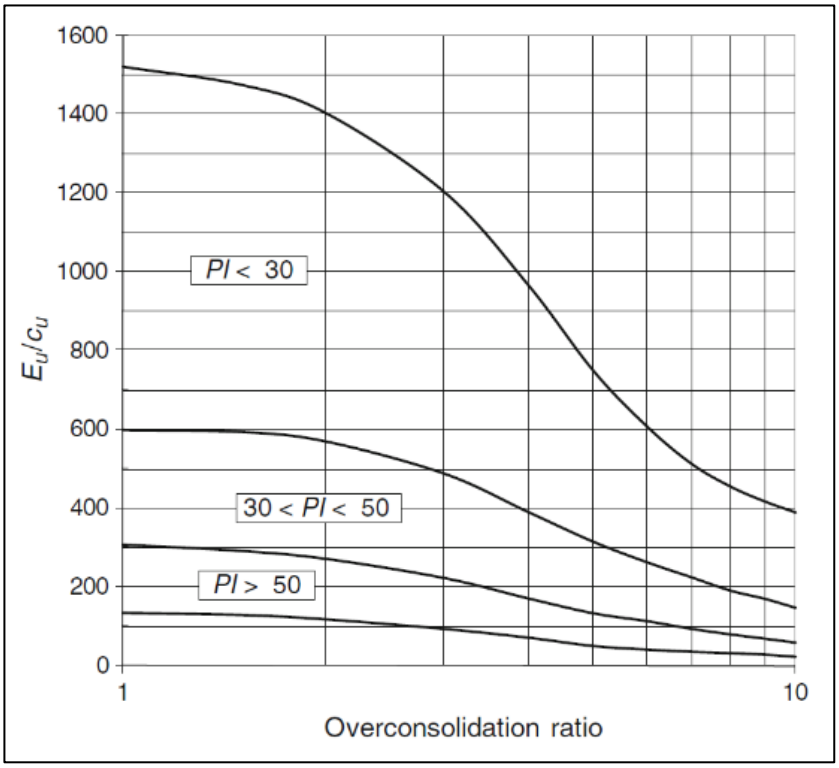

Figure 3.11. E_u/c_u Ratio, Plasticity Index and Overconsolidaton Ratio for Clays (Duncan & Buchignani, 1976)

Poulos & Small (2000) showed the variation of undrained Young's modulus with SPT-N value and plasticity index as shown in Figure 3.12.

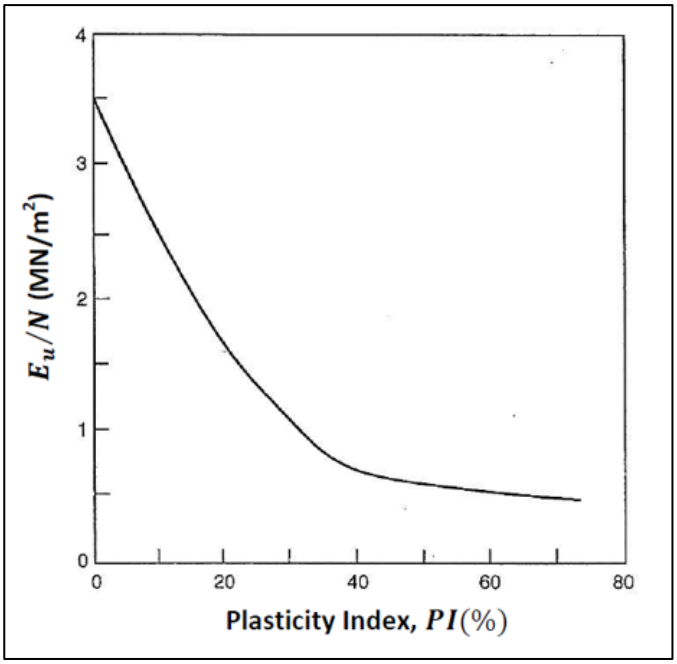

Figure 3.12. The Relationship between E_u/SPT-N Ratio and Plasticity Index (Poulos & Small, 2000)

The lowest undrained Young's modulus estimate was obtained by using the curve based on Poulos & Small (2000) and the highest undrained Young's modulus estimate was obtained by using the table based on CIRIA (1995).

Undrained Young's modulus values obtained by using various relations are shown in Figure 3.11. The Estimation curve shown in Figure 3.11 was plotted to get a linear relation between undrained Young's modulus and depth.

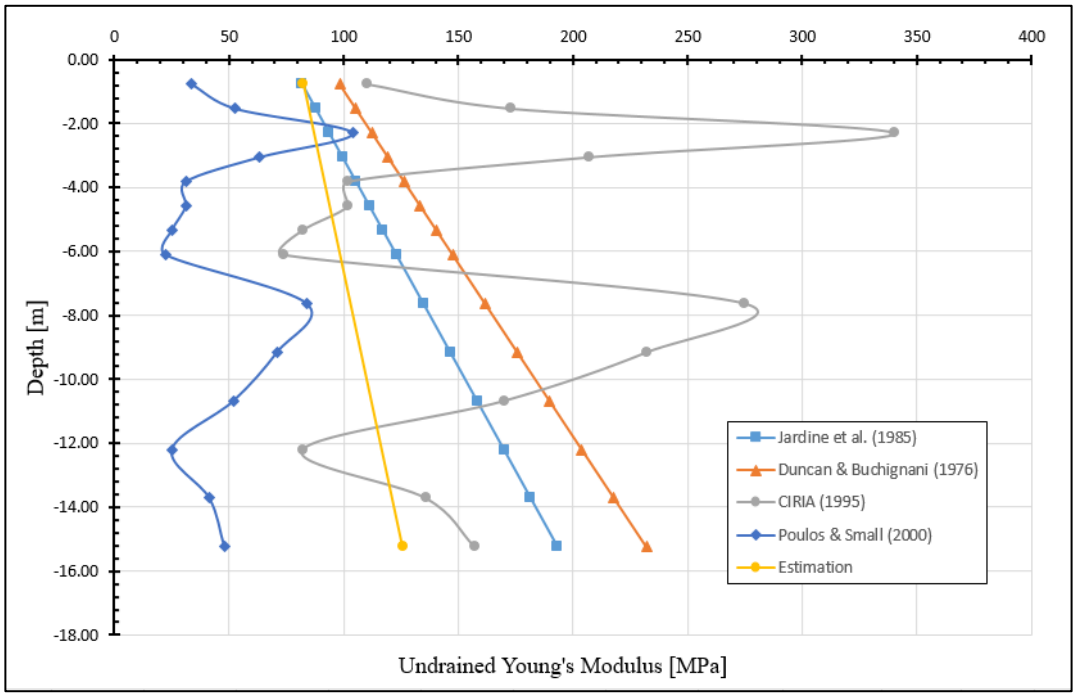

Figure 3.13. The Undrained Young's Modulus Values Obtained Using Various Relations

Poisson's Ratio

Lambe & Whitman (1979), Kulhawy & Mayne (1990) and Bowles (2001) suggested that undrained Poisson's ratio ν_u for saturated clays can be taken as 0.5 and drained Poisson's ratio ν_d can be taken as 0.2-0.4.

Drained Young's Modulus

The following relationship between drained Young's modulus and undrained Young's modulus can be used:

$$E_d = E_u \left(\frac{1 + \nu_d}{1 + \nu_u} \right) \tag{3.9}$$

where $\boldsymbol{\nu_d}$ is drained Poisson's ratio,

ν_u is undrained Poisson's ratio

Table 3.7 presents the results based on the average of SPT-N values SPT-N_{ave} and aforementioned nonlinear relations. Average undrained shear strength $c_{u,ave}$ and average undrained Young's modulus $E_{u,ave}$ were calculated by using Estimation curve in Figure 3.8 and Figure 3.11, respectively. $E_{u,ave}$ was then used to calculate average drained Young's modulus $E_{d,ave}$.

Table 3.7. *The Results Based on the Average of SPT-N Values and Nonlinear Relations*

z [m]	SPT-N_{ave}	SPT-N_{60ave}	σ_v [kPa]	u [kPa]	σ'_v [kPa]	$c_{u,ave}$ [kPa]	$E_{u,ave}$ [MPa]	$E_{d,ave}$ [MPa]
0.76	13	10	14	0	14	82	82	69
1.52	20	15	28	0	28	88	85	71
2.29	40	30	43	2	41	94	87	73
3.05	24	18	60	10	51	99	89	75
3.81	12	9	78	17	61	105	91	77
4.57	12	9	95	25	71	111	94	79
5.33	10	7	113	33	80	117	96	81
6.10	9	7	130	40	90	123	98	83
7.62	32	24	165	55	110	135	103	86
9.14	27	21	200	71	130	146	107	90
10.67	20	15	235	86	149	158	112	94
12.19	10	7	270	101	169	170	117	98
13.72	16	12	305	116	189	182	121	102
15.24	19	14	340	132	209	193	126	106

Table 3.8 presents the undrained shear strength and OCR values calculated by using the available unconfined compressive strength values and nonlinear relations. Undrained shear strength c_{u1} were based on unconfined compressive strength values and undrained shear strength c_{u2} were based on nonlinear relations. Weighted averages of undrained shear strength and OCR values were also calculated and presented in Table 3.8.

Table 3.8. *Undrained Shear Strength and OCR Values Based on Available Unconfined Compressive Strengths and Nonlinear Relations*

Depth [m]	**c_{u1} [kPa]**	**c_{u2} [kPa]**	**Average c_u [kPa]**	**OCR**
0-4	165	203	184	16
4-6	94	82	88	4
6-12	189	164	176	6
12-15	120	112	116	3
		Weighted Average	140	6

Table 3.9 presents undrained and drained Young's modulus values. Undrained Young's modulus values were based on Jardine et al.'s (1985), Duncan & Buchignani's (1976) and Jamiolkowski et al.'s (1979) curves. Weighted averages of undrained and drained Young's modulus values were also calculated and presented in Table 3.9.

Table 3.9. *Different Expressions for Compression Index of the Soil*

Depth [m]	**Jardine et al. (1985) [MPa]**	**Duncan & Buchignani (1976) [MPa]**	**Jamiolkowski et al. (1979) [MPa]**	**Average E_u [MPa]**	**Average E_d [MPa]**
0-4	184	221	64	157	131
4-6	88	105	79	91	76
6-12	176	212	106	165	138
12-15	116	139	127	127	107
			Weighted Average	139	116

3.3.3. Compression Properties of the Soil

Three parameters are necessary to calculate the consolidation settlements. These parameters are preconsolidation pressure σ'_c, compression index c_c and recompression index c_r.

There are several methods (e.g., Casagrande's (1936) Method, the Method of Work, the Log-Log Method) available to obtain the preconsolidation pressure. Although the Casagrande's (1936) method commonly gives somewhat low values (Bowles, 1996).

Also, Mayne & Kemper (1988) showed that:

$$\frac{\sigma'_c}{P_a} = 67N^{0.83} \tag{3.10}$$

Beyond the preconsolidation pressure, the variation is approximately linear with a slope known as compression index. The compression index was obtained by using the equations proposed by various researchers. The results are presented in Table 3.10. It is important to note that such relations may be sufficiently accurate or may yield far more accurate estimates than would be obtained by investing the same money in a few consolidation tests. The results can change by more than 30% within a few meters or less (Reese, 2006).

Table 3.10. *Different Expressions for Compression Index of the Soil*

Reference	Equation	Value
Skempton (1944)	$c_c = 0.009(LL - 10)$	0.117
Nagaraj & Murty (1985)	$c_c = 0.2343\left(\frac{LL\%}{100}\right)G_s$	0.146
Wroth & Wood (1978)	$c_c = 0.5 \times G_s \times \left(\frac{PI\%}{100}\right)$	0.162
Kulhawy & Mayne (1990)	$c_c = \left(\frac{PI\%}{74}\right)$	0.162
Terzaghi & Peck (1948)	$c_c = 0.009 \times (LL - 10)$	0.117
USACE (1990)	$c_c = 0.012 \times w_n$	0.144

The recompression index was obtained by using the limits proposed by Rao (2011) and Ameratunga et al. (2016). The results are presented in Table 3.11.

Table 3.11. *Recompression Index of the Soil*

Reference	**Limit**	**Value**
Rao (2011)	c_c·(1/5 - 1/4)	0.0258 - 0.0323
Ameratunga et al. (2016)	c_c·(1/10 - 1/5)	0.0129 - 0.0258

CHAPTER 4

ANALYSIS USING ANALYTICAL METHOD

4.1. General Information

An Excel 2016 spreadsheet was prepared to check each design consideration according to DNV/RISØ (2002) discussed in Chapter 2. The representative site discussed in Chapter 3 was used as a practical example. A circular foundation was assumed for the sake of simplicity throughout the calculations. The details of the calculations were presented by using Figures. In each table shown below, the tables having solid borders are inputs and the rest are based on calculations.

4.2. Dimensions

The foundation dimensions are presented in Figure 3.3. These dimensions were used to calculate the foundation volume and the backfill volume using the unit weights shown in Figure 4.1.

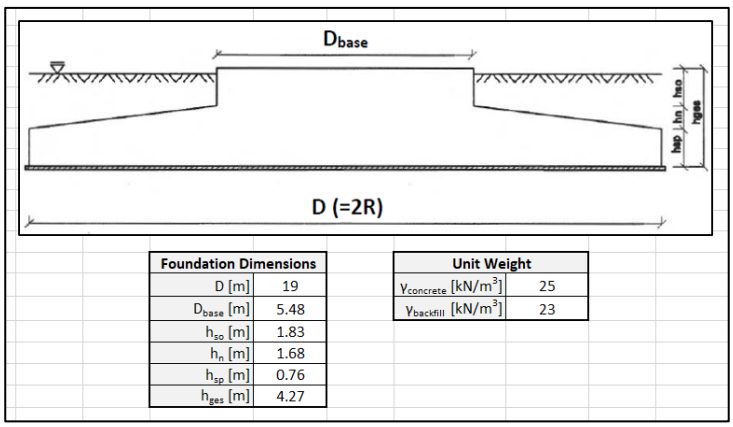

Foundation Dimensions	
D [m]	19
D_{base} [m]	5.48
h_{so} [m]	1.83
h_n [m]	1.68
h_{sp} [m]	0.76
h_{ges} [m]	4.27

Unit Weight	
$\gamma_{concrete}$ [kN/m^3]	25
$\gamma_{backfill}$ [kN/m^3]	23

Figure 4.1. Dimensions and Gravity Weights

4.3. Loads

The loads stated in Table 3.2 were used for each of the criterion. In order to calculate the total vertical load acting to the soil, the normal force and the foundation weight were added together. The final values are shown in Figure 4.2.

Loads (Tower Base)	
F_z [kN]	2269.1
F_x [kN]	667.4
M_r [kN.m]	47736
M_z [kN.m]	0

Loads (at Fnd. Base)	
P [kN]	32374.0
H [kN]	667.4
M [kN.m]	50585.8
T [kN.m]	0.0

Eccentricity	
e [m]	1.56

Figure 4.2. Loads at Tower Base, Loads Foundation Base and Eccentricity

4.4. Effective Area & Eccentricity

The effective area dimensions were calculated once the eccentricity was calculated. There is no need to the correction for torsional moment since the torsional moment was zero. The result of the calculations are shown in Figure 4.3.

Eccentricity	
e [m]	1.56
A [m^2]	283.53
Effective Area Dimensions	
A' [m^2]	224.42
b_e [m]	15.87
l_e [m]	18.74
L' [m]	16.28
B' [m]	13.79

Figure 4.3. Eccentricity and Effective Area Dimensions

All of the above calculations are based on the foundation geometry and the loads provided by the turbine manufacturer. Therefore, these calculations are not site dependent.

4.5. Geotechnical Design Requirements

All geotechnical design requirements were checked for the representative site by using the equations suggested by DNV/RISØ (2002). The factors of safety, the allowable limits for immediate settlement and the minimum required rocking stiffness are shown in Figure 4.4. The rocking stiffness requirement was not available for the wind turbine in the case study. It was assumed as 3000 MN.m/rad by using the rocking stiffness requirement (i.e., 1500 MN.m/rad) for ENERCON E48 (0.8 MW) wind turbine.

Rocking Stiffness	
K_θ [MNm/rad]	3000
Allowable Limits	
δ_V [mm]	25
α_R [rad]	0.003
Factor of Safety	
FS_{bc}	2.26
FS_o	1.5
FS_s	1.5

Figure 4.4. Allowable Limits and Factors of safety

For clay, the initial shear modulus of the soil G_0 can be taken as (DNV/RISØ, 2002):

$$G_0 = 2600 c_u \tag{4.1}$$

Shear modulus ratio G/G_0 can be taken as 0.35 for shear strain level of 10^{-3} using Figure 2.14. Then, G is calculated as the product of G_0 and G/G_0.

The results of the calculations based on analytical method such as the factor of safety against bearing capacity (3.45 > 2.26), overturning (3.65 > 1.5), sliding (7.38 > 1.5), rocking stiffness and immediate settlement are shown in Figure 4.5. As can be seen in Figure 4.5, all design requirements are met and the designed foundation having a diameter of 15.85 m was safe enough under the extreme loading condition.

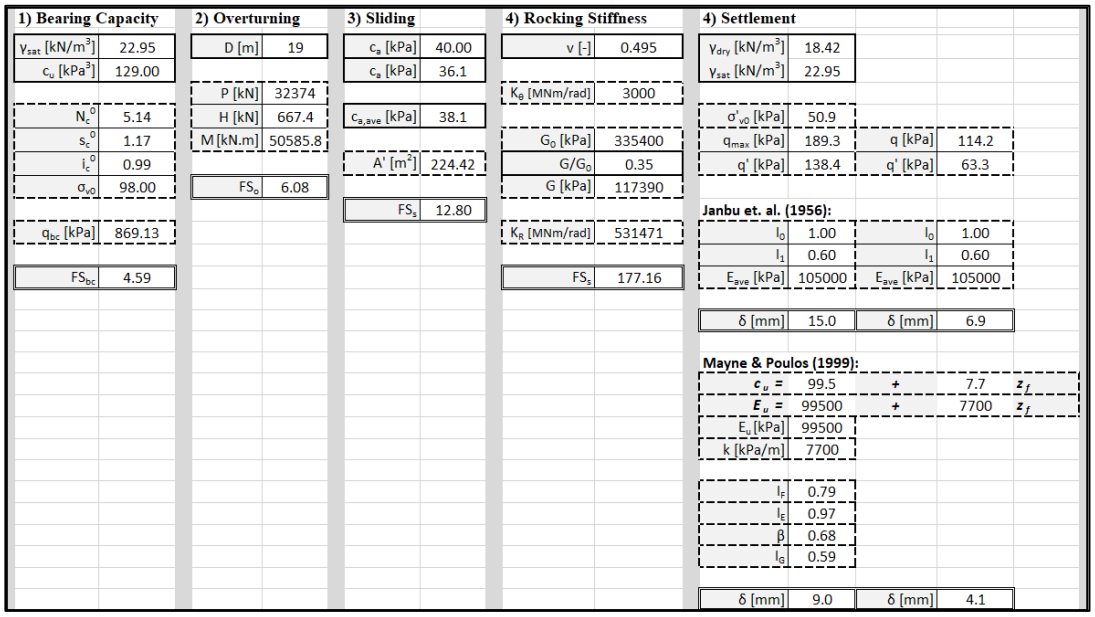

1) Bearing Capacity

γ_{sat} [kN/m^3]	22.95
c_u [kPa^3]	129.00
N_c^0	5.14
s_c^0	1.17
i_c^0	0.99
σ_{vo}	98.00
q_{bc} [kPa]	869.13
FS_{bc}	4.59

2) Overturning

D [m]	19
P [kN]	32374
H [kN]	667.4
M [kN.m]	50585.8
FS_o	6.08

3) Sliding

c_a [kPa]	40.00
c_a [kPa]	36.1
$c_{a,ave}$ [kPa]	38.1
A' [m^2]	224.42
FS_s	12.80

4) Rocking Stiffness

v [-]	0.495
K_θ [MNm/rad]	3000
G_0 [kPa]	335400
G/G_0	0.35
G [kPa]	117390
K_R [MNm/rad]	531471
FS_s	177.16

4) Settlement

γ_{dry} [kN/m^3]	18.42		
γ_{sat} [kN/m^3]	22.95		
σ'_{vo} [kPa]	50.9		
q_{max} [kPa]	189.3	q [kPa]	114.2
q' [kPa]	138.4	q' [kPa]	63.3

Janbu et. al. (1956):

I_0	1.00	I_0	1.00
I_1	0.60	I_1	0.60
E_{ave} [kPa]	105000	E_{ave} [kPa]	105000
δ [mm]	15.0	δ [mm]	6.9

Mayne & Poulos (1999):

c_u =	99.5	+	7.7	z_f
E_u =	99500	+	7700	z_f
E_u [kPa]	99500			
k [kPa/m]	7700			
I_F	0.79			
I_E	0.97			
β	0.68			
I_G	0.59			
δ [mm]	9.0	δ [mm]	4.1	

Figure 4.5. Results of Calculations for Checking Geotechnical Considerations

The factor of safety for bearing capacity, overturning, sliding and rocking stiffness are greater than minimum required factors of safety. Settlements were calculated for both maximum bearing pressure considering the overturning moment and average uniform bearing pressure. Both results are less than the allowable limit. It should be highlighted at this point that rotation limit should be checked using computer-aided methods (e.g., FEM).

4.6. Monte Carlo Simulation

4.6.1. The Reason

A minimum of one borehole at each turbine location is suggested in practice (Tinjum & Christiensen, 2011), as well as in Turkish practice. However, in a large wind farm site, individual boreholes may not be drilled at each wind turbine location. For example, for a proposed 200 MW Búrfell wind park in Iceland consisting of 80 wind turbines, the location of planned boreholes can be seen Figure 4.6.

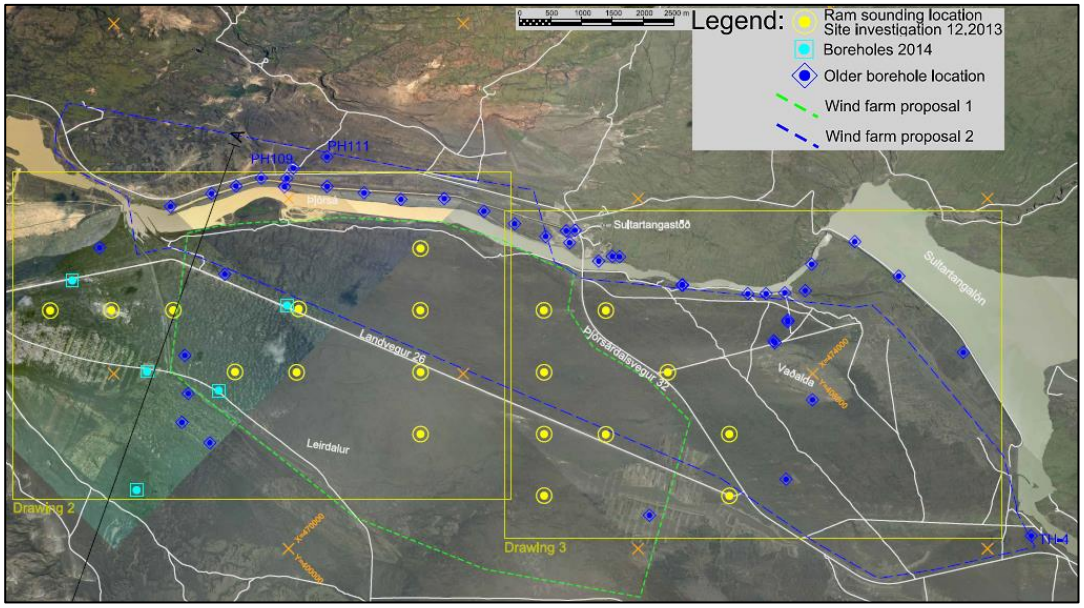

Figure 4.6. The Location of Boreholes for Proposed 200 MW Búrfell Wind Park in Iceland (Landsvirkjun, 2015)

Even if one borehole drilled for each wind turbine location, there is inherent variability in soil profile and properties, which may not be captured with limited number of samples and laboratory tests as shown in Figure 4.7. Consequently, the foundation designer should consider uncertainty and variability of soil properties when s/he carries out wind turbine foundation design.

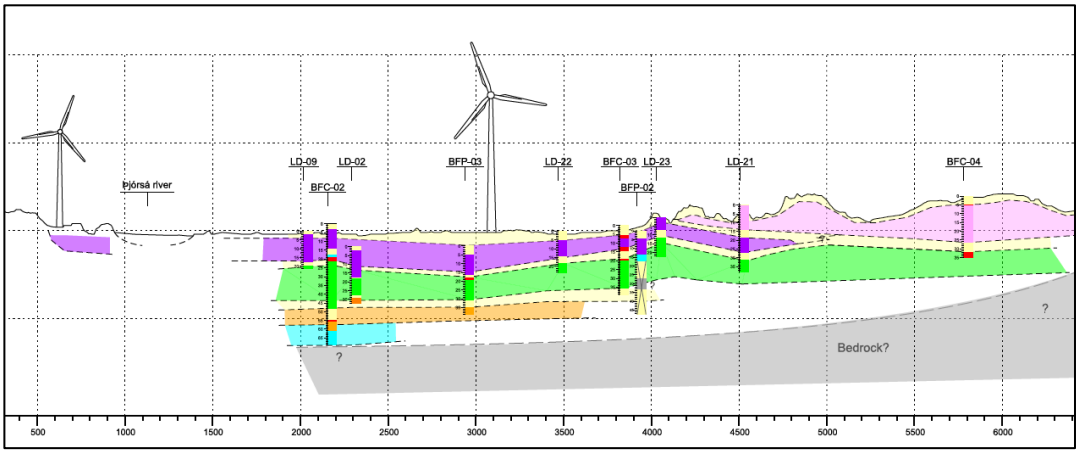

Figure 4.7. Variability of Soil Profile for Proposed 200 MW Búrfell Wind Park in Iceland

For a probabilistic design approach, the mean and standard deviation of all material properties are needed. Ideally, a detailed comprehensive site investigation and laboratory testing program should provide these values. However, significant number of laboratory and in-situ test results are not commonly available in practice. Therefore, these parameters were needed to be assumed from the literature.

4.6.2. The Methodology

In a Monte Carlo simulation for foundation design, all inputs (e.g., loads, soil properties) should be considered as random variables. However, in this study, only the soil properties are considered as random variables. In fact, soil properties are not independent random variables but correlated to each other (e.g., as cohesion increases, friction angle decreases). In this study, since undrained analysis was performed, such cross correlations were neglected.

Generalized steps for a Monte Carlo simulation are outlined below.

(i) Obtain the most likely (mean) values of the required soil parameters,

(ii) For each random variable, choose a relevant coefficient of variation COV (i.e., standard deviation divide by mean) from the literature if site-specific information on soil variability is not sufficient,

(iii) Choose a statistical distribution (e.g., normal, lognormal) for the random variables,

(iv) Determine the required number of sample/run N,

(v) Carry out the analysis N times

Probability of failure, or probability of performance criteria not being met, can be defined as the ratio of 'the number of analyses that end up with criteria not being met' to 'the total number of analyses'.

In this study, only undrained shear strength and unit weight are considered as random variables since undrained Young's modulus depends on undrained shear strength and other soil parameters will not be significantly effective on the results. Therefore, coefficient of variation values for undrained shear strength and unit weight are needed in the analyses. In this study, the effects of low and high COV levels on the results are examined to represent the dispersion around the mean. COV levels were selected for typical COV ranges reported in the literature.

Based on Phoon et al. (1999), who collected extensive information on geotechnical properties by using laboratory and in-situ tests, the COV values of c_u are in the range of 10-60%. Furthermore, Duncan (2000) summarized available literature, added his own data, and reported COV values of 13-40%. Therefore, for undrained shear strength, low and high COV levels were selected as 10% and 70%, respectively. Similarly, for unit weight, low and high COV levels were selected as 3% and 10%, respectively, according to the ranges given by Duncan (2000).

Monte Carlo analysis with "high COV" means COV of undrained shear strength is 70% and COV of unit weight is 10%; "low COV" means COV of undrained shear strength is 10% and COV of unit weight is 3% as shown in Figure 4.8.

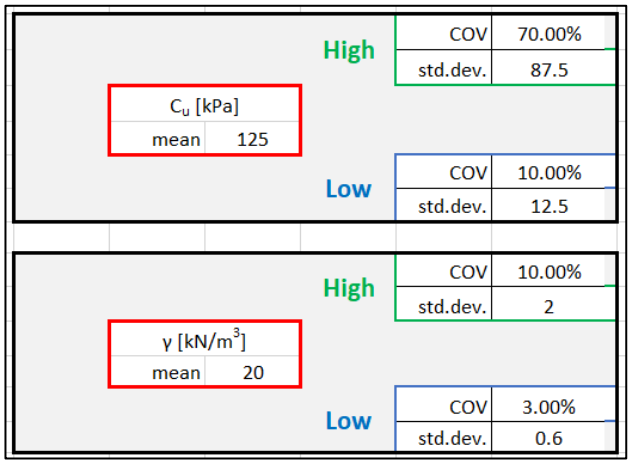

Figure 4.8. Input Values of Random Variables with High and Low COVs

In this study, the lognormal distribution was used since it has been shown to model the inherent spatial variability of geotechnical parameters well (Griffiths et al. 2002; Griffiths & Fenton 2004; Cho 2010) and because the lognormal random variable is a continuous variable which is strictly nonnegative.

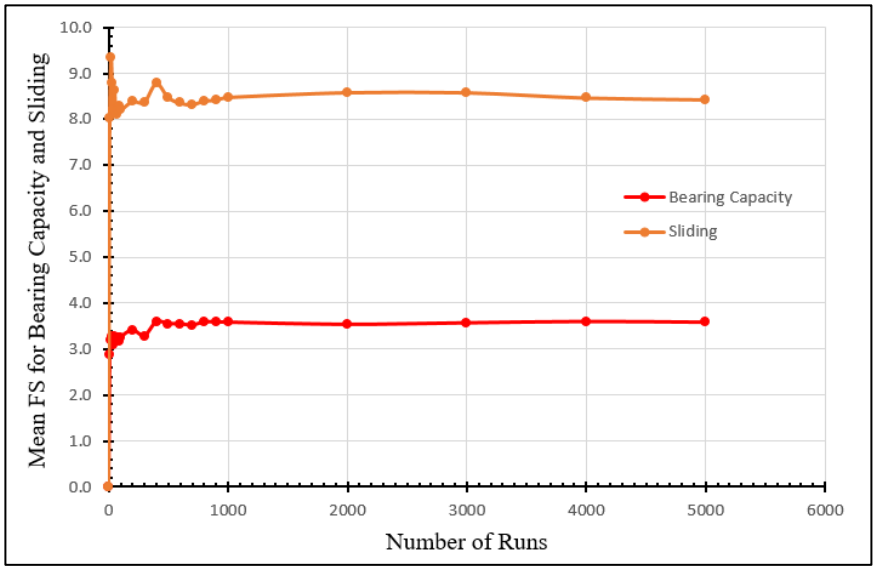

Figure 4.9. Mean Factors of Safety versus Number of Runs for Bearing Capacity and Sliding Checks

Trial runs were carried out to determine the minimum number of runs required to perform accurate Monte Carlo simulations. As can be seen in Figure 4.9 for bearing capacity and sliding, more than 1000 runs do not change the results. For each performance criteria that are dependent on soil variability (e.g., bearing capacity, sliding, rocking stiffness and settlement), this was evaluated and 5000 runs were selected to be on the safe side.

4.6.3. The Results

The results of Monte Carlo simulations using 5000 runs considering high and low COV levels of undrained shear strength and unit weight are presented in Figure 4.10 and Figure 4.11.

Table 4.1 shows that the mean bearing capacity and the mean factor of safety for bearing capacity do not depend on the level of variability in the soil properties. As can be seen in in Figure 4.10, Figure 4.11 and Table 4.1, the corresponding values for high and low COV levels are similar to each other.

Standard deviations of bearing capacity for high and low COV levels are dramatically different from each other as shown in Table 4.1.

In high COV analysis, out of 5000 runs 1945 resulted in FS_{bc} smaller than 2.26 which is the minimum FS_{bc}. This indicates that the probability of unsatisfactory performance (Pf) is 0.39 (39%). On the other hand, for low COV analysis, only 2 runs out of 5000 gave FS_{bc} smaller than 2.26. Probability density functions of 5000 runs for high and low COV levels are presented together with FS_{bc} of 1.0 and FS_{bc} of 2.26 in Figure 4.12.

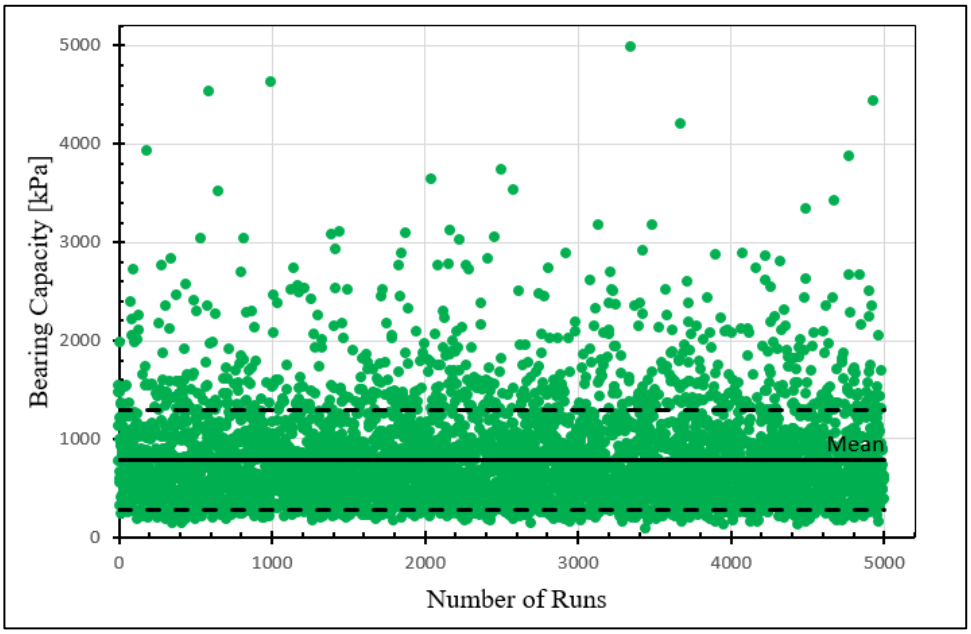

Figure 4.10. Bearing Capacity Values of 5000 runs for High COV Level

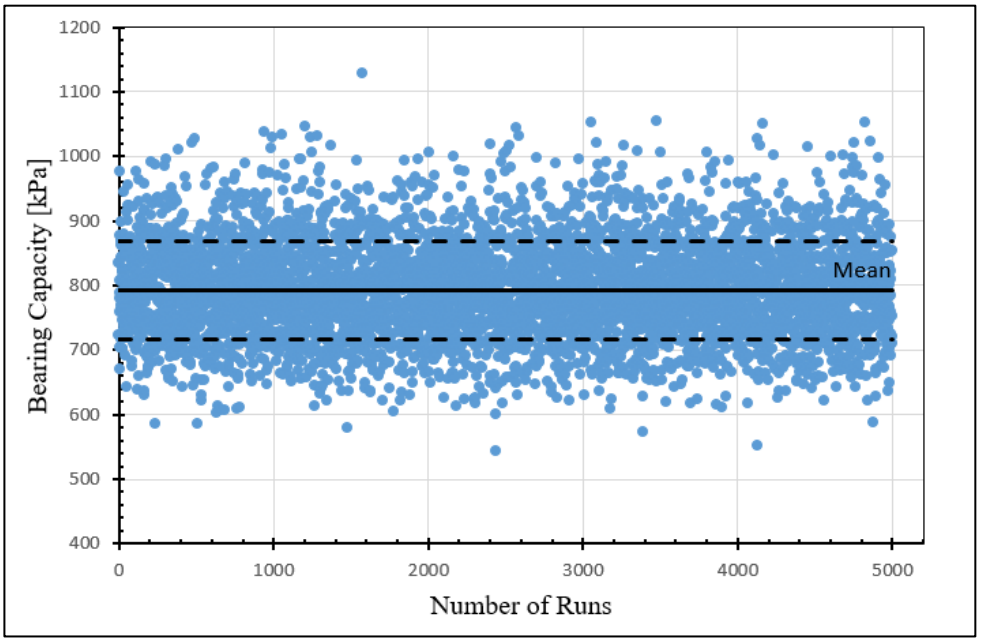

Figure 4.11. Bearing Capacity Values of 5000 runs for Low COV Level

Table 4.1. *Results of Monte Carlo Simulation for Bearing Capacity*

	High COV	**Low COV**
Mean Bearing Capacity [kPa]	790.4	792.6
Standard Deviation Bearing Capacity [kPa]	506.0	75.0
COV Bearing Capacity	64%	9.5%
Mean FS_{BC}	3.19	3.20
Standard Deviation FS_{BC}	2.04	0.30
Number of Runs with $FS_{BC} < 2.26$	1945	2
Probability of $FS_{BC} < 2.26$	0.39	0.0004

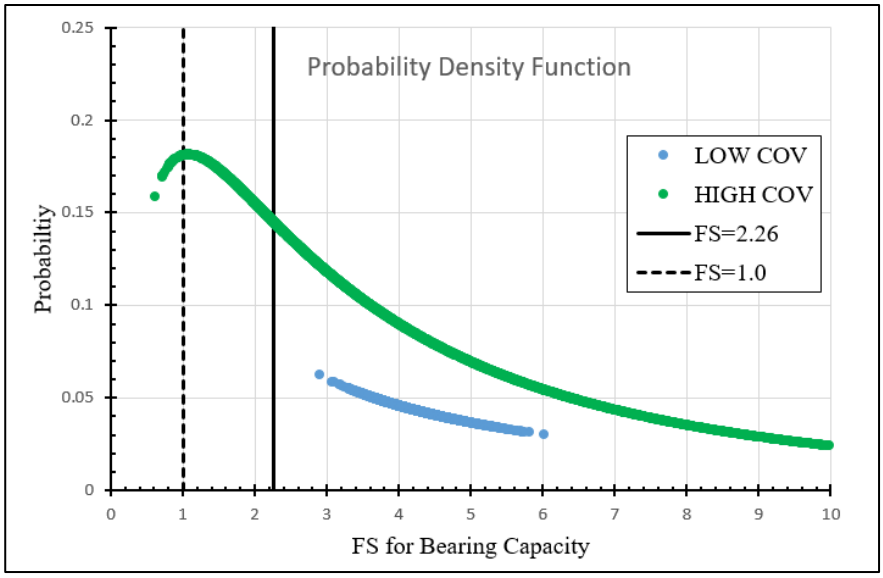

Figure 4.12. Probability Density Function for Bearing Capacity

Table 4.2 presents that the mean factor of safety for sliding 6.73 and 6.77 for high and low COV levels, respectively. Both of these values are greater than FS_s of 1.5.

In high COV analysis, 93 runs out of 5000 gave FS_s smaller than 1.5; whereas this number is zero in low COV analysis. Figure 4.13 presents the probability density

function. As can be seen in Figure 4.13 that the results of low COV analysis is always greater than 1.5 and some of the runs of high COV analysis is smaller than 1.5.

Table 4.2. *Results of Monte Carlo Simulation for Sliding*

	High COV	**Low COV**
Mean FS_S	6.73	6.77
Standard Deviation FS_S	4.72	0.67
Number of Runs with $FS_S < 1.5$	93	0
Probability of $FS_S < 1.5$	0.019	0

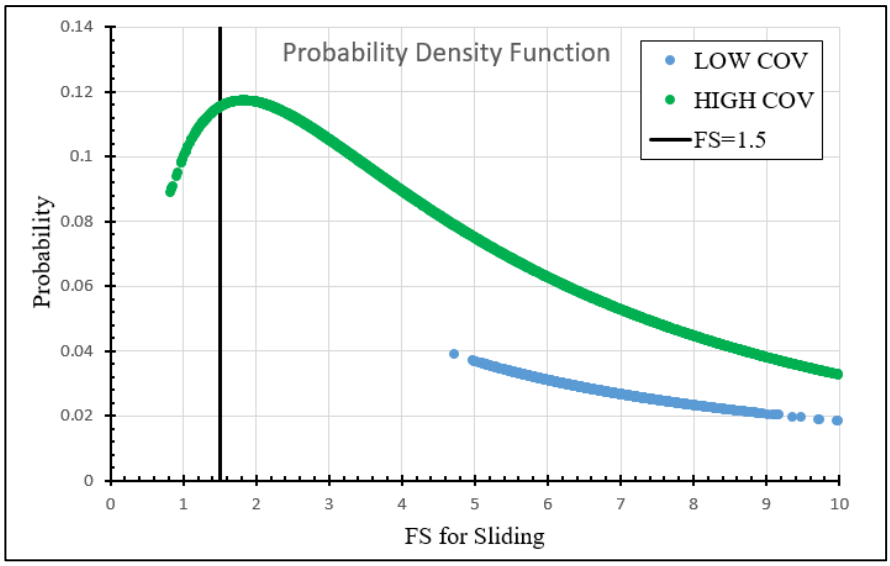

Figure 4.13. Probability Density Function for Sliding

Table 4.3 demonstrates that rocking stiffness is not a major concern if the design is carried out according to DNV/RISØ (2002). For both high and low COV levels, the mean rocking stiffness values are about ten times greater (i.e., ten times rigid) than the design requirement.

Table 4.3. *Results of Monte Carlo Simulation for Rocking Stiffness*

	High COV	**Low COV**
Mean Rocking Stiffness [MNm/rad]	300,861	298,221
Standard Deviation Rocking Stiffness [MNm/rad]	205,740	30,008
Number of Runs with Rocking Stiffness < 3000 [MNm/rad]	0	0
Probability of Rocking Stiffness < 3000 [MNm/rad]	0	0

The mean settlement values of 5000 runs are calculated as 15.6 mm and 10.5 mm for high and low COV levels, respectively as shown in Table 4.4. Corresponding standard deviations are 10.8 mm and 1.06 mm for high and low COV levels of input parameters, respectively. Mean factor of safety for settlement (i.e., 25 mm divided by calculated settlement) is 2.4 mm for both cases.

In high COV analysis, out of 5000 runs, 742 resulted in settlements larger than 25 mm. Therefore, the probability of occurrence of unsatisfactory settlement is 14.8%.

Table 4.4. *Results of Monte Carlo Simulation for Settlement*

	High COV	**Low COV**
Mean Settlement [mm]	15.6	10.5
Standard Deviation Settlement [mm]	10.8	1.06
Mean FS_{SETT}	2.41	2.40
Standard Deviation FS_{SETT}	1.71	0.24
Number of Runs with Settlement > 25 mm	742	0
Probability of Settlement > 25 mm	0.148	0

For an optimum design of wind turbine foundations, the diameter is the major factor, which controls the capital cost of the project. Therefore, the variation in diameter was

investigated in terms of bearing capacity only because all other design criteria were satisfied well beyond the requirements.

Figure 4.14 shows that the bearing capacity is in the range of 724 kPa to 805 kPa for diameters between 11 m and 19 m. As the diameter increases, bearing capacity increases nonlinearly and starts leveling at a diameter of about 18 m. Moreover, the tendency demonstrates that diameter larger than 18 m does not provide any further increase in bearing capacity. Also, the effect of high and low COV levels are insignificant on the mean bearing capacity.

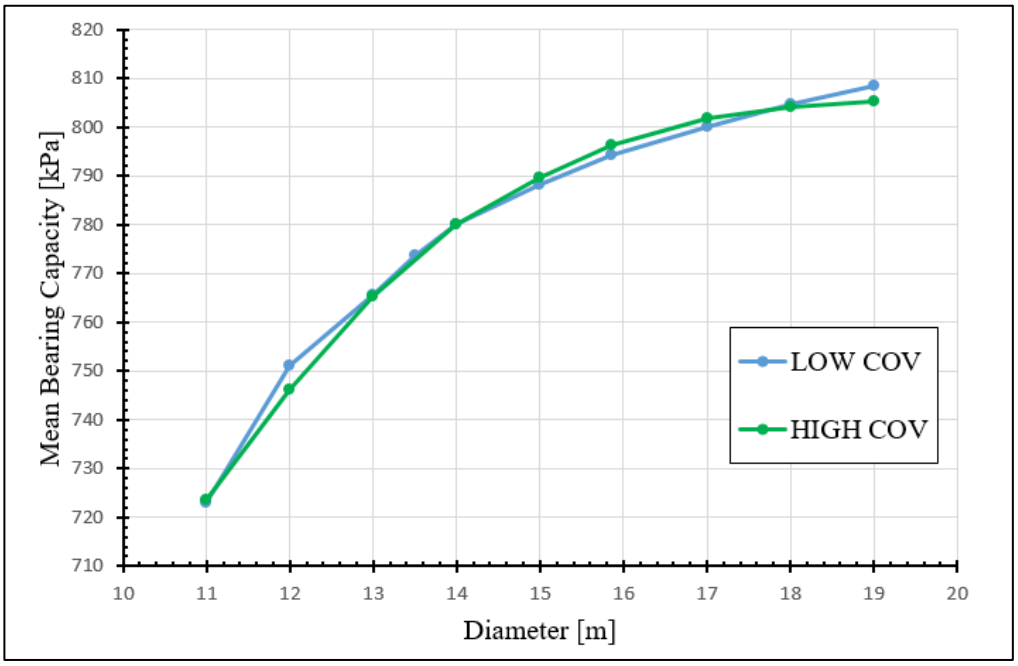

Figure 4.14. Mean Bearing Capacity versus Diameter of the Foundation

The effects of diameter and COV levels on the "probability of $FS_{bc} < 2.26$" are demonstrated in Figure 4.15. For high COV level, as diameter increases from 11 m to 19 m the probability decreases nonlinearly and smoothly from 86% to 22%. For high and low COV level, as diameter less than 12 m, the "probability of $FS_{bc} < 2.26$" is

about 80-100%; therefore, the soil cannot carry the extreme loads. For low COV level, as diameter increases from 12 m to 15 m, there is a dramatic decrease in the probability and diameter beyond 15 m, the design requirement is always satisfied. The designed foundation of 15.85 m has zero probability when COV of soil parameters is low whereas it is 38.3% when COV of soil parameters is high. This means that if the uncertainty in soil parameters are reduced by extensive laboratory and in-situ testing then the probability can be decreased.

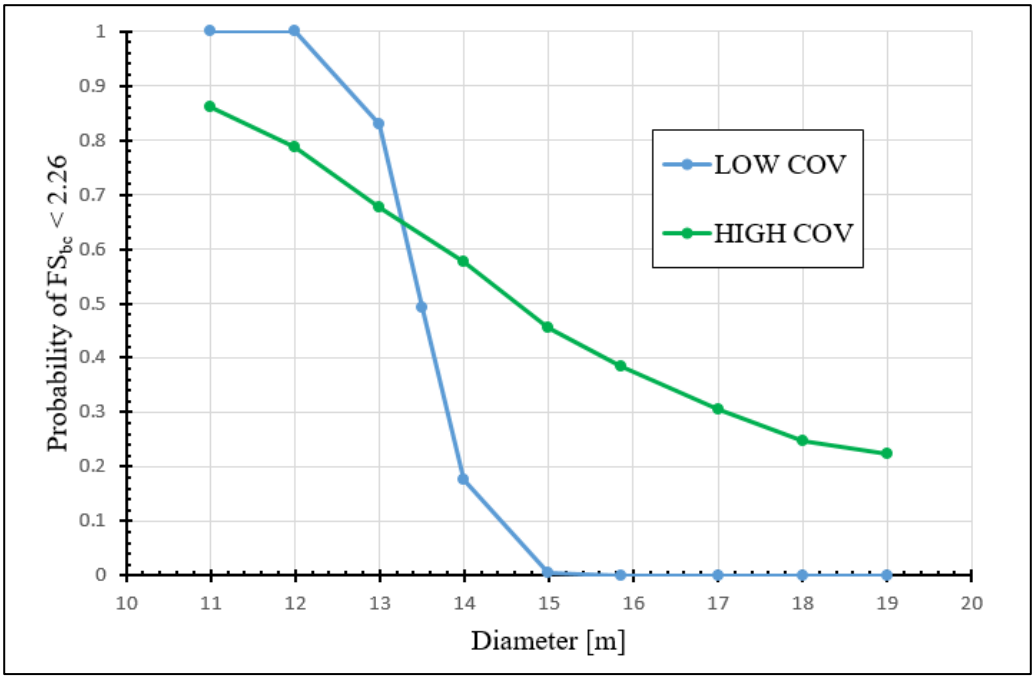

Figure 4.15. Probability of FS_{bc} < 2.26 versus Diameter of the Foundation

CHAPTER 5

ANALYSIS USING 3D FINITE ELEMENT METHOD

5.1. Software

PLAXIS 3D AE.v02 was used to model the wind turbine foundation. PLAXIS mainly consists of two sub-programs (i) input program and (ii) output program. In input program, three-dimensional (3D) geometry composed of points, lines, surfaces and volumes are created, and the material properties and boundary conditions are defined. Also, 3D soil and structure volumes created and meshed in a CAD program can be imported into PLAXIS. These are all done in the first two tabs that are defined as the geometry modes of the input program. Subsequent to these inputs; meshing, defining flow conditions and calculation phases are done. These last three tabs are the calculation modes of the input program.

5.2. Geometry

The geometry of the model should be large enough so that the zone under the foundation wherein the vertical stresses are significant not influenced by the model boundary effects. This zone is frequently termed as stress bulb or stress isobar. The model may become unnecessarily large and need very long analysis time if the model boundaries are located very long away from the stress bulbs to be sure no model boundary effects take place. On the other hand, the model boundaries placed too close to the stress bulbs may start to affect the results of the finite element analysis and probably cause inaccurate results since there may be horizontal and vertical displacements in the real scenario after the construction. However, the model boundaries placed too close to the stress bulbs have fixed the displacements at zero. Therefore, the model boundaries should be placed at the closest possible locations to

the stress zone under the loaded area, wherein the vertical stresses are significant, without any model boundary effects influence the results.

Azizi (2000) suggests that in the case of a shallow foundation with width B on an isotropic homogenous soil, the finite element model should include a volume extending about 10B laterally and 8B vertically from the center of the foundation base. However, the contact pressure from the vertical load is quite low in wind turbines (Tinjum & Christensen, 2011). Therefore, Azizi's (2000) suggestion for the vertical dimension of the model boundary may result excessive analysis time especially for 3D models. Lambe & Whitman (1969) denote that for a circular loaded area, the vertical stresses are less than the ten percent of the stress increment at depth of 4R. Correspondingly, in the literature, the vertical boundary dimension of 6B to 11B is generally recommended if dense sand, gravel, or bedrock is not observed.

In the light of these suggestions, the model boundaries created are shown in Figure 5.1. The model is normally fixed at x_{min} and x_{max}, y_{min} and y_{max}, fully fixed at z_{min} and free at z_{max}. The modeled foundation, excavation and backfill are shown in Figure 5.2.

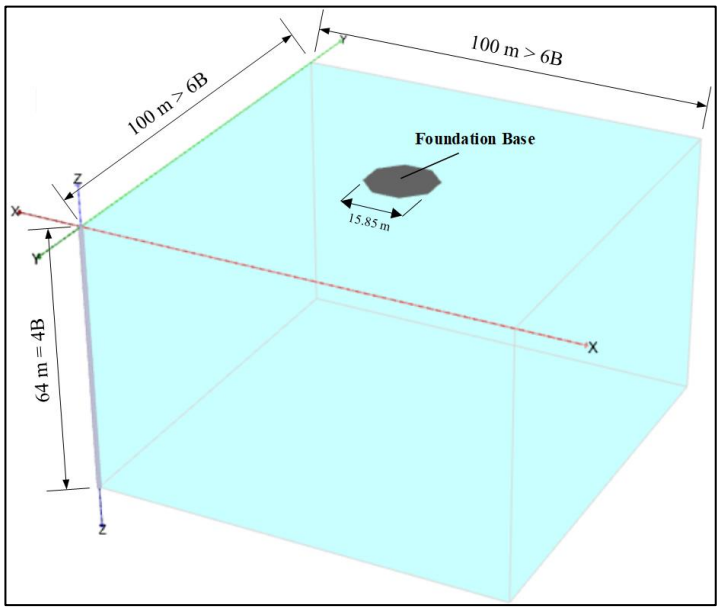

Figure 5.1. The Boundaries of the Model below the Foundation

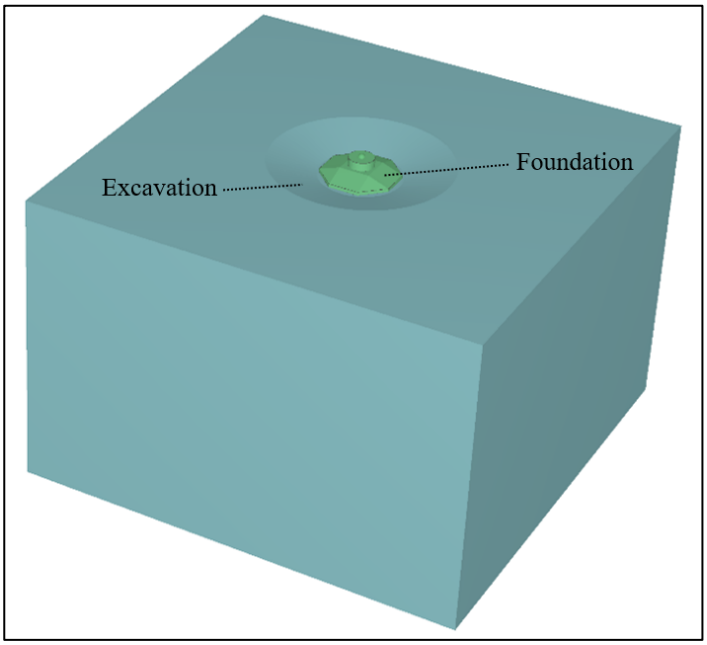

Figure 5.2. The Modeled Foundation and Excavation

5.3. Meshing

When the model is fully defined, it has to be divided into finite elements (i.e., mesh) in order to perform the computations. The mesh should be sufficiently fine to get accurate results. However, unnecessarily fine meshes should be avoided to prevent long calculation times.

10-node tetrahedral element shown in Figure 5.3 is the basic soil element of 3D finite element mesh in PLAXIS 3D. This element can be successfully used to estimate the displacement and stress fields in 3D finite element analyses (Azizi, 2000). They can fit into awkward shapes easily and less susceptible to distortion errors. In addition to the 10-node tetrahedral soil element, special types of elements can be used to model the structural behavior.

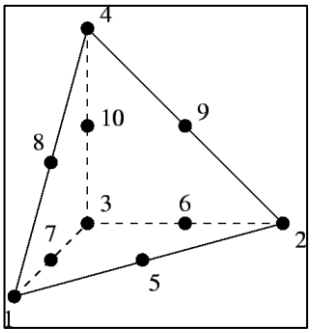

Figure 5.3. 10-node Tetrahedron 3D Soil Element in PLAXIS 3D

The size and arrangement of elements in a mesh can have a critical effect on the accuracy of a finite element analysis. A poorly formed mesh is a common source of error, so a lot of attention needs to be paid to mesh quality. Mesh generation options in PLAXIS 3D are given in Table 5.1 where r_e is defined as the relative element size factor.

Table 5.1. *Mesh Generation Options in PLAXIS 3D AE*

Element Size	$\mathbf{r_e}$
Very Coarse	2.0
Coarse	1.5
Medium	1.0
Fine	0.7
Very Fine	0.5

Optional local refinement settings are also available in PLAXIS 3D. This option is to refine the mesh in the areas where the stresses and the displacements are expected to be large and at the surfaces where material properties change. The element sizes should be increased progressively in a way ensuring a smooth transition from small to larger sizes. This can be achieved if the ratio of the areas of two adjacent elements does not exceed two (Azizi, 2000).

Large stress concentrations and zone of rapid stress or strain change need smaller elements. A good finite element mesh is graded with small elements where they are needed and larger elements remote from the area of interest and where stresses and strains are uniform (Lees, 2016). The optimum number of elements minimizing calculation time and ensuring accurate results was determined by a mesh sensitivity study. The results of the study are presented in Table 5.2 and graphically shown in Figure 5.4.

The results show that the optimal meshed model ensuring reliable outputs and preventing excessive calculation time should contain at least 50,000 elements. When number of elements is increased ~2.3 times as much, the maximum vertical displacement changes by only 1.7%. However, the calculation time increases approximately 2.6 times as much.

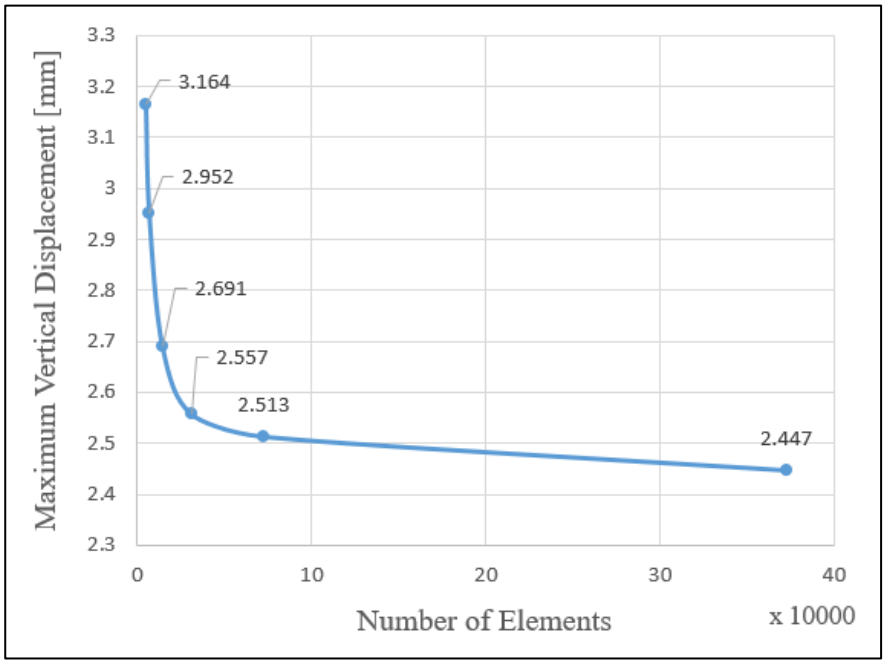

Figure 5.4. Graphical Presentation of Mesh Sensitivity Analysis

Table 5.2. *Results of the Mesh Sensitivity Analysis*

Number of Elements	r_e	Max. u_z [mm]
4902	2.0	3.164
6794	1.5	2.952
14319	1.0	2.691
30937	0.7	2.557
72546	0.5	2.513
372577	0.3	2.447

In the light of the suggestions presented and the results of the sensitivity study, the model is meshed using fine to very fine size 128353 soil elements. The meshed model is presented in Figure 5.5.

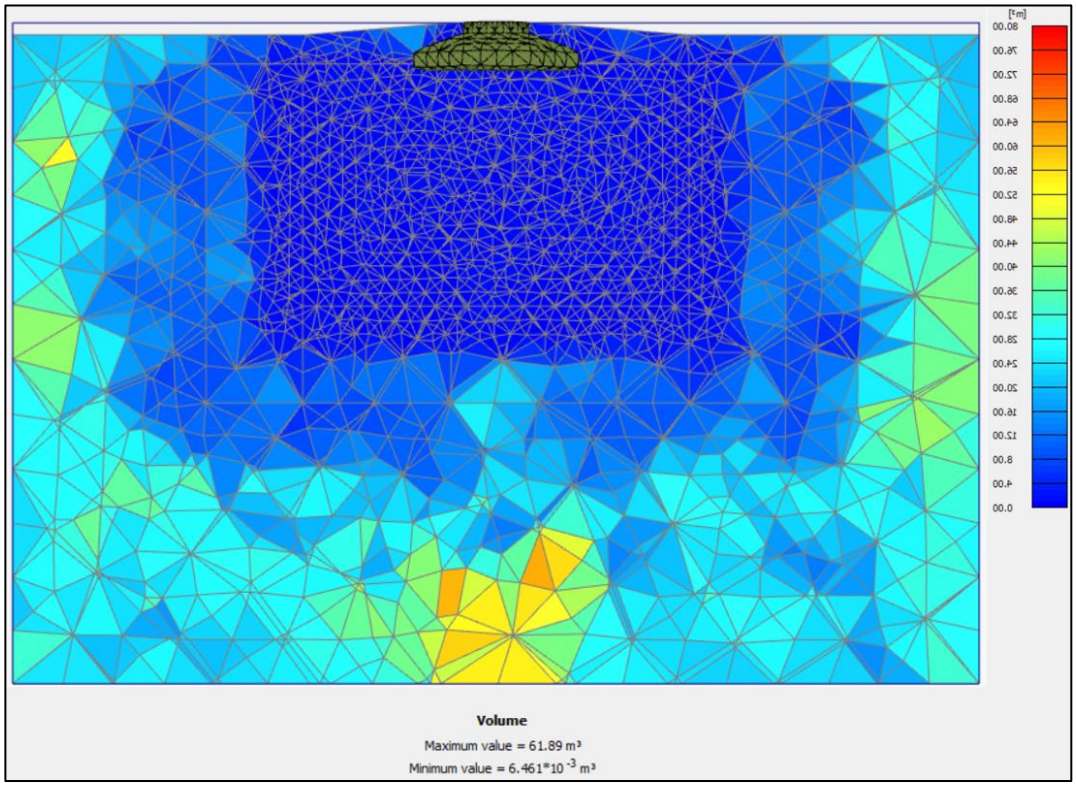

Figure 5.5. Meshed Model with Fine to Very Fine Sized Soil Elements

5.4. Constitutive Models

Constitutive models should be selected to simulate soil behavior with sufficient accuracy under all loading conditions to be imposed. To avoid unnecessary complexity, the simplest constitutive model that satisfies this requirement should be selected (Lees, 2016).

PLAXIS 3D supports various constitutive models from very simple linear elastic model to user-defined soil models. Mohr-Coulomb model, a linear-elastic perfectly plastic model, and Hardening model, a hyperbolic model, were preferred for the analyses to simulate soil behavior.

Mohr-Coulomb model requires five input parameters to express the stress-strain behavior: (i) Young's modulus, (ii) Poisson's ratio, (iii) friction angle, (iv) cohesion and (v) dilatancy angle which comes from the use of non-associated flow rule used to model a realistic irreversible change in volume due to shearing.

Among constitutive models, Mohr-Coulomb model has more applications than other models because of the simplicity of formulation as well as the lesser data input determined by simple tests. The linear-elastic part of the model is based on Hooke's law of isotropic elasticity and the perfectly-plastic part is based on the Mohr-Coulomb failure criterion.

Mohr-Coulomb model is applicable to analyze shallow foundations and it was well suited to the project because the soil strain level at full power production was calculated as 0.006% just beneath the foundation and approximately 80% of this strain dissipates within 1.7 m beneath the foundation (Yılmaz, 2014).

Undrained behavior was considered since the soil was saturated and pore water could not freely flow through the clay skeleton under loading. Drainage type C which is the only type enables simulation of undrained behavior using a total stress analysis with undrained parameters was selected.

Constant cohesion and constant stiffness across the depth are estimated for the soil by default in PLAXIS 3D. However, in real cases, these properties significantly depend on the stress level. This means that cohesion and stiffness increases with depth. Therefore, the cohesion increment $s_{u,inc}$ and the stiffness increment $E_{u,inc}$ per unit depth should be used. Subsequently, a reference depth z_{ref} has to be defined. For any depth above the reference depth, the cohesion is equal to $s_{u,ref}$ and the stiffness is equal to $E_{u,ref}$. For any depth z below the reference depth, these properties are automatically computed using the following equations (PLAXIS Material Models Manual, 2015):

$$s(z) = s_{u,ref} + (z_{ref} - z)s_{u,inc} \tag{5.1}$$

$$E(z) = E_{u,ref} + (z_{ref} - z)E_{u,inc} \tag{5.2}$$

Hardening model accounts for stress-dependency according to a power law m. Three types of stiffness are defined in this model (i) loading stiffness E_{50}, based on the results of triaxial pressure test; (ii) unloading stiffness E_{ur}, based on the results of triaxial unloading pressure test; and (iii) stiffness loading E_{oed}, based on the results of a one-dimensional consolidation test as shown in Figure 5.6. Failure is based on Mohr-Coulomb model with three parameters: friction angle, cohesion and dilatancy angle.

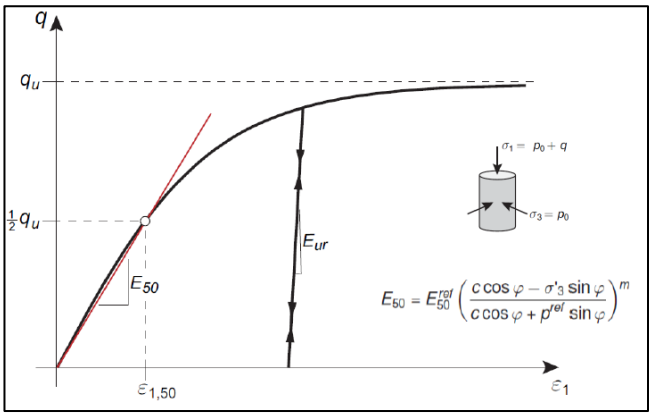

Figure 5.6. Hyperbolic Stress-Strain Relation in Primary Loading for a Standard Drained Triaxial Test (PLAXIS Material Models Manual, 2015)

Hardening model can be used to accurately predict displacement and failure for general types of soils in various geotechnical applications.

The basic idea of the Hardening model is the hyperbolic relationship between the deviator stress and the vertical strain in triaxial loading. However, triaxial test data to obtain the model parameters were not available for the project.

The oedometer loading stiffness can be taken equal to the triaxial loading stiffness and the triaxial unloading stiffness can be taken three times of the triaxial loading stiffness (PLAXIS Material Models Manual, 2015). In addition to these parameters, the power for stress-level dependency of stiffness m plays an essential role and can be estimated by using the curve proposed by Viggiani & Atkinson (1995).

Drainage type B, which is the only type in which strength is defined as undrained shear strength, was selected.

The properties of the soil for Mohr-Coulomb Model, Hardening model and the reinforced concrete are given in Table 5.3 to Table 5.7, respectively.

Table 5.3. *Soil Properties Obtained by Using the Estimation Curve for Mohr-Coulomb Model*

	Parameter	**Value**	**Unit**
General	Material Model	*Mohr-Coulomb*	
	Drainage Type	*Undrained C*	
	Unsaturated Unit Weight γ_{unsat}	18.42	kN/m^3
	Initial Void Ratio e_{init}	0.324	-
Strength Parameters	Young's Modulus $E_{u,ref}$	89	MPa
	Poisson's Ratio ν_u	0.495	-
	Shear Strength $s_{u,ref}$	87	kPa
	Increase of Young's Modulus $E_{u,inc}$	3.0	MPa/m
	Increase of Shear Strength $s_{u,inc}$	4.0	kPa/m
	Reference Depth z_{ref}	-3.05	m
	Coeff. of Earth Pressure at Rest K_0	Automatic	-
	Dilatancy Angle ψ	0	^{o}

Table 5.4. *Soil Properties Obtained by Using the Weighted Averages for Mohr-Coulomb Model*

	Parameter	Value	Unit
General	Material Model	*Mohr-Coulomb*	
	Drainage Type	*Undrained C*	
	Unsaturated Unit Weight γ_{unsat}	18.42	kN/m^3
	Initial Void Ratio e_{init}	0.324	-
Strength Parameters	Young's Modulus $E_{u,ref}$	139	MPa
	Poisson's Ratio ν_u	0.495	-
	Shear Strength $s_{u,ref}$	140	kPa
	Coeff. of Earth Pressure at Rest K_0	Automatic	-
	Dilatancy Angle ψ	0	^{o}

Table 5.5. *Soil Properties Obtained by Using the Estimation Curve for Hardening Model*

	Parameter	Value	Unit
General	Material Model	Hardening Soil	
	Drainage Type	Undrained B	
	Unsaturated Unit Weight γ_{unsat}	18.42	kN/m^3
	Saturated Unit Weight γ_{sat}	22.95	kN/m^3
	Initial Void Ratio e_{init}	0.324	-
Strength Parameters	Shear Strength s_u	87	kPa
	Increase of Shear Strength $s_{u,inc}$	4.0	kPa/m
	Reference Depth z_{ref}	-3.05	m
	U-R Poisson's Ratio ν_{ur}	0.2	-
	Loading Stiffness E_{50}^{ref}	75	MPa
	Stiffness Loading E_{oed}^{ref} $(=E_{50}^{ref})$[1]	75	MPa
	Unloading Stiffness E_{ur}^{ref} $(=3E_{50}^{ref})$	225	MPa
	Power for stress-level dependency of stiffness m	0.65	-
	Overconsolidation Ratio OCR	6	-
	Coeff. of Earth Pressure at Rest K_0	Automatic	-

Note. [1] From "PLAXIS 3D Reference Manual" by PLAXIS, 2015

Table 5.6. *Soil Properties Obtained by Using the Weighted Averages for Hardening Model*

	Parameter	Value	Unit
General	Material Model	Hardening Soil	
	Drainage Type	Undrained B	
	Unsaturated Unit Weight γ_{unsat}	18.42	kN/m^3
	Saturated Unit Weight γ_{sat}	22.95	kN/m^3
	Initial Void Ratio e_{init}	0.324	-
Strength Parameters	Shear Strength $s_{u,ref}$	140	kPa
	Loading Stiffness E_{50}^{ref}	115	MPa
	Stiffness Loading E_{oed}^{ref} (=E_{50}^{ref})	115	MPa
	Unloading Stiffness E_{ur}^{ref} (=$3E_{50}^{ref}$)	345	MPa
	Power for stress-level dependency of stiffness m	0.65	-
	Overconsolidation Ratio OCR	6	-
	Coeff. of Earth Pressure at Rest K_0	Automatic	-

Table 5.7. *Reinforced Concrete Properties for Linear-Elastic Model*

	Parameter	Value	Unit
General	Material Model	Linear-Elastic	
	Drainage Type	Non porous	
	Unit Weight γ	25	kN/m^3
Strength Parameters	Young's Modulus E	30,000	MPa
	Poisson's Ratio ν	0.15	-

5.5. Analysis Stages

The analysis can be proceeded after meshing is completed. In the engineering practice, a project is divided into project phases. Similarly, finite element calculations should be divided into sequential calculation stages in PLAXIS 3D. Each stage corresponds to a particular phase in the practice. Calculation stages are necessary to accurately simulate the nonlinear behavior of the soil.

The calculation stages of a wind turbine foundation analysis may include (i) initial stage, (ii) excavation stage, (iii) foundation installation stage, (iv) tower loading stage and (v) combined loading stage as shown in Figure 5.7. Each stage is outlined below.

(i) Initial Stage

Initial stage is automatically created in PLAXIS 3D. It is the initial ground condition comprises the initial geometry, initial water level and initial stress state. The initial stress state can be generated using either K_0 procedure or gravity loading.

(ii) Excavation Stage

Excavation stage should be modeled after the initial stage by deactivating the soil volume to be excavated. If the intention is to simulate a dry excavation, the water must be deactivated in this stage.

(iii) Foundation Installation Stage

The wind turbine foundation is modeled as a rigid body. It is installed after the excavation. Each rigid body has a reference point associated to it. The reference point is defined by three coordinates and needed to apply external forces and moments. If any interfaces are created in the modeling, they should be activated in this stage. In this study, surface friction between reinforced concrete foundation and clay soil is represented by choosing a suitable value for the strength reduction factor R_{inter} which relates the interface strength to the soil strength. As suggested by PLAXIS Manual, in the absence of detailed information it may be assumed that R_{inter} is of the order of 0.67. Soil volume corresponds to backfill soil is also activated to finish the foundation installation.

(iv) Tower Loading Stage

The vertical load is applied on the foundation along the negative z-axis in the tower loading stage to calculate the effect of the tower self-weight,

(v) Combined Loading Stage

The horizontal load along x-axis (or y-axis) and the overturning moment around y-axis (or x-axis) are applied on the foundation to model the effect of wind load.

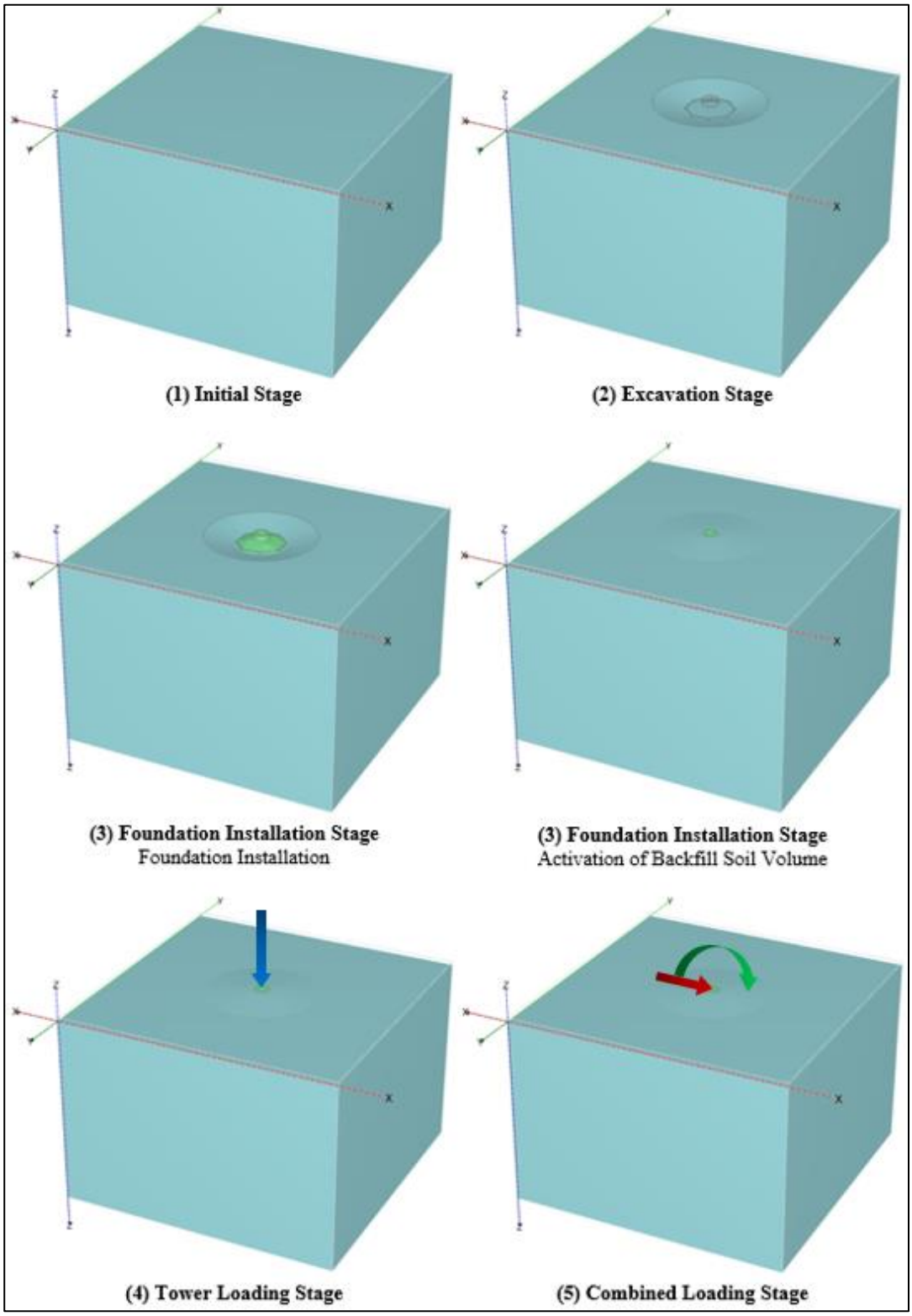

Figure 5.7. Calculation Stages for Analysis of a Wind Turbine Foundation

5.6. Results

Analyses were conducted using two different soil constitutive models, namely Mohr-Coulomb and Hardening models for soil parameters presented in Table 5.3 to Table 5.6. The results shown in figures belong to the analysis conducted using Mohr-Coulomb model and soil properties given in Table 5.3. All results are presented in Table 5.8. Unless otherwise specified, all of the figures are for combined loading stage and the negative values of pressure indicates compression.

The deformed mesh is shown in Figure 5.8, where the maximum total deformation |u| was 3 mm and the foundation was observed to tilt towards the side where the overturning moment was applied.

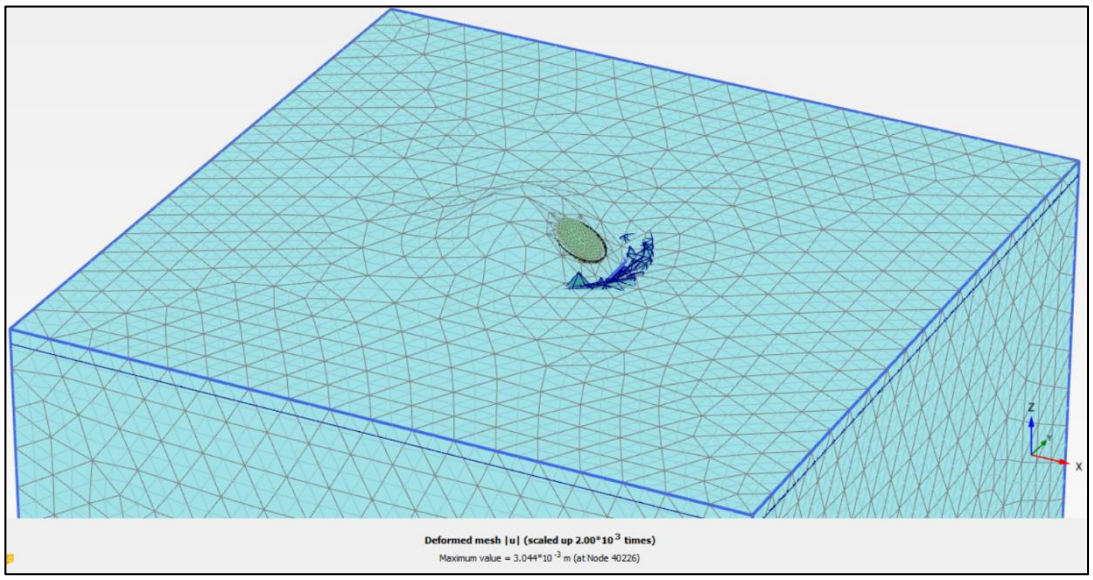

Figure 5.8. The Deformed Mesh for Mohr-Coulomb Model

Figure 5.9 presents the movement vectors in a side view of a cross section at centerline of the foundation. The original ground surface moves vertically down all over the model geometry due to the gravity loading at initial stage. The foundation tilt is visible

in movement vectors. The zone of deformations is observed to be about 1.5xD depth from the ground surface, where D is the diameter of the foundation.

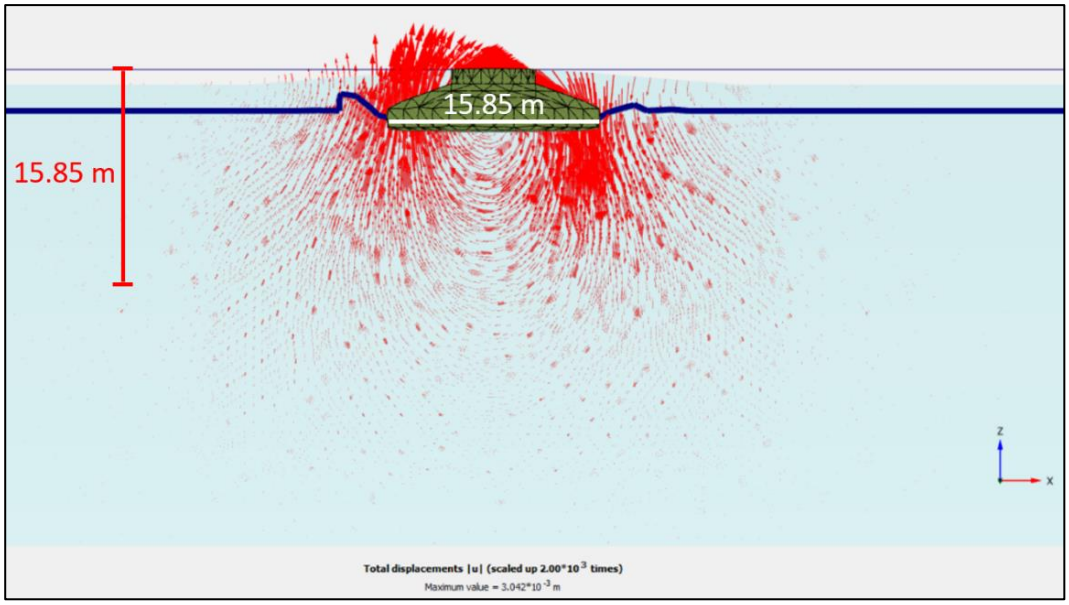

Figure 5.9. The Arrows of Total Displacement for Mohr-Coulomb Model

The total vertical displacement u_z contours are shown in Figure 5.10. The maximum vertical displacement is - 3 mm in downward direction and the minimum is + 3 mm in upward direction. The rotation of the foundation was calculated as the differential settlement divided by the diameter of the foundation. The rotation was computed as 0.00038 rad.

The total deviatoric strain contours γ_s can be seen in Figure 5.11, where the maximum strains are on the order of 0.4×10^{-3}. The strain localization at edges of the foundation is significant as compared the central area of the foundation.

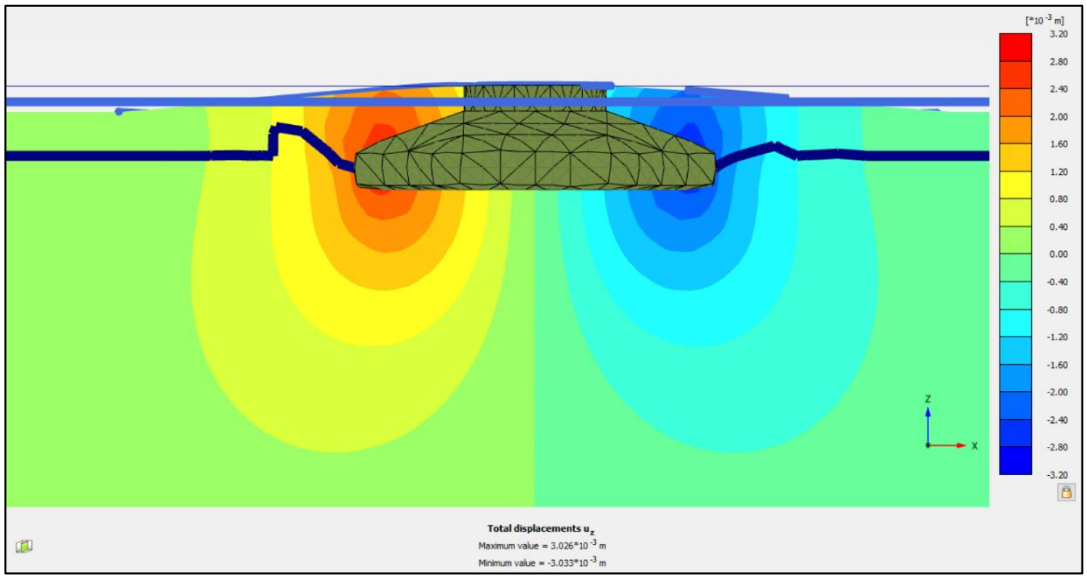

Figure 5.10. The Total Vertical Displacement for Mohr-Coulomb Model

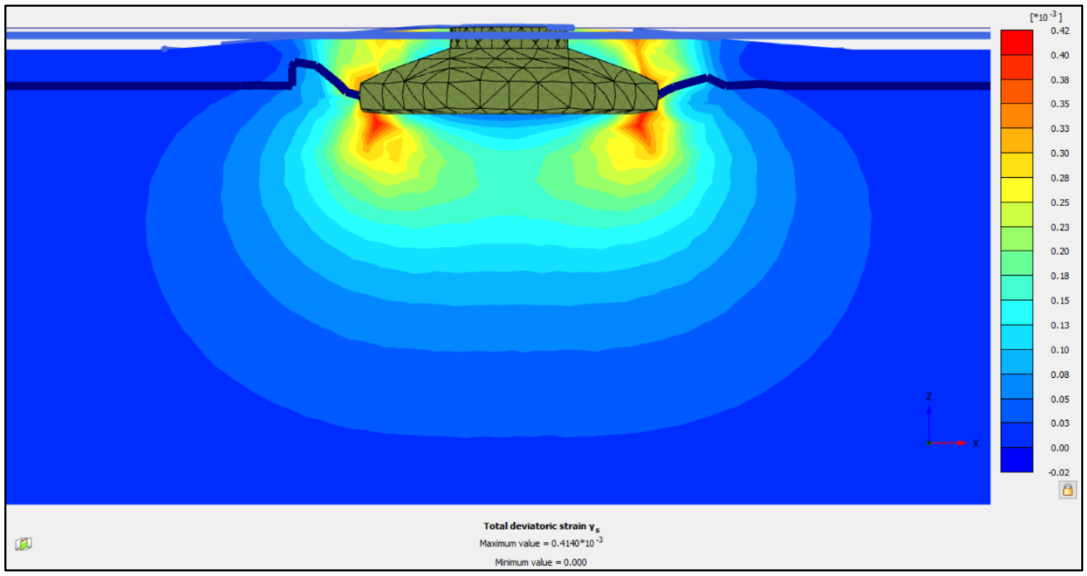

Figure 5.11. The Total Deviatoric Strain for Mohr-Coulomb Model

To investigate the pressure distribution beneath the foundation, the Cartesian total vertical stresses at a depth of 3.1 m from ground surface (which is 5 cm below the

foundation base) is shown in Figure 5.12 and Figure 5.13, at tower loading and combined loading stages, respectively.

Figure 5.12 indicates that the maximum contact pressure is - 42.8 kPa at the central part of the foundation and whereas the minimum value is - 155.8 kPa occurs at the edges of the foundation base.

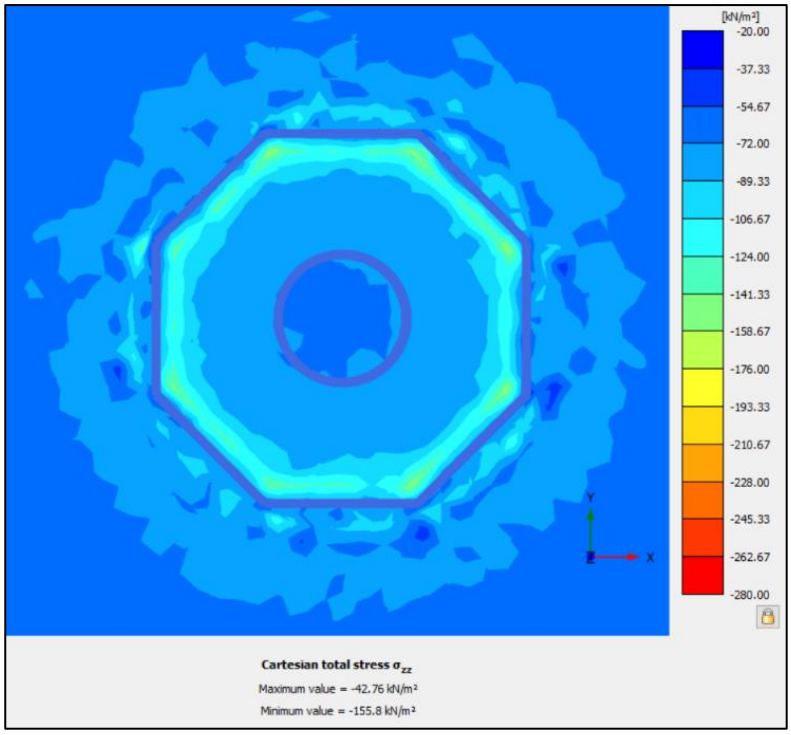

Figure 5.12. The Pressure Distribution beneath the Foundation at Tower Loading Stage for Mohr-Coulomb Model

The pressure distribution beneath the foundation at combined loading stage is presented in Figure 5.13. The maximum and the minimum values are - 26.3 and - 278.1 kPa, respectively. It can be concluded that even in extreme loading condition, the soil beneath the foundation is always under compression (i.e., there is full contact between the foundation base and the soil). Due to the octagonal shape of the foundation, there are stress concentrations at the corners as shown in Figure 5.13.

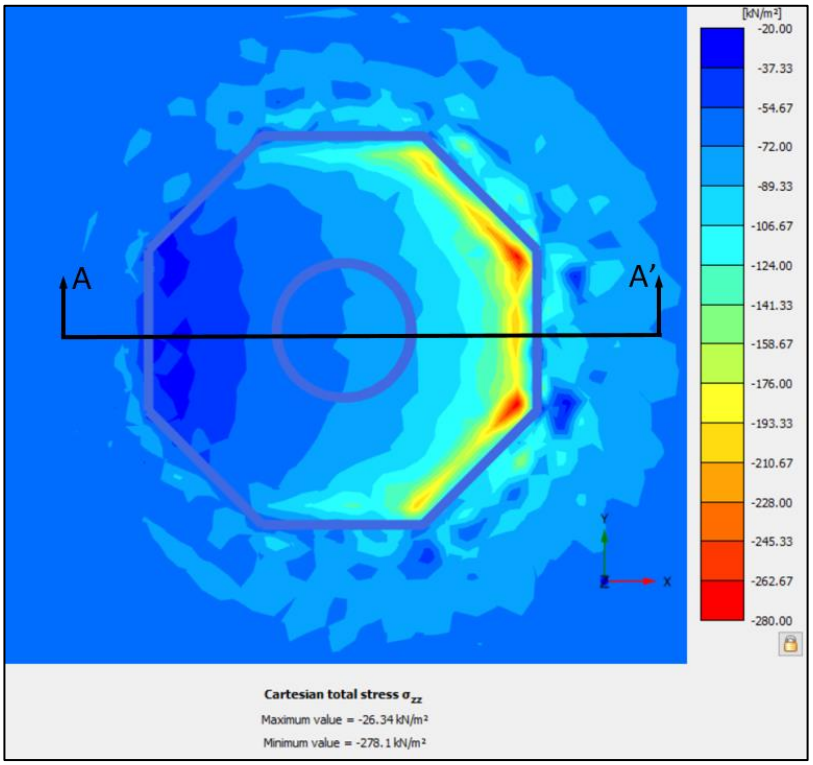

Figure 5.13. The Pressure Distribution beneath the Foundation at Combined Loading Stage for Mohr-Coulomb Model

The distribution of Cartesian total vertical stresses beneath the foundation along the cross section A-A' in Figure 5.13 can be seen in Figure 5.14. The maximum and minimum values are - 33.9 kPa and - 209.5 kPa, respectively, which are smaller than the stresses at the corners. As expected, there is constant in-situ overburden pressure outside of the foundation area.

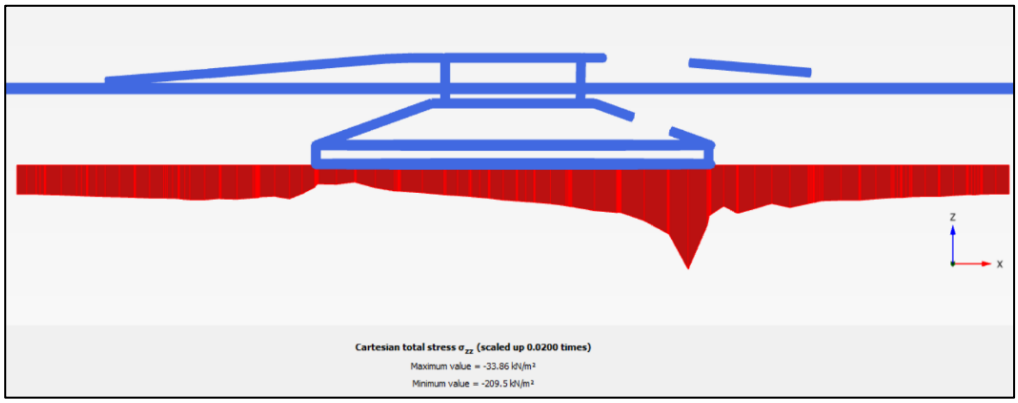

Figure 5.14. The Cartesian Total Stress beneath the Foundation for Mohr-Coulomb Model

The pressure distribution beneath the foundation at combined loading stage for Hardening model is given in Figure 5.15. The maximum and the minimum values are 4.72 kPa and – 263.2 kPa, respectively. In extreme loading condition, the soil beneath the foundation subjected to tensile pressure in only a small portion of the base area.

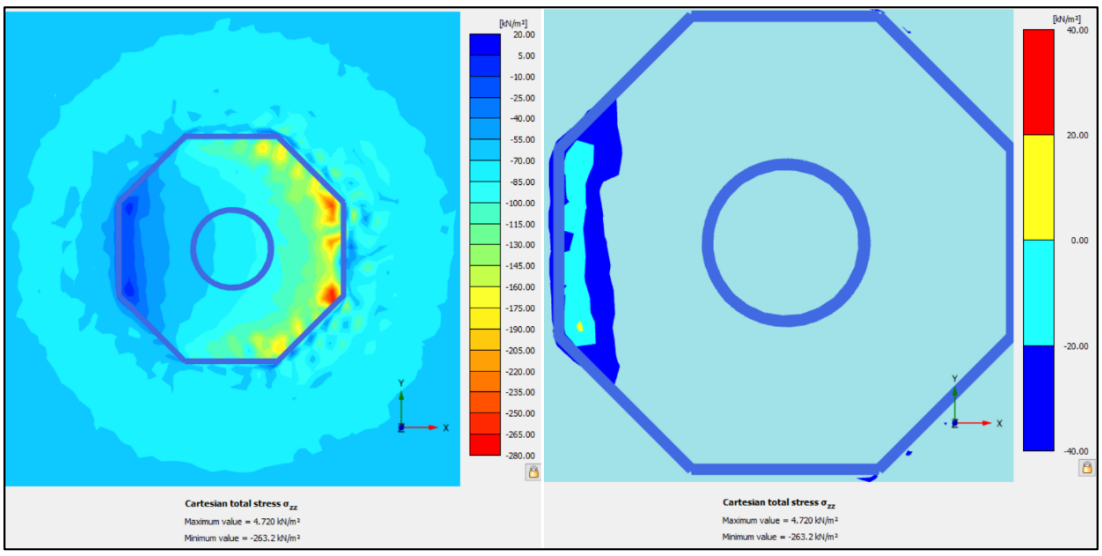

Figure 5.15. The Pressure Distribution beneath the Foundation at Combined Loading Stage for Hardening Model

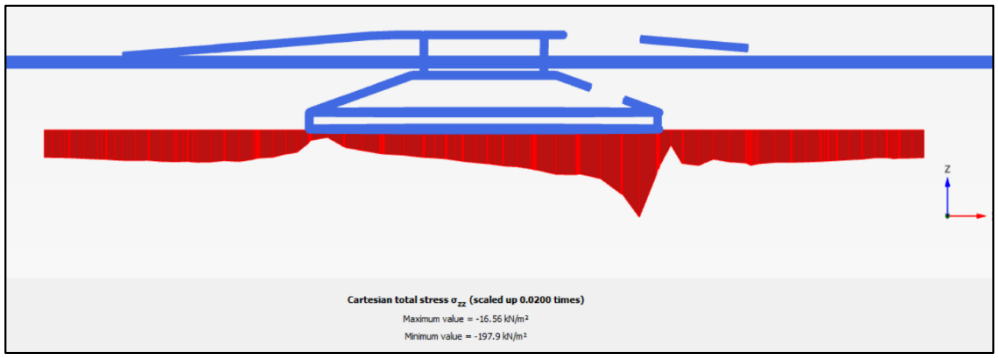

Figure 5.16. The Cartesian Total Stress beneath the Foundation (Centerline) for Hardening Model

The results of the 3D finite element analyses made by using Mohr-Coulomb and Hardening models are presented in Table 5.8 and Table 5.9.

Table 5.8. *Results of the 3D Finite Element Analyses Using Estimation Curve*

Variable	MOHR-COULOMB MODEL		HARDENING MODEL	
	Maximum Value	Minimum Value	Maximum Value	Minimum Value
Deformed Mesh Maximum Total Displacement |u| [mm]	3.044	-	1.530	-
Total Vertical Displacement u_z [mm]	3.026	-3.033	1.185	-1.528
Total Deviatoric Strain γ_s [-]	0.4140×10^{-3}	-	0.7870×10^{-3}	-
Total Vertical Stress at Centerline [kPa]	-33.9	-209.5	-16.6	-197.9
Pressure Distribution at Tower Loading [kPa]	-42.8	-155.8	-27.6	-153.3
Pressure Distribution at Combined Loading [kPa]	-26.3	-278.1	4.7	-263.2
Difference [kPa]	-16.5	122.3	-32.3	109.9
Rotation [rad]	0.00038		0.00017	

Note: (-) signs in pressure indicate compression.

Table 5.9. *Results of the 3D Finite Element Analyses Using Weighted Averages*

Variable	MOHR-COULOMB MODEL		HARDENING MODEL	
	Maximum Value	**Minimum Value**	**Maximum Value**	**Minimum Value**
Deformed Mesh Maximum Total Displacement |u| [mm]	2.279	-	1.981	-
Total Vertical Displacement u_z [mm]	2.227	-2.274	1.853	-1.962
Total Deviatoric Strain γ_s [-]	0.5803×10^{-3}	-	0.4592×10^{-3}	-
Total Vertical Stress at Centerline [kPa]	-20.7	-219.2	-13.1	-209.2
Pressure Distribution at Tower Loading [kPa]	-45.9	-137.3	-45.6	-153.8
Pressure Distribution at Combined Loading [kPa]	-18.8	-275.3	-1.1	-268.0
Difference [kPa]	-27.1	138.0	-44.5	114.2
Rotation [rad]	0.00028		0.00024	

Note: (-) signs in pressure indicate compression.

The results from Hardening model indicate smaller total and vertical displacements because of the modeling differences in the stiffness of the soil. All of the stresses in Table 5.8 and Table 5.9 resulted from Hardening model are similar to Mohr-Coulomb model. Using Hardening model, the maximum value of base pressure at combined loading stage was obtained as 4.7 kPa in tension. This means that the foundation lost contact with soil under extreme loading condition. However, this is insignificant because this loading occurs instantaneously at a smaller portion of the foundation. The maximum and minimum rotation calculated 0.00038 rad and 0.00017 rad for Mohr-Coulomb and Hardening models, respectively.

5.7. Discussion of Results: Field Measurements, Analytical Solution and Three-Dimensional Finite Element Method

According to the analytical solution based on DNV/RISØ (2002) guideline, the maximum base pressure was calculated to be 247.6 kPa in compression. The corresponding values were – 278.1 kPa and - 268.0 kPa for Mohr-Coulomb and Hardening models, respectively. This indicates that analytical solution can be used to obtain foundation dimensions, which can be used in a more elaborate and complicated 3D numerical models for further detailed analyses.

Yılmaz (2014) measured daily vertical elastic displacements at 0.5 m below the base of the foundation only on several days in 2013 and 2014. The maximum wind speed observed was 9 m/s and in all measurements, the maximum daily vertical elastic displacement was 0.0215 mm. The magnitudes of the loads acting on the foundation corresponding to these measurements are unknown. Therefore, the results of this study can not be directly compared with Yılmaz's (2014) measurements. Vertical elastic displacements under extreme loading condition presented in Table 5.8 and Table 5.9 are 1.5 to 3.0 mm, which are greater than the field measurements as expected. The maximum elastic settlement calculated by analytical method was 17.8 mm under the extreme loading condition. 3D finite element analysis using sophisticated constitutive models can be used to capture the real soil behavior. However, the analytical method can be used to make a conservative estimate of the settlement.

The rotation under extreme loading condition in Table 5.8 and Table 5.9 are 0.00017 and 0.00038 rad, which are greater than the observed rotation in the field $4x10^{-6}$ rad recorded by Yılmaz (2014). The allowable rotation for wind turbine foundations is 0.003 rad to 0.0045 rad (ASCE/AWEA, 2011; Ntambakwa et al., 2016). Therefore, finite element analyses using two different constitutive models resulted in safe rotation condition.

CHAPTER 6

CONCLUSION

6.1. Summary

In this study, a wind turbine with 1.5 MW capacity on stiff clay taken as a case study is carried out by using analytical method with Monte Carlo simulation and 3-dimensional finite element method (3D FEM) for the extreme loading condition. The 3D FEM results are compared with analytical solutions as well as limited amount of field measurements of settlements. In analytical method based on DNV/RISØ (2002), bearing capacity, overturning, sliding, rocking stiffness and elastic settlements are calculated. Monte Carlo simulations are carried out considering the inherent variability of soil properties namely undrained shear strength and unit weight at different coefficient of varitation levels via lognormal statistical distribution and no cross correlation between soil parameters. In 3D FEM, Mohr-Coulomb and Hardening models are used and base pressures, settlements and rotations are investigated.

6.2. Conclusions

Some of the conclusions reached at this study are provided below.

(i) It is observed that base pressure distribution and localized stress concentrations under the corners of the foundation can be obtained by using 3D finite element analyses whereas this is not possible with analytical method,

(ii) The maximum strains in the soil obtained by 3D finite element analyses are within the expected strain limits for wind turbine foundations,

(iii) The differential settlement and the rotation (tilt) are important design considerations for wind turbine foundations. Settlement and rotation calculations based on analytical solution may not be reliable because of the assumptions and simplifications involved (Coduto et al., 2015). Therefore, 3D finite element analyses are becoming a necessity to obtain the settlement and rotation of wind turbine foundations accurately,

(iv) Analytical method is based on the assumption of circular shaped foundation. Therefore, the differences (e.g., in base pressures) between a hexagonal and an octagonal shaped foundation can not be observed in analysis made by using analytical method, whereas foundations with any shape can be studied in 3D FEM, together with shape optimization. However, analytical solution based on DNV/RISØ (2002) can still be used to obtain an initial foundation dimension for further analyses,

(v) In recent decades, the geotechnical engineering requires decision-making based on risk assessment considering soil variability. Deterministic analyses resulting in a single factor of safety value is no longer sufficient to evaluate the safety of a foundation and the effects of soil variability should be considered for better geotechnical risk evaluation, together with deterministic approaches. For wind parks, individual boreholes may not be drilled at each wind turbine location. Therefore, the foundation design should consider uncertainty and variability of soil properties. Either the variability in material properties should be reduced via extensive laboratory and in-situ testing, or variability should be considered in the design (e.g., via different coefficient of variation levels). If the uncertainty in soil parameters can be reduced, the probability of unsatisfactory performance (Pf) can be decreased,

(vi) The diameter is a major factor in wind turbine foundation design directly affecting the capital cost of the project. In this study, the variation in diameter was investigated together with different COV levels in soil properties. The effects of diameter and COV levels on satisfactory performance was shown. As demonstrated in this study, the diameter versus Pf could be plotted to obtain the optimum diameter,

(vii) As it was noted by Oguz et al. (2017) for slope stability problems, low and high COV levels can influence the probability of failure nonlinearly, in a steep or smooth manner. Pf for bearing capacity was demonstrated to be influenced significantly by COV level and diameter of foundation, in a steep or smooth manner. Increase of COV level (i.e., more variability in the soil properties) causes increase in Pf for Pf smaller than 50%. As COV level decreases, Pf decreases. Similar conclusions were reported by Oğuz et al. (2017),

(viii) Settlement criteria was satisfied for all analyses (analytical, probabilistic and 3D FEM) in this study for elastic settlement. Therefore, the optimum design for settlement could not be investigated. However, settlement together with bearing capacity should be used in optimum design,

The results presented in this study could be useful for further understanding of optimum wind turbine foundation design demonstrating a methodology for practicing engineers. It will be useful to reach robust, safe and economical foundation design for wind turbines considering the effects of soil variability.

6.3. Recommendations for Future Studies

- This study can be conducted for other soil and rock types as well as different foundation shapes.
- Other soil properties such as Young's modulus etc. can considered as random variables and cross correlation between parameters can be considered.
- Site-specific COV values based on extensive laboratory tests and field investigations can be determined.
- Consolidation settlement can be considered.
- Soil structure interaction investigations via 3D FEM with cyclic loading can be studied.

- Settlement measurements of specific turbine foundations in field can be used to verify and validate 3D FEM results.
- Metaheuristic optimization algorithms can be used for optimization of wind turbine foundations.
- Allowable Stress Design method and Load and Resistance Factor Design method can be compared for design of a wind turbine foundation.

REFERENCES

AASHTO Officials. (2012). *AASHTO LRFD Bridge Design Specifications* (6th ed.). Washington, DC: AASHTO.

Adaramola, M. (2014). *Wind Turbine Technology Principles and Design.* Boca Raton: CRC Press.

Ameratunga, J., Sivakugan, N., & Das, B. M. (2016). *Correlations of Soil and Rock Properties in Geotechnical Engineering.* India: Springer.

ASCE/AWEA. (2011). *Recommended Practice for Compliance of Large Land-based Wind Turbine Support Structures.* Washington, DC: AWEA.

Azizi, F. (2000). *Applied analyses in geotechnics*. London: E & FN Spon.

Baban, T. M. (2016). *Shallow Foundations: Discussions and Problem Solving.* Chichester: John Wiley & Sons.

Bowles, J. E. (2001). *Foundation Analysis and Design.* New York: McGraw-Hill.

Branca, B., & Ben-Hassine, J. (2009). Dynamic Analysis of a Wind Turbine and Foundation to Assess Liquefaction Potential of Bearing Soils. *Structures Congress 2009* (pp. 1-12). Austin: ASCE.

Briaud, J. L. (2013). *Geotechnical Engineering: Unsaturated and Saturated Soils.* Hoboken: John Wiley & Sons.

British Standards Institution. (2004). *Eurocode 7: Geotechnical Design - Part 1: General Rules.* London: BSI.

Brown, L. R., Larsen, J., Roney, J. M., & Adams, E. E. (2015). *The Great Transition: Shifting from Fossil Fuels to Solar and Wind Energy.* New York: W. W. Norton & Company.

Brumund, W. F., & Leonards, G. A. (1972). Subsidence of Sand Due to Surface Vibration. *Journal of the Soil Mechanics and Foundations Division*, 27-42.

Budhu, M. (2010). *Soil Mechanics and Foundations* (3rd ed.). Hoboken: John Wiley & Sons.

Burton, T., Jenkins, N., Sharpe, D., & Bossanyi, E. (2011). *Wind Energy Handbook* (2nd ed.). Chichester: John Wiley & Sons.

Casagrande, A. (1936). Determination of the preconsolidation load and its practical significance, *in Proceedings of the International Conference on SMFE*, Harvard University, Cambridge, MA, Vol. III, pp. 60–64.

Chen, W., & McCarron, W. O. (1991). Bearing Capacity of Shallow Foundations. In H. Y. Fang, *Foundation Engineering Handbook* (2nd ed., pp. 144-161). New York: Van Nostrand Reinhold.

Cho S. E. (2010). "Probabilistic Assessment of Slope Stability That Considers the Spatial Variability of Soil Properties." Jour*nal of Geotechnical and Geoenvironmental Engineering*, Vol. 136, Issue 7, pp. 975-984.

Construction Industry Research and Information Association (Great Britain). (1995). *The standard penetration test (SPT): Methods and use*. London: CIRIA.

Coduto, D. P., Kitch, W. A., & Yeung, M. R. (2015). *Foundation Design: Principles and Practices* (3rd ed.). Upper Saddle River: Pearson.

Das, B. M. (2015). *Principles of Foundation Engineering* (8th ed.). Boston: Cengage Learning.

Das, B. M. (2017). *Shallow Foundations: Bearing Capacity and Settlement* (3rd ed.). Boca Raton: CRC Press.

Das, B. M., & Luo, Z. (2016). *Principles of Soil Dynamics* (3rd ed.). Boston: Cengage Learning.

Das, B. M., & Shin, E. C. (1996). Laboratory Model Tests for Cyclic Load-induced Settlement of a Strip Foundation on a Clayey Soil. *Geotechnical and Geological Engineering*, 213-225.

DNV/RISØ. (2002). *Guidelines for Design of Wind Turbines* (2nd ed.). Copenhagen: Det Norske Veritas & Risø National Laboratory.

Dobry, R., Gazetas, G., & Stokoe, K. H. (1986). Dynamic Response of Arbitrarily Shaped Foundations: Experimental Verification. *Journal of Geotechnical Engineering*, 136-154.

Duncan, J. M. (2000). "Factors of Safety and Reliability in Geotechnical Engineering." *Journal of Geotechnical Engineering*, Vol. 126, Issue 4, pp. 307-316.

Duncan, J. M., & Buchignani, A. L. (1976). An engineering manual for settlement studies. Berkeley: University of California, Dept. of Civil Engineering.

El-Sharkawi, M. A. (2016). *Wind Energy: An Introduction.* Boca Raton: CRC Press.

Faber, T. (2014). Tower and Foundation. In A. Schaffarczyk, *Understanding Wind Power Technology: Theory, Deployment and Optimization* (G. Roth, Trans., pp. 253-272). Chichester: John Wiley & Sons.

Gao, Q., Dong, H., Deng, Z., & Mae, Y. (2017). Wind-induced Dynamic Amplification Effects on the Shallow Foundation of a Horizontal Axis Wind Turbine. *Computers and Geotechnics*, 9-17.

Gazetas, G. (1991). Foundation Vibrations. In H. Y. Fang, *Foundation Engineering Handbook* (2nd ed., pp. 553-569). New York: Van Nostrand Reinhold.

Germanischer Lloyd (2010). *Rules and Guidelines: IV-Industrial Services, I-Wind Energy, 1. Guideline for the Certification of Wind Turbines.* Hamburg: Germanischer Lloyd Industrial Services GmbH.

Griffiths D. V., & Fenton G. A. (2004). "Probabilistic Slope Stability Analysis by Finite Elements." *Journal of Geotechnical and Geoenvironmental Engineering*, Vol. 130, Issue 5, pp. 507-518.

Grünberg, J., & Göhlmann, J. (2013). *Concrete Structures for Wind Turbines.* Berlin: Ernst & Sohn.

Hansen, J. B. (1970). A Revised and Extended Formula for Bearing Capacity. *Danish Geotechnical Institute, Bulletin No.28*.

Hara, A., Ohata, T., & Niwa, M. (1971). Shear modulus and shear strength of cohesive soils. Soils Found 14(3):1–12.

Hau, E. (2013). *Wind Turbines: Fundamentals, Technologies, Application, Economics* (3rd ed.). (H. Von Renouard, Trans.) Berlin: Springer.

Heller, L. W. (1964). Failure Modes of Impact Loaded Footings on Dense Sand. Port Hueneme: U.S. Naval Civil Engineering Laboratory.

Hemami, A. (2012). *Wind Turbine Technology.* New York: Cengage Learning.

IRENA. (2012). *Renewable Energy Technologies: Cost Analysis Series: Wind Power.* Bonn: IRENA.

Jain, P. (2011). *Wind Energy Engineering* (1st ed.). New York: McGraw-Hill.

Jamieson, P. (2011). *Innovation in Wind Turbine Design* (1st ed.). Chichester: John Wiley & Sons.

Jamiolkowski, M., Lancellota, R., Marchetti, S., Nova, R., & Pasqualini, E. (1979). Design parameters for clays, State of the Art Report, 7th European Conf. On Soil Mechanics, Brighton.

Jamiolkowski, M., Ladd, C. C., Germaine, J., & Lancellotta, R. (1985). New developments in field and lab testing of soils. In: Proceedings 11th international conference.

Janbu, N., Bjerrum, L., & Kjaernsli, B. (1956). Soil Mechanics Applied to Some Engineering Problems. *Norwegian Geotechnical Institute, Publication No. 18*, 30-32.

Jardine, R. J., Fourie, A., Maswoswe, J., & Burland, J. B. (1985). Field and laboratory measurements of soil stiffness. In Proc. 11th International Conference on Soil Mechanics and Foundation Engineering. San Francisco (Vol. 2, pp. 511-514).

Knappett, J. A., & Craig, R. F. (2012). *Craig's Soil Mechanics* (8th ed.). London: Spon Press.

Kramer, S. L. (1996). *Geotechnical Earthquake Engineering.* Upper Saddle River: Prentice Hall.

Kulhawy, F. H., & Mayne, P. W. (1990). Manual on estimating soil properties for foundation design, Report EL-6800, Electric Power Research Institute, Palo Alto, California, USA.

Ladd, C. C., Foott, R., Ishihara, K., Schlosser, F., & Poulos, H. G. (1977). Stress-deformation and strength characteristics. Proceedings of 9th ICSMFE, Tokyo, pp 421–494.

Lancellotta, R. (2009). *Geotechnical Engineering* (2nd ed.). (A. A. Balkema, Trans.) New York: Taylor & Francis.

Lambe, T. W., & Whitman, R. V. (1969). *Soil mechanics*. New York: Wiley.

Lambe, T. W., & Whitman, R. V. (1979). *Soil mechanics*. New York: Wiley.

Lees, A., & Institution of Civil Engineers (Great Britain). (2016). *Geotechnical finite element analysis: A practical guide*.

Li, C., Bao, G., Cao, Y., Zhou, J., & Liu, M. (2014). Wind-induced Fatigue Loading and Its Effect on the Stability of Wind Power Foundation. *New Frontiers in Geotechnical Engineering* (pp. 78-87). Shanghai: ASCE.

Lommler, J. C. (2012). *Geotechnical Problem Solving.* Chichester: John Wiley & Sons.

Lynn, P. A. (2012). *Onshore and Offshore Wind Energy: An Introduction.* Chichester: John Wiley & Sons.

Madaschi, A., Gajo, A., Molinari, M., & Zonta, D. (2016). Characterization of the Dynamic Behavior of Shallow Foundations with Full-Scale Dynamic Tests. *Journal of Geotechnical and Geoenvironmental Engineering, 142*(7).

Marchetti, S. (1997). The Flat Dilatometer: Design Applications. *Proceedings of the Third International Conference on Geotechnical Engineering*. Cairo: ISSMGE.

Mathew, S. (2006). *Wind Energy: Fundamentals, Resource Analysis and Economics.* Berlin: Springer.

Mawer, B. W. (2015). *An Introduction to Geotechnical Design of South African Wind Turbine Gravity Foundations (Master's Thesis).* University of Cape Town.

Mayne, P. W., & Kemper J. B. (1988). Profiling OCR in stiff clays by CPT and SPT. Geotech Test J ASTM 11(2):139–147.

Mayne, P. W., & Poulos, H. G. (1999). Approximate Displacement Influence Factors for Elastic Shallow Foundations. *Journal of Geotechnical and Geoenvironmental Engineering*, 453-460.

McCarthy, D. F. (2007). *Essentials of Soil Mechanics and Foundations* (7th ed.). Upper Saddle River: Pearson.

Mesri, G. (1989). A reevaluation of $s_{u(mob)} \approx 0.22\sigma'_{0p}$ using laboratory shear tests. Can Geotech J 26(1):162–164.

Meyerhof, G. G. (1963). Some Recent Research on the Bearing Capacity of Foundations. *Canadian Geotechnical Journal*, 16-26.

Morgan, K., & Ntambakwa, E. (2008). Wind Turbine Foundation Behavior and Design Considerations. *AWEA Windpower Conference 2008* (pp. 1-14). Houston: AWEA.

NAVFAC. (1986). *Foundations & Earth Structures Design Manual 7.02.* Alexandria: U.S. NAVFAC.

Ntambakwa, E., Yu, H., Guzman, C., & Rogers, M. (2016). Geotechnical Design Considerations for Onshore Wind Turbine Shallow Foundations. *Geotechnical and Structural Engineering Congress 2016* (pp. 1153-1165). Phoenix: ASCE.

Oguz, E. A., Yalcın Y., Huvaj, N. (2017). Probabilistic Slope Stability Analyses: Effects of the Coefficient of Variation and the Cross-Correlation of Shear Strength Parameters. ASCE Geo-Congress 2017, Geotechnical Frontiers 2017, Geotechnical Special Publication 278: Walls and Slopes, 363-371.

Oztoprak, S., & Bolton, M. D. (2013). Stiffness of Sands through a Laboratory Test Database. *Géotechnique, 63*(1), 54-70.

Partnership for Renewables. (2013, 12 06). *Oakdale Wind Turbines Begin to Take Shape*. Retrieved 12 12, 2016, from Partnership for Renewables: http://www.pfr.co.uk/image-library/Oakdale//Completed%20foundation.jpeg

Pasten, C., Shin, H., & Santamarina, J. C. (2013). Long-Term Foundation Response to Repetitive Loading. *Journal of Geotechnical and Geoenvironmental Engineering*, 1-11.

Phoon K. K. and Kulhawy F. H. (1999). "Evaluation of geotechnical property variability." *Canadian Geotechnical Journal*, Vol. 36, Issue 4, pp. 625-639.

PLAXIS 3D Manuals 2015, P.O. Box 572, 2600 AN Delft, The Netherlands.

Poulos, H. G., & Small, J. C. (2000). Development of Design Charts for Concrete Pavements and Industrial Ground Slabs, In book: *Design Applications of Raft Foundations*. Thomas Telford Limited.

Prakash, S. (1981). *Soil Dynamics.* New York: McGraw-Hill.

Priest, J. (2012). Dynamic and Seismic Loading of Soils. In J. Burland, T. Chapman, H. Skinner, & M. Brown, *ICE Manual of Geotechnical Engineering* (pp. 259-269). London: ICE Publishing.

Rao, N. S. (2011). *Foundation Design: Theory and Practice.* Singapore: John Wiley & Sons (Asia).

Reese, L. C., & Wang, S. (2008). Design of Foundations for a Wind Turbine Employing Modern Principles. *From Research to Practice in Geotechnical Engineering Congress* (pp. 351-365). New Orleans: ASCE.

Reese, L. C., Isenhower, W. M., & Wang, S. (2006). *Analysis and Design of Shallow and Deep Foundations.* Hoboken: John Wiley & Sons.

Richart, F. E., Hall, J. R., & Woods, R. D. (1970). *Vibrations of Soils and Foundations.* Upper Saddle River: Prentice Hall.

Salgado, R. (2008). *The Engineering of Foundations*. New York: McGraw-Hill.

Schmertmann, J. H. (1978). *Guidelines for Cone Penetration Test: Performance and Design.* Washington, DC: FHWA.

Sivakugan, N., & Pacheco, M. (2011). Design of Shallow Foundations. In B. M. Das, *Geotechnical Engineering Handbook* (pp. 3.2-3.50). Fort Lauderdale: J. Ross Publishing.

Skempton, A. W. (1951). The Bearing Capacity of Clays. *Proceedings* (pp. 180-189). London: Building Research Congress.

Smil, V. (2010). *Energy Myths and Realities: Bringing Science to the Energy Policy Debate*. Washington, DC: AEI Press.

Smoltczyk, H. U., Netzel, D., & Kany, M. (2002). Spread Foundations. In H. U. Smoltczyk, *Geotechnical Engineering Handbook* (Vol. III, pp. 1-81). Berlin: Ernst & Sohn.

Stroud, M. A. (1975). The standard penetration test in insensitive clays and soft rocks. In: Proceedings, European symposium on penetration testing 2, pp 367–375.

Szerző, A. (2012). Optimization of Foundation Solutions for Wind Turbines. *Mathematical Modeling in Civil Engineering*, 215-224.

Terzaghi, K. (1943). *Theoretical Soil Mechanics.* New York: John Wiley & Sons.

Tinjum, J. M., & Christensen, R. (2011). Site Investigation, Characterization and Assessment for Wind Turbine Design and Construction. In J. D. Sørensen, & J. N. Sørensen, *Wind Energy Systems: Optimising Design and Construction for Safe and Reliable Operation* (pp. 28-45). Cambridge: Woodhead Publishing.

Tomlinson, M. J., & Woodward, J. (2015). *Pile design and construction practice*. Boca Raton: CRC Press.

Twele, J., Heilmann, C., & Schubert, M. (2012). Design and Components. In R. Gasch, & J. Twele, *Wind Power Plants: Fundamentals, Design, Construction and Operation* (2nd ed., pp. 46-113). Berlin: Springer.

U.S. EIA. (2016). *International Energy Outlook 2016.* Washington, DC: U. S. Energy Information Administration.

Vardanega, P. J., & Bolton, M. D. (2011). Practical Methods to Estimate the Nonlinear Shear Stiffness of Fine Grained Soils. In C. K. Chung, H. K. Kim, J. S. Lee, & Y. H. Jung, *Proceedings of the Fifth International Symposium on Deformation Characteristics of Geomaterials* (pp. 372-379). Amsterdam: IOS Press BV.

Viggiani, G., and J. H. Atkinson. 1995. “Interpretation of bender element tests.” *Géotechnique* 8 (2): 149–154.

Vesic, A. S. (1973). Analysis of Ultimate Loads of Shallow Foundations. *Journal of the Soil Mechanics and Foundations Division*, 45-73.

Vesic, A. S. (1975). Bearing Capacity of Shallow Foundations. In R. F. Winterkorn, & H. Y. Fang, *Foundation Engineering Handbook.* New York: Van Nostrand Reinhold.

Wagner, H. J., & Mathur, J. (2013). *Introduction to Wind Energy Systems: Basics, Technology and Operation* (2nd ed.). Berlin: Springer.

Warren-Codrington, C. J. (2013). *Geotechnical Considerations for Onshore Wind Turbines: Adapting Knowledge and Experience for Founding on South African Pedocretes (Master's Thesis).* University of Cape Town.

Willey, L. D. (2010). Design and Development of Megawatt Wind Turbines. In W. Tong, *Wind Power Generation and Wind Turbine Design* (pp. 187-253). Southampton: WIT Press.

WRD-K of ENERCON GmbH. (2010). *Foundation Data Sheet E48/S/49/3K/01*. WRD-K. Aurich: ENERCON GmbH.

Wu, Z. (2014). *Measuring Dynamic Properties of Wind Turbine Foundation Soil in Resonant Column - Issues and Challenges (Master's Thesis).* University of Wisconsin-Madison.

Xiao, M., & Barreto, D. (2015). *Geotechnical Engineering Design.* Chichester: John Wiley & Sons.

Xu, S., Fan, Y., & Wang, Z. (2015). A Study about Security of Wind Turbine Foundation in Different Width and Height Ratios. *Advanced Materials Research*, 566-573.

Yilmaz, M. (2014). *Foundation Soil Response to Wind Turbine Generator Loading (Master's Thesis).* University of Wisconsin-Madison.